UNIVERSITÄT FÜR BODENKULTUR WIEN
University of Natural Resources
and Life Sciences, Vienna

Doctoral Dissertation

Development of a modelling and analysis procedure for renewable energy potential: application for the case study ´Gaza Strip´

submitted by

Heyam Khamis AL-NAJJAR, M.Sc.

in partial fulfilment of the requirements for the academic degree

Doktorin der Bodenkultur (Dr.nat.techn.)

Vienna, February 2023

Supervisor:

Christoph Pfeifer, Univ.Prof. Dipl.-Ing. Dr.techn.
Institute of Chemical and Energy Engineering (IVET)
Department of Material Science and Process Engineering (MAP)

Affidavit

I hereby declare that I have authored this dissertation independently, and that I have not used any assistance other than that which is permitted. The work contained herein is my own except where explicitly stated otherwise. All ideas taken in wording or in basic content from unpublished sources or from published literature are duly identified and cited, and the precise references included. Any contribution from colleagues is explicitly stated in the authorship statement of the published papers.

I further declare that this dissertation has not been submitted, in whole or in part, in the same or a similar form, to any other educational institution as part of the requirements for an academic degree.

I hereby confirm that I am familiar with the standards of Scientific Integrity and with the guidelines of Good Scientific Practice, and that this work fully complies with these standards and guidelines.

Vienna, 11August Heyam

This thesis is dedicated to my parents, family, and friends.

Be in time.

2022

Supervisory team and reviewers

Supervisory team

Rafat Al Afif, Ph.D.
Senior Scientist
Institute of Chemical and Energy Engineering (IVET)
Department of Material Science and Process Engineering (MAP)

Prof. Dr. Hala Jarallah El Khozondar
Electrical Engineering Department
Islamic University of Gaza

Reviewers

Tobias Pröll, Univ.Prof. Dipl.-Ing. Dr.techn.
Institute of Chemical and Energy Engineering (IVET)
Department of Material Science and Process Engineering (MAP)

Associate Professor Muhammad Abu-Khaizaran
Department of Electrical and Computer Engineering
Birzeit University

Preface

This research was financed by Austrian Development Agency and Appear scholarship, grant number ICM-2019-13718. Supported by BOKU Vienna Open Access Publishing Fund.

The financial support from the Austrian Development Agency is gratefully acknowledged: Appear project155—MakingEnergy4Palestine (Developing maker-movement-inspired training courses on renewable energy sources in the Gaza Strip) as well as Appear scholarship (Reference number ICM-2019-13718).

Acknowledgements

First of all, all thanks and appreciation to ALLAH for his unlimited blessings and for giving me Islam and the strength to complete this thesis.

My sincere gratitude goes out to Austria, a beautiful, peaceful, and charming country, for granting me the chance to study at BOKU, one of its esteemed universities. Through the Austrian Development Agency and Appear Scholarship, thanks go to the Islamic University of Gaza (IUG), which is to be commended for its generosity, as are all the staff in the department of electrical engineering.

I would like to thank Mrs. Elki and her work team for their follow-up, support, and interest in overcoming obstacles to the success of this work, as well as for the beautiful entertainment programs and everything else that they have provided.

I would like to extend my sincere thanks to my supervisor, Prof. Christoph Pfeifer, without whom this work would not have been possible. And thanks very much for his continuous guidance, support, and humanity. I very much see him as an approach. I would like to thank Dr. Rafat Al-Afif. I would like to appreciate his effort. From his vision and in-depth discussion, he was concerned about the quality of the work from the beginning. I would like to thank Prof. Hala Jarallah El Khozondar for her guidance and considerable recommendations at work.

I would like to thank Eng. Christian Hardt, BOKU, for the IT technical support. I would like to thank all my colleagues at the institute for their kind treatment.

I'd like to thank everyone involved in the energy sector, especially engineers Raed Abu Al-Hajj at the Palestinian energy and natural resources authority, Ahmed Abu Aklien from the Gaza electricity distribution company, Dr. Sami Hamdan, and Abdul Halim Al-Kurd from the Coastal Municipalities Water Utility.

I would like to thank Dr. Sami Alalwani from the Kingdom of Saudi Arabia, a consultant in solar systems. Thank you for providing information and consultants related to solar power systems.

Many thanks and gratitude to my family, especially my parents, who always support me. I would like to thank my small family, who are always happy with my successes, my precious husband “Mohammed” and my children. Thanks much to everyone who gave me help, guidance, and encouragement. Thank you very much.

Table of content

List of publications

This dissertation is based on the work in the following papers. The papers are listed chronological order based on the steps of the methodology applied to analysis the renewable energy sources in the field study and the its contribution in electric energy supporting.

Al-Najjar H, Pfeifer C, Al Afif R, J. El-Khozondar H. Estimated View of Renewable Resources as a Sustainable Electrical Energy Source, Case Study. *Designs*. 2020; 4(3):32. https://doi.org/10.3390/designs4030032

Al-Najjar, H., H. J. El-Khozondar, C. Pfeifer and R. Al Afif (2021). "Hybrid grid-tie electrification analysis of bio-shared renewable energy systems for domestic application." Sustainable Cities and Society: 103538. https://doi.org/10.1016/j.scs.2021.103538

Al-Najjar H, Pfeifer C, Al Afif R, El-Khozondar HJ. Performance Evaluation of a Hybrid Grid-Connected Photovoltaic Biogas-Generator Power System. *Energies*. 2022; 15(9):3151. https://doi.org/10.3390/en15093151

Abstract

Electricity is very important in modern life, as it is used in many different sectors and has a significant impact on the economy, society, and the environment. It allows us to access numerous types of energy. Electricity can be obtained from traditional or renewable energy sources. Due to the energy crisis caused by the lack of some of these sources, as well as other political and economic considerations, a serious problem has arisen in Gaza City, which is located in the southwest of Palestine. The goal of this research is to develop modeling and analytical procedures for renewable energy potential. To construct a renewable grid-connected hybrid system that employs solar energy and biomass that achieve the optimal hybrid system design, a mathematical model as well as a hybridized energy simulation tool were employed. To this aim a brief survey has been conducted on the energy sources in the Gaza Strip, which included their availability, and mix types, as well as the current organization framework. Estimating the amount of electricity generated by renewable resources such as solar, biomass, wind, and wave is the initial step in the research. From this point of view, it is possible to construct a hybrid renewable system that uses solar and biomass as the main renewable energy sources. The hybrid system is designed to serve residential load with peak demand 84.5 kWp and daily consumption of around 1078.8 kWh. The system components capacities and full connections are evaluated using a pre-calculated mathematical model, which is then drawn to imitate the reality installed. The mathematical model implementation concern related arts and operators work in such field in the Strip. In the next step, HOMER Pro software has been used to design the desired system based on locally accessible components at a reasonable price. Biomass shared in the hybrid system regard to the biogas extraction in anaerobic digestion assumption, which is chosen among various biomass conversion technologies based on types and quantities of biomass, moisture content, and the amount of organic matter. Based on the economic and technical requirements and input data of the system into HOMER Pro, the results reveal in the optimal hybrid system, that combined grid tied solar and biomass components and exclude diesel generator and batteries. Solar energy harvest by PV panels, while the biogas engines generate electricity to introduce cost of energy (COE) (US$0.438/kWh) and (US$2.30M) Net Present Cost (NPC), as well as to comply with the limits of simulation input parameters and constraints. Finally, performance basic indicators, namely, energy efficiency, system sizing, and economic parameters have been evaluated. These results can be a helpful tool in the design of such types of hybrid system.

Kurzfassung

Elektrizität ist im modernen Leben sehr wichtig, da sie in vielen verschiedenen Sektoren verwendet wird und erhebliche Auswirkungen auf die Wirtschaft, die Gesellschaft und die Umwelt hat. Sie ermöglicht uns den Zugang zu zahlreichen Energiearten. Elektrizität kann aus traditionellen oder erneuerbaren Energiequellen gewonnen werden. Aufgrund der Energiekrise, die durch den Mangel an einigen dieser Quellen verursacht wurde, sowie aufgrund anderer politischer und wirtschaftlicher Erwägungen ist in Gaza-Stadt, das im Südwesten Palästinas liegt, ein ernstes Problem entstanden. Das Ziel dieser Forschungsarbeit ist die Entwicklung von Modellierungs- und Analyseverfahren für das Potenzial erneuerbarer Energien. Um ein netzgekoppeltes Hybridsystem aus erneuerbaren Energien, das Solarenergie und Biomasse nutzt, zu konstruieren und ein optimales Hybridsystemdesign zu erreichen, wurden ein mathematisches Modell sowie ein hybrides Energiesimulationstool eingesetzt. Zu diesem Zweck wurde ein kurzer Überblick über die Energiequellen im Gazastreifen, einschließlich ihrer Verfügbarkeit und ihrer Mischungsarten, sowie über die derzeitigen organisatorischen Rahmenbedingungen gegeben. Die Schätzung der durch erneuerbare Ressourcen wie Sonne, Biomasse, Wind und Wellen erzeugten Strommenge ist der erste Schritt in der Untersuchung. Unter diesem Gesichtspunkt ist es möglich, ein hybrides System aus erneuerbaren Energien zu konstruieren, das Solar und Biomasse als wichtigste erneuerbare Energiequellen nutzt. Das hybride System ist für die Versorgung von Haushalten mit einem Spitzenbedarf von 84,5 kWp und einem Tagesverbrauch von etwa 1078,8 kWh ausgelegt. Die Kapazitäten der Systemkomponenten und Vollanschlüsse werden mit Hilfe eines vorberechneten mathematischen Modells bewertet, das dann gezeichnet wird, um die installierte Realität nachzuahmen. Die Implementierung des mathematischen Modells bezieht sich auf verwandte Künste und Betreiber, die in diesem Bereich in dem Streifen arbeiten. Im nächsten Schritt wurde die Software HOMER Pro verwendet, um das gewünschte System auf der Grundlage von lokal verfügbaren Komponenten zu einem vernünftigen Preis zu entwerfen. Die im Hybridsystem verwendete Biomasse bezieht sich auf die Biogasgewinnung durch anaerobe Vergärung, die unter verschiedenen Technologien zur Umwandlung von Biomasse auf der Grundlage der Art und Menge der Biomasse, des Feuchtigkeitsgehalts und der Menge der organischen Stoffe ausgewählt wird. Basierend auf den wirtschaftlichen und technischen Anforderungen und den Eingabedaten des Systems in HOMER Pro zeigen die Ergebnisse ein optimales Hybridsystem, das netzgebundene Solar- und Biomassekomponenten kombiniert und Dieselgenerator und Batterien ausschließt. Solarenergie Ernte von PV-Panels, während die Biogas-Motoren Strom erzeugen, um die Kosten der Energie (COE) (US$0.438/kWh) und (US$2.30M) Kapitalkosten (NPC), sowie mit den Grenzen der Simulation Eingangsparameter und Zwänge entsprechen einzuführen. Schließlich wurden die grundlegenden Leistungsindikatoren, d.h. die Energieeffizienz, die Systemdimensionierung und die wirtschaftlichen Parameter, bewertet. Diese Ergebnisse können ein hilfreiches Verfahren für die Planung solcher Hybridsysteme sein.

1. Introduction

This chapter introduces the research. It first gives an overview of the research including a background about the study as well as the frame conditions, the research problem, the research objectives, the importance of this research area, scopes and limitations, and the research methodology that is followed to achieve the research objectives. Finally, the research structure is presented.

1.1. Background

The significance of energy is related to the extent to which a human needs energy in all aspects of his life, from ancient to present time. Humans have known and used energy through its original forms, such as the sun, wind, waves, fire, and so on, since an early time. With the passage of time, energy has been experimented with in new and varied forms, devised techniques of utilization, and developed new technologies to produce them.

Energy sources vary from conventional to renewable resources. Coal, fossil fuel, and gas are considered conventional resources for generating electrical power, while the sun, wind, wave, biomass, hydrogen, and geothermal, for instance, are considered renewable resources. The quest for alternative or sustainable energy resources manifests itself as a result of conventional energy being exhausted, unclean, and not renewable.

This work aims to analyze the energy sources involved, traditional and renewable, in the study area of Gaza, Palestine, and conduct a feasibility study of the echo-economic design of the hybrid renewable energy system HRES. Hence, provide a tool to suggest HRES depending on the frame conditions. The study addresses a residential area in Gaza city that contains 94 homes with electricity subscriptions. A hybrid grid-connected power system utilizes solar energy by using photovoltaic technology as well as biogas generators as two abundant kinds of renewable resources in the study area. In addition to diesel genset that are already frequently used to generate electricity due to long power cuts, and discuss the possibility of adding a battery storage as a backup. To this aim, analytical procedures that are well-known in the literature community are followed, beginning with identifying and assessing resources, calculating the load to be covered, and investigating the location. The basic components of the system were then introduced, which are compatible with the technologies used to generate energy from both types of resources. Finally, the HOMER Pro software has been applied, through which an optimum design from an economic, technological, and environmental point of view could be developed. As a conclusion, the literature review shows that the development of renewable energy nowadays is being encouraged as a green solution. But utilizing energy from biomass sources is slow and still rare in Middle East/North Africa (MENA) countries, especially in the Arab Gulf States region, where it is insufficient compared to traditional fuels due to high operating and capital costs (Rehman and Al-Hadhrami 2010) (Salameh et al. 2020).

1.2. Problem description and motivation

The Gaza Strip has suffered from a continuous shortage of energy supplies for a long period of time, not less than 25 years. The crisis has increased since 2006, mostly due to the political framework conditions. This problem has worsened and exacerbated over time as a result of the steady increase in population and the accompanying activities that they carry out, which necessitate the use of various sources of energy, particularly electric energy. Gazans need energy to pump and desalinate water. Its sewage system also depends on energy-intensive cleaning procedures. On the other hand, the sources of energy and their quantities remained the same or increased only slowly. This caused a deficit that led to a permanent, daily, and continuous power outage for long hours, exceeding an average of eight hours. This resulted in paralysis in the wheel of the economy and development and disrupted the provision of basic services to citizens, on top of which are health and education, even in the darkest natural and abnormal conditions.

The other side of the problem lies in the sector’s dependence on external parties or neighbouring countries to import energy or fuel to operate the sole diesel-fueled power plant, whose electricity production does not exceed a third of domestic consumption.

The foregoing prompted officials, decision-makers, and even researchers to study and assess the energy crisis situation to come up with solutions and strategies that would alleviate the energy crisis. These solutions include the optimal use of the renewable resources available in the geographical area, such as solar energy and biomass. It is worth mentioning that the investment in biomass does not only generate electricity, but rather disposes of the amount of waste that is considered an environmental burden for the study area.

1.3. Research Objectives

Main Objective

The main aim of the research is to provide a tool to suggest HRES depending on the frame conditions. Design an optimal grid-tied hybrid renewable energy system for residential neighborhood electrification using renewable energy resources available in the study area, to achieve an affordable techno-economic power system.

Specific Objectives

- To identify the various types of renewable resources in the study area, including solar irradiation, biomass, wave, and wind, and appreciate the energy yield of each one. In the “Estimated View of Renewable Resources as a Sustainable Electrical Energy Source, Case Study” (Paper I).
- To define a mathematical model for analyzing and calculating hybrid system capacity, which includes the number of components and their power capacities.
- To evaluate the techno-economic optimum solution of a hybrid system by using the simulation software HOMER Pro and obtain an optimized system for the chosen case depending on the cost of energy and total cost of energy. “Hybrid grid-tie electrification analysis of bio-shared renewable energy systems for domestic application” (Paper 2).
- Provide methods to develop and optimize HRES´s and to provide a toolbox of developers from other regions (eventually but not necessarily with similar frame conditions).

1.4. Research Methodology

To fulfill the research's main and specific objectives, thereby problem solving, the following methodology steps are followed:

First Step: State of the art and literature review

An investigative overview of the energy supply and its capabilities in the Gaza Strip was presented, with reference to the dimensions of the energy sector and its institutions. The study has demonstrated hybrid systems, photovoltaic technologies and their topologies, and biogas technologies have been demonstrated. For this, principles in the design and analysis processes are needed. As a consequence, a literature analysis of related work has been conducted, with a focus on solar and biomass in hybrid systems, both connected and unconnected to the utility grid, as well as biomass technology techniques used in such systems.

Second Step: Design hybrid system

The designed system includes three stages as follow:

Assessment of traditional and renewable energy resources' availability

Energy resources available at the study location have been estimated as being of both traditional and renewable types. and provide a brief description of the energy situation in the geographic area. The assessment methodology uses mathematical equations and a software tool to compute the amount of energy that can be harvested from solar, biomass, wind, and wave energy. Then nomination of the resources that will take part in the hybrid system is based on the results obtained.

System components and data collection

After energy source candidates are fixed for the hybrid system, the next step involves the components associated with and technologies assumed to build the hybrid system. For that, information such as load profile, hybrid system component manufacture, their local market prices, and their technical and economic parameters have been collected and defined, respectively. This step required conducting interviews and consultation with experts in this community. Hence, it dealt with many specialized agencies in the energy sector. Gaza Electricity Distribution Company (GEDCo) provides utility grid and load profile information. Energy and Natural Resources Authority to stand on the latest development in the renewable energy sector. As well as the local sole diesel-fueled power plant, Gaza Power Plant, and its ability to cover residential loads. Meeting with consultant engineers involved in the installation and sizing of solar and hybrid systems.

Set-up of the hybrid system

Definition of the optimal design of hybrid renewable bio-shared renewable energy systems for domestic-based applications. Firstly, traditional and nontraditional energy sources system's components have been determined. The energy capacity and size numbers of each have been evaluated by using the mathematical model. Secondly, the HOMER Pro software program is used to conduct simulation experiments for optimum solutions over input parameters and sensitivity analysis, concerning economic and manufacturing values. Multiple values were used to provide input parameters as a trade-off between many options in order to find a winner solution. The output displays the techno-economic optimum for a hybrid system with a set of possible combinations based on the cost of energy and total energy cost.

Third step: Results and conclusions

The outputs of this research are the resulting economic and technical values of the system and its components that meet the optimal solution of grid-tied hybrid renewable energy system design, as well as the values of the emissions due. Discussion for these outputs has been presented, and finally, the conclusion and recommendation of the study were drawn up.

1.5. Outline of the theses

Chapter 2: State of the Art of energy supply and potential in the Gaza Strip provides an overview of the energy sector, its institutional structure, and the functionality of Gaza's power plants. There are outline reviews of common sources of energy used in the study area, as well as its potential. **Energy technologies and applications are covered in Chapter 3.** In this chapter, the technologies utilized in the Gaza Strip to convert traditional fuel, diesel, into electrical energy, as well as the concepts and technologies that are commonly employed to transform renewable energy into electrical energy, are displayed and discussed. The creation of biogas from anaerobic digestion will be discussed, as will the factors that influence the calorific value of the gas. Moreover, definitions and terminologies throughout the work are demonstrated, as well as biomass conversion technologies that include thermochemical and bio-chemical conversion. **In Chapter 4: Methodology,** the research methodology steps for the work will be presented, which includes collecting data, estimating available renewable energy, calculating the possible electrical energy from these resources along the Strip, and determining the sources that will be candidates to be included in a hybrid system. Following that, a mathematical model was created to determine the capacities of the input system components as well as appropriate technologies, taking into account many criteria such as related work in a similar environment and resource characteristics. According to the various system inputs and constraints, the hybrid renewable energy system was developed. The findings developed by using the HOMER Pro software are presented in the following chapters. **Chapter 5: Implementation of the Hybrid Renewable Energy System** HOMER Pro software with a flow chart regarding renewable energy resources is applied. A mathematical model is proposed to evaluate the desired hybrid systems' components for residential district electrification. Basic values and datasheet characteristics of system components needed in the design process, as well as site location and load profile of household electricity, the energy source contributing to the main components, are selected and presented. The economic parameters used to determine a more affordable system are explained. Finally, simulation experiments with technical, economic, and emission characteristics were conducted. building single line diagrams for the microgrid are developed. **Chapter 6: Results and Discussion** reviews the optimum hybrid system chosen solution among the combinations associated with sensitivity parameters and apace values of the input parameters. The following discusses the numerical and graphic results, as well as the differences with the modified mathematical model, in order to investigate the effects of economic and emission features that are considered in HOMER calculations. Finally, **Chapter 7: Conclusion,** concludes the research by stressing that the results meet the research objectives. And in **chapter 8,** consideration and future research are stated.

2. State of the art OF Energy Supply and potential in the Gaza Strip

2.1. Overview

Energy enters into every aspect of daily life. It is the backbone of economic and industrial development, the development of social life and the achievement of prosperity. According to the Palestinian Central Bureau of Statistics (PCBS), the energy dependency rate (%) in 2019 is 86.4%, an increase of 6.1% compared to 2014. The average annual electricity consumption per capita (kWh/capita) in 2019 is 1,280 kWh (PCBS 2020). The energy consumption of the household sector as a percentage of the total energy consumption is actually 38.8%. The percentage of households in the Gaza Strip varies according to their use of the form of energy. As shown in **Figure 2.1**, the percentage of residents who have access to electricity service in the Gaza Strip for the year 2019 is 99.8%, followed by liquefied petroleum gas (LPG) by 93%, then firewood and solar energy usage are 43.3% and 43.8%. Household utilization of gasoline, kerosene, and diesel is reported to be 13.5, 3.1, and 2.9%. As for the renewable sources of energy, solar energy is still mainly used to heat water through solar boards installed on rooftops and indirectly through the use of firewood and peat for heating, which constitutes about 18% of the total energy consumption.

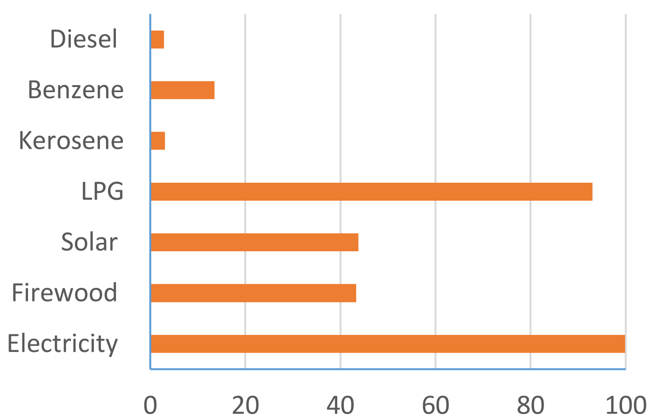

Figure 2.1: GS households percentage according to their use of the form of energy

The Gaza Strip (GS) requires some 500 MW of electricity, of which only 180 MW are currently available. Gaza currently has three sources of electricity: Israel, which provides 120 MW (66.6%); Egypt, which supplies 32 MW (8.5%); and the strip's sole power plant, which generates between 40 and 60 MW (24.9%).

The national strategy for the energy sector in Palestine includes a set of steering and guiding policies aimed at achieving a comprehensive vision to meet the challenges of energy demand in Palestine in the coming years. The vision includes the sustainability concept's achievement and continuity of development. raising the percentage of clean energy in the total energy supplied to the market and reducing the negative environmental impacts of energy supply and consumption. In addition to energy efficiency and security, a possible realization is important. Moreover, encouraging the private sector to invest in the energy sector is vital. This will lead to attracting investment to the local market, which will create jobs and stabilize capital within the country. Finally, the energy sector could become more productive and produce financial income for the state treasury.

The energy sector in Palestine consists of three sub-sectors: electricity, renewable energy and energy efficiency, and hydrocarbons (natural gas and petroleum). The Palestinian Energy and Natural Resources Authority (PENRA) supervises electricity, renewable energy, and energy efficiency. The General Petroleum Authority (GPA) supervises the gas and petroleum products sectors. This authority was incorporated under the umbrella of the Ministry of Finance. The Gaza Power Plant (GPP) has already been built by the Palestinian private sector.

Statistical studies of previous years indicate a significant increase in the rate of energy consumption in Palestine, where the annual capacity growth rate is 5.8% per year, while the rate of energy consumption amounts to 7% per year.

PENRA has conducted several studies on the expectations of growth in energy demand and local market needs in the Palestinian territories up to 2030. **Figure 2.2** shows the future prospects of the domestic electricity market; the blue curve displays the power (MW) demand increase indicator, the red curve for the energy (GWh) consumption increase indicator.

According to data published in 2020 by PENRA, in particular, the Gaza Strip's maximum demand is 640 MW (with 200 MW of capacity available), while the anticipated demand for 2025 is 828 MW. PENRA provides renewable energy solutions for households across Gaza with the support of the United Nation Office for Project Services (UNOPS). in support of PENRA’s aim to achieve 10% of domestic electricity generation coming from renewable energy by 2020. UNOPS installed hybrid solar systems, with a peak capacity of around 5 kilowatts (kW), on the rooftops of 400 households distributed along the strip, equivalent to 2MW.

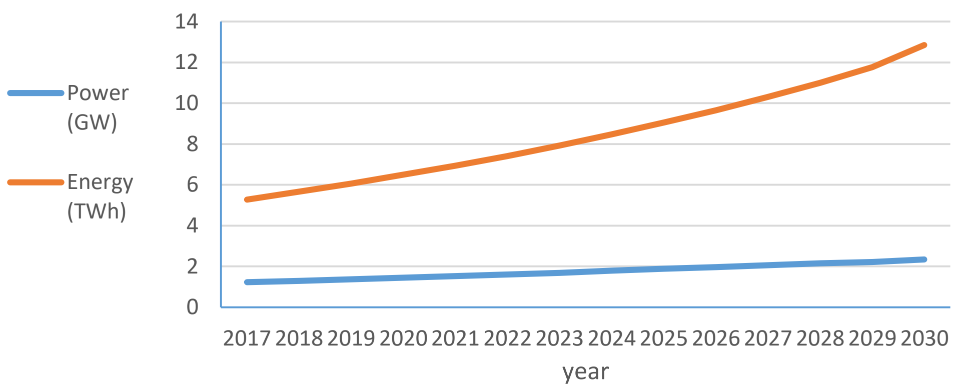

Figure 2.2: Future prospects of the domestic electricity market in Palestine (PENRA)

2.2. Traditional resources

In general, Palestine's energy sources are: first, petroleum and natural gas derivatives; second, electricity; and third, renewable energy sources (including solar power, wind power, and biofuels) (PENRA 2019). Fossil fuels and gas represent the main energy sources (TJ), and are mainly diesel, liquefied petroleum gas, and gasoline. PT imports most of its energy needs from outside. About 369 GWh of electricity is locally generated, which is about 6.2% of the total electricity demand for the year 2017 (meetMED 2020a).

The total imported energy in GS by type of energy for the year 2019 is presented in **Table 2.1**. Small amounts of biomass energy (olive cake and wood) are utilized for heating applications. The only large-scale generation capacity in the PT is the troubled sole Gaza Power Plant with a 140 MW capacity.

Higher heating value (HHV) of both charcoal and wood, **Table 2.1** was taken as standard based on the weight of each type as 15.81 GJ/ton (PCBS 2020). LPG has a typical specific calorific value of 46.1 MJ/kg (Hussain 2015), and bitumen coal heating values range from 24.423 to 32.564 kJ/kg (Schumacher and Juniper 2013), where their relative density is about 0.5–0.58 kg/L, and 1.0366 kg/L, respectively (Razali 2016).

Table 2.1: Imported Energy in Gaza Strip by Type of Energy in physical units, 2019

Electricity (MWh)	**Gasoline (k liter)**	**Diesel (k liter)**	**Fuel Oil (k liter)**	**Kerosene (k liter)**	**LPG (ton)**	**Bitumen (ton)**	**Wood & Charcoal (ton)**
1,095,266	13,861	203,221	188	38	50,230	683	668

Source:
Palestinian Energy and Natural Resources Authority (PENRA). Energy statistics reports 2020.
Palestinian Central Bureau of Statistics, 2020. Database of Foreign Trade Data 2019. Ramallah - Palestine.

2.3. Renewable resources

The Comprehensive National Strategy of the Energy Sector in Palestine (2017-2022) vision includes an energy system that is capable of securing energy from multiple sources to meet the needs of comprehensive sustainable development, at prices that reflect the real cost of supply and consumption. All available sources of energy locally available have to be included, especially clean energy sources, which are essential to achieve the principle of sustainability of the sector. The renewable energy (RE) strategy establishes targets for increasing electricity mix production and increases energy independence, flexibility, and reduces problems caused mainly by the environmental impact of using fossil fuels and the depletion of its reserves (Juaidi et al. 2016). Renewable energy sources that can be used in Gaza Territory include: solar either as photovoltaic cell or thermal solar plates, and biomass (e.g., the project at the waste water plant to utilize energy from the residues). Concentrated solar plates, wind power, and geothermal energy are used in the West Bank territory. Wave energy resources are still under research and were not made in practice (El-Zaza 2009) since the sea is controlled by Israel and there is a need for more research and experiments to be conducted. Each of these resources is discussed in the following sub-chapters:

2.3.1. Solar energy (irradiation and heat)

The Gaza Strip has about 3000 sunshine hours per year and a high annual average of global solar radiation amounting to 6.121 kWh/m^2/day on its south-facing tilted surface. And about 5.543 kWh/m^2/day on the horizontal surface. The solar radiation on a tilted surface varies from 3.72 kWh/m^2/day to 7.54 kWh/m^2/day, based on the global solar atlas website. That encourages us to exploit solar energy for electricity generation. **Figure 2.3** shows the GeoModel long-term averages of solar resources: Global Horizontal Irradiation (GHI) and Global Tilted Irradiation (GTI), Direct Normal Irradiation (DNI), and Specific Photovoltaic Power Output (PVOUT) kWh/kW$_p$. Analysis of (GHI) and (GTI) is required for (PV) technologies in the solar power sector. The coastal side region of the strip has higher solar radiation than the inner region with respect to photovoltaic electricity output. The global solar atlas is adequate for the initial stages of a solar energy project's lifecycle: prospection and preliminary evaluation. While in the next project stages, high-quality solar resource and meteorological data are needed, such data is typically generated from at least 10 years or more of continuous climate records at sub-hourly time resolution (Fathi Nassar and Yassin Alsadi 2019).

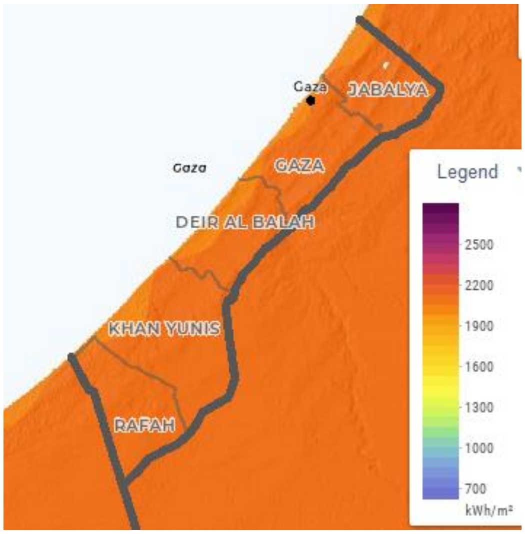

Global Horizontal Irradiation (GHI)

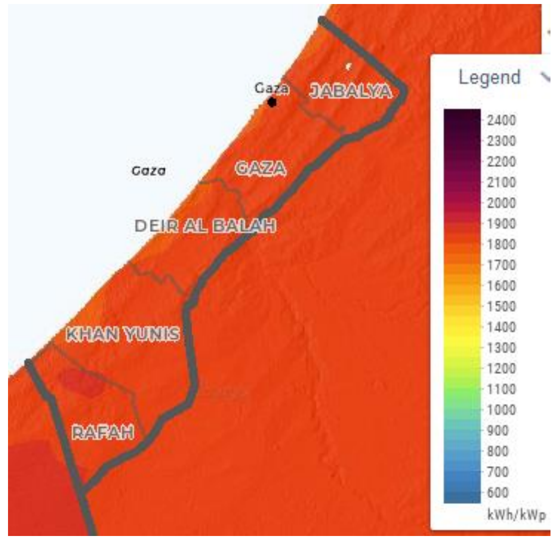

Specific photovoltaic power output (PVOUT)

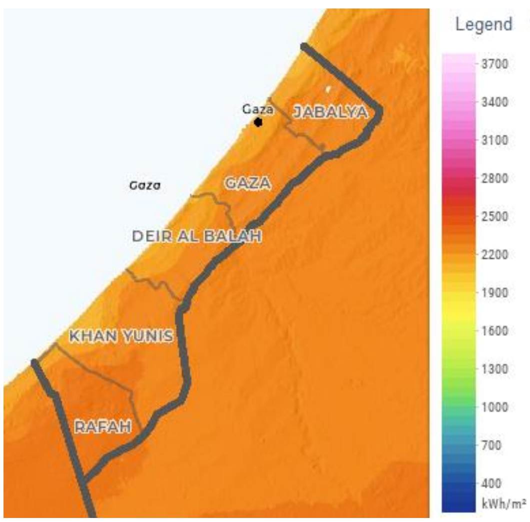

Direct Normal Irradiation (DNI)

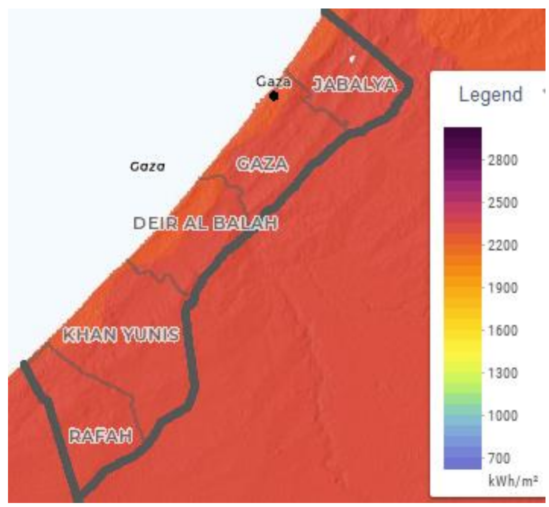

Global Tilted Irradiation (GTI)

Figure 2.3: Long-term averages of solar resource (GHI, DNI, GTI, DIF) and TEMP of Gaza Strip. [Source: http://globalsolaratlas.info/.]

Solar energy is a very popular source of energy since it can be used as a source for heat and electricity. It can be used in different ways and there are different technologies that can be implemented. The most commonly used concepts are solar thermal collectors and photovoltaic modules.

Concentrated solar power

Concentrated solar power (CSP) is a technology that produces electricity by concentrating solar energy into a single focal point or line using mirrors and lenses. As seen in **2.4**, there are three main types of concentrating solar power: system linear concertation (Parabolic trough and Linear Fresnel reflector) (a), power tower systems (b), and dish/engine (c). CSP technology systems use reflective surfaces to gather and concentrate un-scattered ("direct normal") solar radiation to create heat(MÜLLER-STEINHAGEN et al. 2004).

Figure 2.4: Different Concentrated solar power (CSP) technologies (a) linear, (b) tower, (c) Dish/engine [Source: https://en.wikipedia.org/wiki/Concentrated_solar_power.]

In **Figure 2.4-a** and **Figure 2.4-b** systems, reflected sunlight heats a heat-transfer fluid in the receiver. The receiver is a pipe in system a and a tower in system b, which are used to generate steam (Rankine cycle steam) to produce electricity. Some tower systems have the energy storage capability, that is, thermal storage, which allows the system to continue to dispatch electricity during the night. The dish/engine system **Figure 2.4-c)** engine absorbs and collects heat and transfers it to the engine generator (single Brayton cycle). The Stirling engine, the most common type of heat engine, is used in such a system.

Concentrating Solar Technologies can be classified according to operating temperature in medium temperature, line focusing at 400ºC in the linear concentrated system. High temperature (> 400ºC), point focusing in tower and dish system, **Figure 2.4-b** and **Figure 2.4-c**. In the utility / commercial scale, concentrated solar power is used in electricity generation (stand alone, grid project, and hybrid projects), industrial process heat (boiling melting), and cooling systems.

Abundant solar energy radiation in Palestine (5.46 kWh/m^2/day), and the average annual sunshine hours exceeds 3000 hours, making its heat utilization feasible, following some applications that can be used in the Palestinian Territories (Abu-Hafeetha 2009), see **Figure 2.5**.

In low temperature (<100ºC) the technologies applied are: flat plate collectors, solar chimney, and solar pond. Domestic/small scale feasible applications of CSP such as hot water collectors, solar steam cooking, solar Ovens/cookers, solar food dryers.

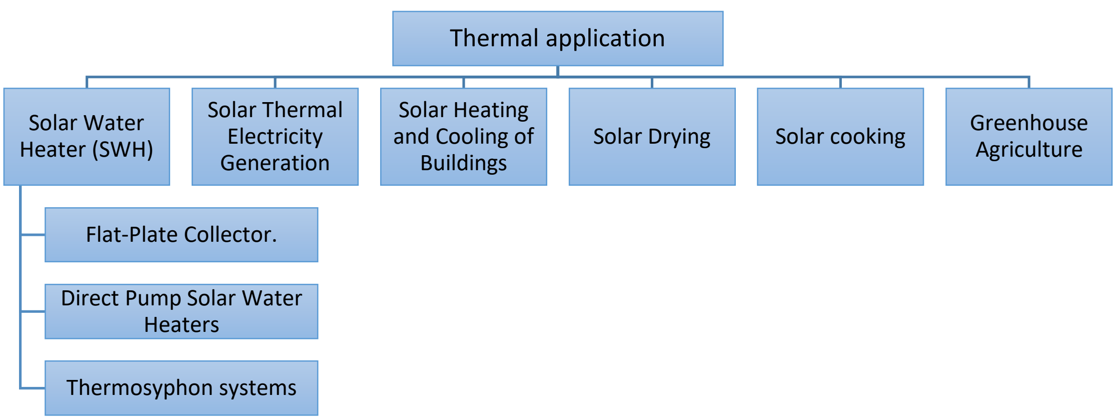

Figure 2.5: Applications that can be utilized heat solar power in the Palestinian Territories

Hot water is used in residential, service, commercial, and industrial sectors. Solar water heaters (SWH) are widely used in the residential sector. Solar water heaters are present for 56.5% of the households., although they are less common in the service and industrial sectors (PCBS, 2015).

The study found that installing SWH systems can effectively contribute to reducing CO_2 emissions. Utilizing SWH technology is considered one of the important measures to save fuel or reduce the amount of imported electricity. Two types of SWHS are commonly used in Palestine. The first and the most widespread type is with flat plate collectors (FPC), which has an accumulated area in operation by the end of 2016 of 1,826,625 m^2. The second type is the evacuated tube collector (ETC). ETC has started to gain market share with a total collector area in operation by the end of 2016 of 8,225 m^2 (Abusafa and Mansour 2019).

In Palestine, the residential sector occupies the largest share of the country's electrical consumption about 31.41% of total consumption as depict in **Figure 2.6**, and of domestic consumption goes to water heating in the first place, almost a third of this percentage (PCBS 2020). Palestine leads the MENA region for total district heating capacity in operation, with more than 1 GW at the end of 2020. Solar thermal energy represents only a small fraction of the Palestinian Energy mix (8%) (Alsadi and Foqha 2021). Power cut hours in Gaza reach 18/24 hours, which prompted people there to rely on solar collectors instead of electrical water heaters. In 2019, the Gaza Strip had 43.8% of households having solar water heater based on the final report of World Bank, 2018(2016).

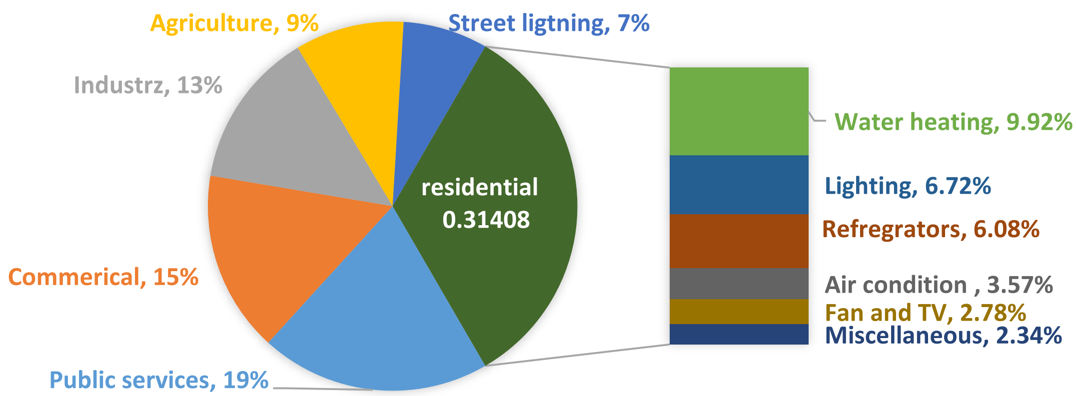

Figure 2.6: Distribution of electricity load in Palestine, residential load, water heating

2.3.2. Biomass

The Gaza Strip is a densely populated coastal region. The economic activities vary between agricultural activities, construction, trade, transportation and storage, services and others. Consequently, biomass could be grown everywhere. The potential of biomass in the Gaza Strip is limited to the following types: agriculture residues, municipal waste, and sludge produced in waste water treatment. Biomass is a strategic sustainable energy resource; it helps with environmental protection (Abu Hamed et al. 2017). According to the (meetMED 2020b) report, the assumed potential for wind and biomass in PT is 72 MW in 2017. Small amounts of biomass energy (olive cake and wood) are utilized for heating applications as shown in **Table 2.1**, where the biomass types are limited in wood, olive oil cake, biogas, and municipal waste. Gaza has huge amounts of biomass from agricultural and livestock breeding, municipal waste, and sludge from waste water treatment plants. Biomass energy is used in PT, but only on an individual basis, and no specialized companies are involved. For the year 2018 agricultural statistics, the Gaza Agriculture Directorate (GAD) of tree horticulture areas and the estimated productivity in Gaza governorate is 27,689.1 tons distributed over horticulture, olives, citrus fruits, grapes, and fruit. And the annual vegetable crops are 15,387 tons, while the area used in cereal production for field crops is 355 ha. **Figure 2.7** shows the percent distribution of agriculture (MOA 2018).

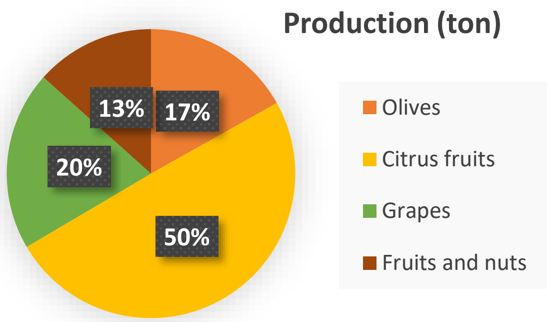

Figure 2.7: Horticulture tree production in Gaza city

Basic changes are observed in livestock in Palestine during the time interval 2006–2019. The number of cows, sheep, and goats slaughtered in Palestine is shown in **Figure 2.8**, as well as the number of broiler and laying chicks produced (per thousand). It is noticed that the consumption of poultry is increasing due to the local market's dependence on it, as well as the increase in the number of consumers. Poultry is raised locally on farms in rural areas. The same applies to Gaza city, which constitutes a tenth of the Palestinian population on a much smaller area, obviously.

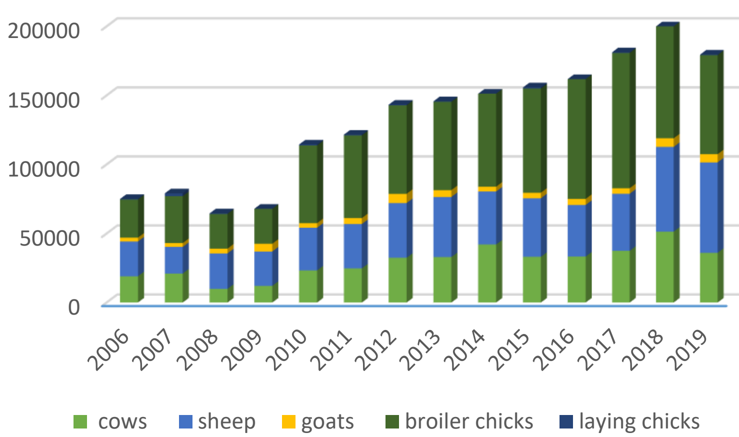

Figure 2.8: Changes in livestock in Palestine, 2006-2019

According to the Ministry of Agriculture (MoA) annual report 2016, the quantity of agricultural waste production in the Strip is approximately 436,618 tons per year (1,197 tons per day). Practically no agricultural waste is collected and used as fuel. A maximum utilization of 10% of the overall quantity is reported. Just a few amounts are used to prepare compost, which is about 4000 tons of the total agricultural waste per year.

Municipal solid waste (MSW) in the Gaza Strip is normally composed of paper, plastic, organic waste, and metals, among others. Results obtained by comparison between different studies conducted by the governorate and international organizations such as Gaza municipality, MoA, and the last by the United Nations Development Program UNDP/DHV 2012 in the Gaza Strip show a high organic content of around 65% for the solid waste. This percentage is an indication of how to calculate the density of the waste and the amount of gas that would be obtained from aerobic and anaerobic chemical decomposition.

Based on the UNDP/DHV 2012 study, the forecasts of total generated municipal waste streams are classified as household waste and street littering, commercial waste (offices and shops), and market waste without agricultural waste. For the North Gaza and Gaza Municipality, the forecasted generated waste quantities are presented in **Figure 2.9**. The study is assumed that the per capita waste will gradually raise to a maximum of 1.05 kg/(person*day) for all governorates, including Gaza city, assuming that the economic situation of Gaza people will improve staring from now to 2040 (MDLF 2017).

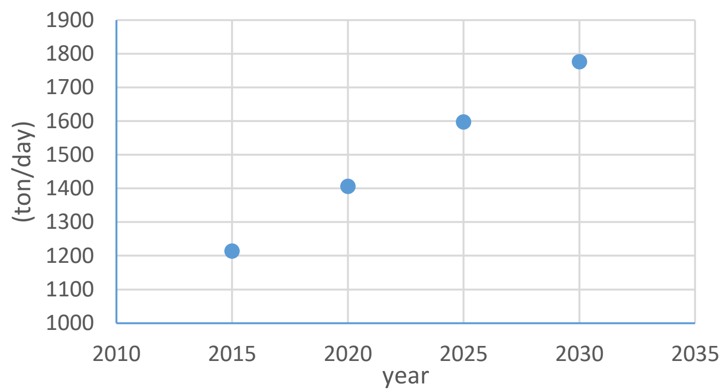

Figure 2.9: Forecasts of Generated Waste Quantities for North Gaza and Gaza Municipality (ton/day)

There are three main waste water treatment plants (WWTP) located in the Beit Lahia, Gaza and Rafah areas, as well as two treatment plants in Khan Younis (Mawasi area) and Wadi Gaza WWTP. The current and projected WWTP all over the Gaza Strip produce over 240,000 m^3/day, and the average daily flow m^3/day Gaza Waste Water Treatment Plant (GWWTP) is 54,000. In Buriej WWTP, followed by GWWTP biogas production capacity is 12,000 m^3/day of 60–65vol% methane.

2.3.3. Wave energy

The western coast of GS territory overlooks the Mediterranean basin, with an extension of 41 km from the south to the north. Wave energy is a promising, underutilized source of energy that could help to expand the energy mix and reduce reliance on fossil fuels. It is an endless and sustainable source that can make coastal countries less energy-dependent and provide essential benefit.

For the Mediterranean region, a detailed study of wave energy resource assessment and wave energy converters (WECs) in real-world settings has been evaluated. The installed power of the Mediterranean Sea's various deployed WECs ranges from 3–2500 kW. The point absorber is the most typical form of WEC fitted. The Mediterranean, in comparison to the Atlantic coasts, is a semi-enclosed sea with medium wave energy power. The eastern Mediterranean Sea includes the Levantine Sea. The numerical wave model and in situ observations were used to analyze the Levantine Sea's wave energy resources (Liberti et al. 2013) (Dialyna and Tsoutsos 2021).

In (Besio et al. 2016) analysed 35-year data and detected the powerful regions, and found that the wave energy power is intermediate in the eastern and central Mediterranean, about 6–7 kW/m, and that the wave energy potential varies significantly during the seasons in the whole basin (Zodiatis et al. 2014b) identified the locations with the highest wave energy potential in the Levantine Basin: the western coastline of Cyprus and the coasts of Alexandria, Lebanon, and Israel.

The most wave-energetic offshore areas of the Levantine Basin are discussed in (Zodiatis et al. 2014b). They are characterized by a relatively low 10-year mean wave energy potential of about 2.5 kW/m. **Figure 2.10** shows that the available power along the coasts of Cyprus, Lebanon, and Egypt is five times more than the average potential, reaching 10 kW/m during the winter months.

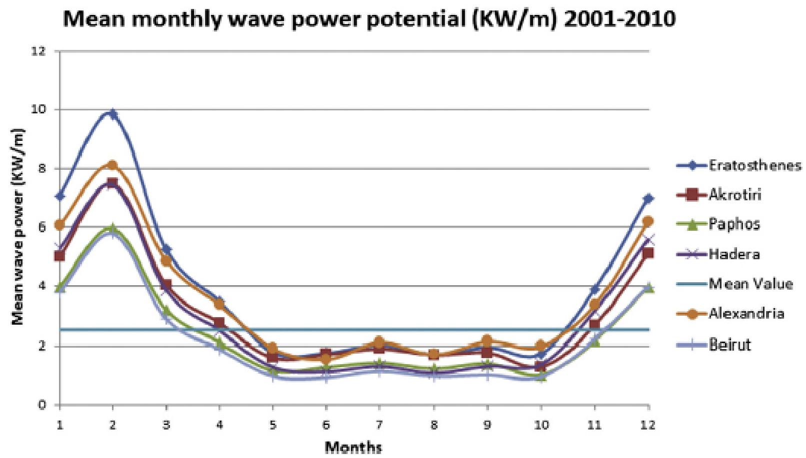

Figure 2.10: Mean monthly wave power potential (kW/m) for the period 2001e2010 over different areas of the Levantine.

2.3.4. Wind energy

The Gaza Strip has a pleasantly mild Mediterranean climate with separate seasons: warm and dry summers and mild winters. During the autumn, most of the rain can be expected. When spring starts, temperatures rapidly rise. The absolute maximum temperature recorded in May was 43.5°C and the absolute minimum temperature in January was 2.0°C (Abu-Zarifa 2014) .

The average wind speed throughout the months of the `typical meteorological year` for the period from 1991 to 2010 of Gaza is shown in the **Figure 2.11**. The average monthly speed, as seen in the figure, is usually greater than 4 m/s, with the exception of October and November. The highest average wind speeds are recorded in February and September. The wind data rely on Ashdod climate data, since there is no typical meteorological year data for Gaza and similarity between two these cities. (Elnaggar et al. 2017) Fed these wind into a small wind turbine of 5kW power rating installable on the roof of residential buildings. One wind turbine and one PV system together could provide enough energy for 3.7 households. The expected annual energy output at a height of 10 m amounts to 2695 kWh, but it can be increased by 35-125% at higher altitude between 20 and 70 m

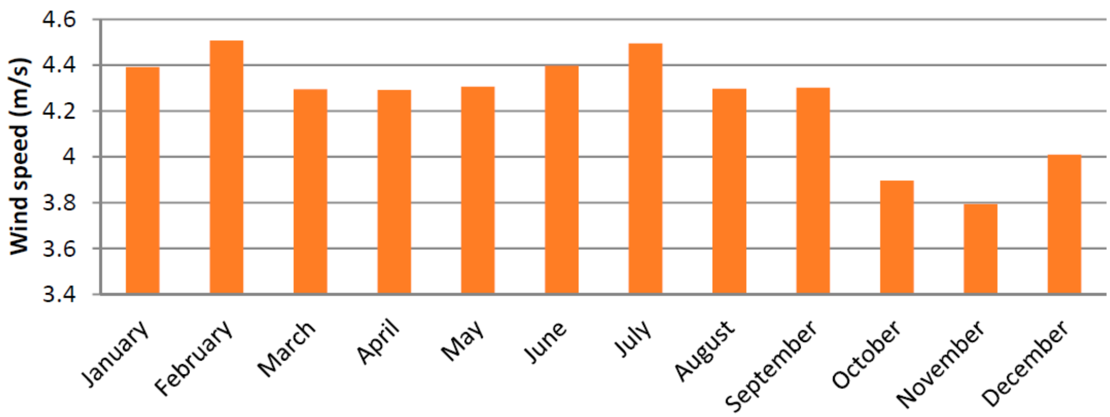

Figure 2.11: Monthly average wind speed in a typical meteorological year.

The study conducted by (Nassar et al. 2018) estimate the annual energy production for three sites in the Gaza Strip, using Gamesa G128-4.5 MW turbines. The results showed that Rafah City has the highest wind energy potential, with an annual average wind speed of 6.38 m/s and a speed higher than 7 m/s for 3118 hours per year (36%) and about 200 hours of rated wind speed. In order to determine the best location to build the first wind power farm in the Palestinian territory, they deal with 16 years of hourly climatic data provided by Meteoblue (www.meteoblue.com). With an estimated annual energy production of 15,962 MWh/turbine, with an average utility factor of 40.4% and at 80 m altitude, to cover the shortage of 200 MW, they need 110 wind turbines (WTs). The required area for the wind farm is estimated to be 43 km^2.

The researchers in (Salem 2019) investigated the wind energy potential in GS at the present time are infeasible economically, average speed of wind, for the year 2005, was recorded in the city of Gaza and is equivalent to approximately 3.53m/s. Wind energy utilization in particular is severely limited in GS for a variety of reasons, including a lack of suitable land, funding, qualified professional ability. and others.

2.3.5. Geothermal energy

Geothermal energy is considered a clean source of energy. A geothermal system essentially uses a stable temperature, hence offering energy that is constant, and available on demand. It provides an important alternative to fossil fuels as clean energy and could allow a reduction in energy costs, for heating in winter and cooling in summer. The Palestinian land has been discovered to be ideal for geothermal energy utilization, with two particularly high sources being the Gaza Strip and the north of Palestine. The only known project in Palestine is a residential building in Ramallah, West Bank, that demonstrated a significant reduction in energy expenses, paying for heating and cooling by more than 70% with a 4.5-year payback period (Juaidi et al. 2016).

2.4. Institutional framework of the energy sector

Electrical energy in Gaza Strip comes from Israel 161 kV, 260 kV connection with Egypt, and Gaza power plant. Power is generated on the Israeli side and is transmitted via 161 kV main transmission lines, then transformed to 33 kV transmission lines or 22 kV transmission lines. Then, in the middle of these transmission lines, a coupling point that controls the amount of electricity that flows toward the Palestinian side is placed. The Israeli Electricity Company (IEC) owns transmission lines up to the coupling point, while the Palestinian Electricity Transmission Line (PETL) Company possesses the remaining part until the low voltage power substation, which can be 33 kV/0.4 kV, 22 kV/0.4 kV or 33 kV/6.6 kV. After the low voltage substation, the electricity networks are possessed by Gaza electricity distribution company (GEDCo), which is responsible for supplying electricity to the end users in Gaza. They have close links to the Israeli civil administration, the DCO, the Energy and Natural Resources Authority, PENRA, Egypt, Qatar, and PETL.

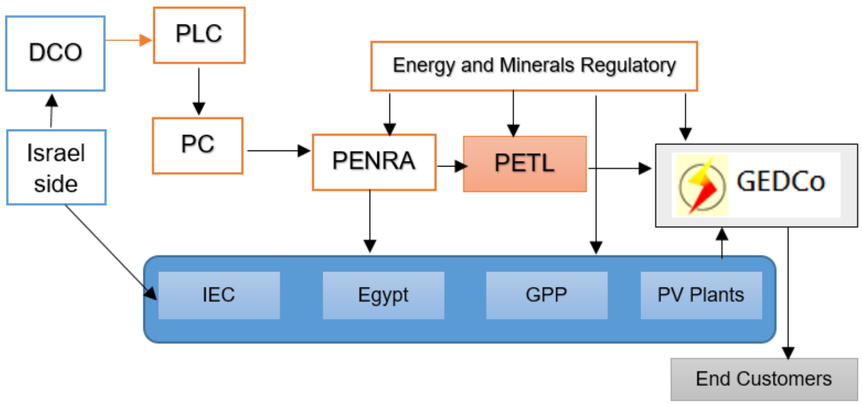

Figure 2.12: Gaza Strip institutional energy framework

Figure 2.12 shows the desired Palestinian institutional energy framework. Based on this model, DOC is a coordination office to manage issues including electricity between the PA and Israel. The Palestinian Legislative Council (PLC) represents the people of Palestine and it is in charge of approving any act regarding electricity. The Palestinian Cabinet (PC) is the head of PENRA, and it has two rules: first, it proposes act drafts to the PLC; and second, it directs PERNA to carry out the authorized acts through agreed-upon regulations and laws. PENRA acts as a ministry of energy. he Energy and Minerals Regulatory Commission should keep an eye on the rules and regulations and assist in their development, including shares, rules, markets, concession areas, and prices. Generally, the energy sector includes three main sectors: the electricity sector, renewable energy and energy efficiency sector, and hydrocarbons sector. Where these sectors include many institutions as shown in brief:

2.4.1. Electricity sector

Energy and Natural Resources Authority: It undertakes the task of developing the general policies and rules related to the development of the electricity sector. It oversees all activities related to the management and development of the renewable energy and energy efficiency sectors through its Energy Research Center.

The National Transport Company for Electricity: It is entrusted with the tasks of building, developing, managing and owning the electrical transmission system, and purchasing the energy either from the local supply sources, or by importing from the neighboring countries and selling them to the electricity distribution companies on the basis of the sole buyer model.

The Electricity Distribution Companies: Electricity distribution companies have been established to carry out the tasks of managing, building and developing medium and low voltage distribution networks, purchasing energy from the National Transport Company and selling it to the consumer. The Gaza Electricity Company manages the electricity distribution sector in Gaza Strip. Work is continuing on the transfer of electricity service from the municipalities to these companies to reach an electricity distribution sector that is managed only by the distribution companies.

The Electricity Sector Regulatory Council: It is entrusted with the tasks of monitoring and regulating the generation, transmission, and distribution sectors and recommending to the Energy Authority to identify the electrical tariff, accept, reject, renew, withdrew or waiver of generation, transmission, and distribution licenses; and ensure the quality of the technical and administrative services provided by the distribution companies to consumers.

2.4.2. The Renewable Energy and Energy Efficiency sector

The Palestinian Center for Energy and Environmental Research: It works under the umbrella of the Energy and Natural Resources Authority, and it is concerned with all matters related to the development and exploitation of alternative energy sources. One of its main functions is to encourage the use of alternative energy, which increases awareness of the local consumer in terms of rationalization of energy consumption and raises the efficiency of its use to ensure the reduction of energy losses. It also contributes to the preservation of the environment and reduces the emission of toxic gases.

Energy research centers in public and private universities that prepare studies and research on alternative sources of energy. In spite of the efforts by the Energy and Natural Resources Authority to establish the necessary institutional frameworks to manage and develop the electricity sector, renewable energy, and energy efficiency, there are still many political and economic conditions that prevent the complete activation of these frameworks.

2.4.3. Hydrocarbon sector

The hydrocarbon sector is currently directed by the Ministry of Finance and has a supervisory role in the financial and administrative supervision of the sector. And the General Petroleum Authority's role, which is summarized as follows: concluding the agreements necessary to purchase and supply the needs of oil and gas derivatives from all sources. supervise the establishment of strategic storage reservoirs for oil and gas. setting the monthly prices of fuel and gas. Grant the necessary licenses for the construction of fuel and gas stations and obligate them to abide by the technical specifications and public safety. Grant the necessary licenses. Fuel stations are privately owned by the private sector and deliver these products to the consumer.

2.5. Gaza Power Plant

The only Palestinian electricity production is from the Gaza power plant **Figure 2.13**; with 140 MW of production total capacity installed, which covers a part of Gaza city and other surrounding areas. It currently generates a little more than 80 MW, with a daily fuel consumption of 420,000L. The dieselfired power plant is located in the middle of the strip. It was crippled in a July 2006 bombing. Electricity production is based on four gas turbines of type "ABB GT10B2" which operate as a combined cycle with two steam turbines. Hence, the station consists of two generation units. Each unit contains two gas turbines and one steam turbine. Currently, the gas turbines fire liquid fuel (diesel oil distillate No. 2). According to reported energy infrastructure in the Gaza Strip in the annual bulletin (June 2017) of the World Bank planning plant, the plant is so expensive to operate due to the high cost of diesel – costing NIS 1.05-1.65 (US$ 0.29-0.46) per kilowatt-hour – that it can typically be run only at half capacity. It has also suffered repeated damage during armed conflict, affecting its fuel storage capacity. The diesel fuel price maximizes 1.4 (US$/L) in 2021 with the same operating capacity of the power plant (2017) (Fathi Nassar and Yassin Alsadi 2019) (Juaidi et al. 2016).

The plant's operating costs would be reduced by at least a third if it were converted to run on natural gas. Natural gas, rather than diesel oil, could be used to power the station. The cost of constructing a gas line from Israel to supply the gas station and replacing torches in the combustion chamber to make the station fit to work with gas is estimated to be around million US$25.

Figure 2.13: The Gaza Power Plant, Gaza, August 2020. ©(EDITION 2020).

3. Energy technologies and applications

3.1. Overview

Energy is used effectively in different aspects of life: in industry, transportation, domestic, agriculture, commerce, and public service. In Palestine, the energy reliability rate reached 86.4 percent in 2019, representing a 6% increase over 2014. The transportation sector is one of the most energy-consuming sectors, followed by residential, while the industrial sector recorded the lowest rate according to the Palestinian energy sector indicators during (2014–2019) as depicted in **Figure 3.1**. Also, the monthly per capita share of consumed electric energy is 106,6 (kWh/capita). As for renewable energy, it contributes 11.7% of the total final energy consumption.

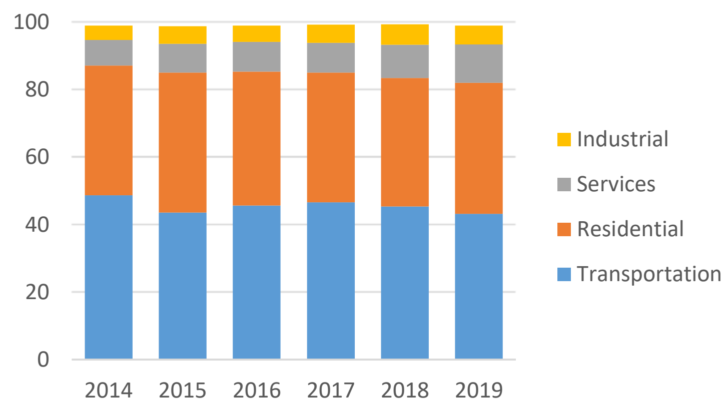

Figure 3.1: Indicators of energy consumption for different sectors in Palestine.

The form of energy flowing to the domestic sector varies between electricity, diesel, kerosene, liquefied petroleum gas (LPG), peat, wood and coal, and solar energy. The total domestic consumption in the Palestinian territories is 27384.4 TJ, with renewable energy accounting for 27% of it.

Energy supplied to the domestic sector in the Gaza Strip is generated from temporary and renewable energy sources through machines and different techniques associated with them. The Gaza Power Plant (GPP) is one of the important sources of electricity generated from traditional sources, as it relies on two types of turbines (gas and steam) connected to generators. Solar energy is increasingly being used in traditional and modern ways. With the first step of manufacturing biogas from a waste water plant in northern Gaza, bioenergy is finding its way to energy and environmental benefits.

The production of electricity from PV panels is one of the rapidly spreading technologies that leads to the purpose. In the event of power outages of 18/24 per day, the total installed capacity amounted to about 22,380 kWp in the year 2020, to involve residential, service, agriculture, public, and industrial sectors. In a separate study (paper 1) estimated study, evaluates the potential of PV solar energy and biomass, it is found that both renewable resources as a hybrid system could cover electrification of the residential sector. Therefore, in this chapter, some of the technologies and many basic concepts in the field of energy, specifically solar and biomass, are explained and discussed.

3.2. Steam Turbine and Gas Turbine:

Generally, a turbine is a device or machine that converts the kinetic energy of a fluid (air, water, steam, or other gases) to mechanical energy. Basically, turbines are classified by the type of fluid inlet used. There are four types of turbines: water turbines, steam turbines, gas turbines, and wind turbines. Two kinds of turbines are used in GPP: steam turbine and gas turbines.

Steam turbine extracts energy from the high-pressure steam and converts it into electrical energy through coupling with a generator. It can be classified into five types according to: mode of steam action; direction of steam flow; exhaust condition of steam; pressure of steam; and number of stages. The basic classification is according to the mode of steam action, which involves impulse turbines and reaction turbines; in an impulse turbine, the steam available at the inlet has only kinetic energy, while in a reaction turbine, the steam available at the inlet has kinetic energy as well as pressure energy, hence the name reaction turbine. The major components of such a turbine are: casing, rotor, and blades. The casing should withstand all conditions due to temperature and pressure. The rotor is the main component in a steam turbine and is fitted inside the casing that converts thermal energy by rows of moving blades penetrating between the rows of fixed blades (nozzles). The thermal efficiency of practical steam turbines can reach values of up to about 50% in a 1200 MW turbine; as the turbine gets smaller in size, they have lower efficiencies. The working of a steam turbine is based on the thermodynamic cycle called the "Rankine Vapor Cycle" (Vasserman and Shutenko 2017).

Gas turbine extracts energy from the hot moving gas and converts it into electricity. It divided into two types: working substance path (closed cycle, open cycle, semi-closed) and heat absorption process (constant pressure, constant volume). A simple gas turbine is composed of a compressor, a combustor, and an exhaust turbine. During operation, air enters the compressor at the ambient temperature and is compressed to a higher pressure and temperature. Upon leaving the compressor, the air enters the combustor, where fuel is injected and combustion occurs. The gases in the chamber rapidly expand during combustion, gaining kinetic energy; and because of this kinetic energy, the air can do mechanical work to rotate the turbine. Currently, gas turbines are achieving plant efficiencies of as high as 64%, with outputs in the 900 MW range (Langston 2020). The thermodynamic process used in gas turbines is the Brayton cycle.

Combined cycle power plant

A combined cycle power plant (CCPP), also known as a combined cycle gas turbine (CCGT), consists of a gas turbine generator generating electricity while waste heat is used to make steam to generate additional electricity via a steam turbine. A combined cycle power plant produces high power outputs at high efficiency (up to 55%) and with low emissions. Compared to a conventional power plant that produces 33% of electricity and the remaining 67% as waste, we are getting 68% of electricity by using a combined cycle power plant. A combined-cycle power plant uses both a gas and a steam turbine together to produce electricity. The waste heat from the gas turbine is routed to the nearby steam turbine, which generates extra power (Breeze 2016) (Dev et al. 2012).

The combine cycle employs two thermodynamic cycles, Brayton and Rankine cycles. It improves the simple Brayton cycle efficiency by capturing wasted energy in the Brayton cycle and using it in the Rankine cycle. The gas turbine is a fast-spinning turbine that drives a generator that converts a portion of the spinning energy into electricity, then the heat recovery system captures exhaust heat and creates steam to deliver it to the steam turbine. Therefore, the steam turbine sends its energy to the generator drive shaft, where it is converted into additional electricity. In addition to its high efficiency, the combine cycle (CC) has fewer moving parts, a higher operating speed, and less vibration than a reciprocating engine, and it can run on a variety of fuels. However, there is a high cost, a lack of responsiveness to power demand, and shrill whining noise on the other side.

3.3. Biomass conversion routes

Biomass in this study was classified as agricultural residues and waste (MSW, industrial waste, manure, and sewage sludge). Organic elements (C, H, O, N) and (S, Cl) are hopefully the only side elements that make up the bulk of biomass. These elements are found in agricultural residues, which are composed of the following substance groups: cellulose, hemicellulose, lignin, lipids, and proteins. For example, cellulose makes up around 40% of wood and 25% of grass. Biomass content causes a challenge in terms of energy utilization.

Plant biomass also contains macronutrients such as (N, P, K, Mg, S, Ca), that are required as inorganic and essential for plant production and life cycle. Plants also require trace amounts of micronutrients like (Cl, Fe, B, Mn, Zn, Cu. Mo, Ni). Trace elements like Si, Se, Ti, V, Co, Al and other heavy metals may also be present in plant biomass at different levels depending upon the plant species and the environment. inorganic materials such as Na in lignocellulose biomass (LCB) called ash. The ash content in LCB depends on feedstock type, the environment in which it was grown, fertilizer use, and contamination with soil particles. For wood typically ash contents below 1wt% can be found whereas for straw and similar materials it can be up to 10wt% and even higher. Various biomass components can be used to produce bio-fuels and potentially limit the use of fossil fuels. Biomass residues and wastes (such as agricultural residue, food waste, animal manure, and municipal solid waste) as resources for bioenergy production are promising alternatives to reduce environmental issues concerning waste management and disposal, greenhouse gas emissions, pest breeding, insects, and foul odor.

Straw and other agricultural residues usually have a high ash content and contain chlorides and potassium compounds, which can cause high levels of corrosion in boilers. The problems of corrosion and slagging can be mitigated by burning biomass at lower temperatures. The drawback with most non-woody energy crops is that their chemical properties generally make them less suitable for combustion due to their high ash and salt content.

Biomass is analyzed in terms of volatile matter (VM), ash content, fixed carbon (FC), and moisture (M). The VM of biomass are the condensable and non-condensable gases released from the biomass during heating. That depends on the heating rate and the final temperature to which biomass is heated. Ash is the solid residue left after the biomass is completely burned. FC shows the percentage of biomass burned in the solid states.

The composition of ash depends on the type of biomass, which includes mostly inorganic residues. The ash content plays a significant role in biomass combustion or gasification. If biomass contains alkali metals, it can cause severe agglomeration, fouling, and corrosion in boilers or gasifiers, even though it is very small.

FC is the solid carbon (non-volatile) in the biomass that remains in the char following devolatilization in the pyrolysis process. The following equation relates the amount of FC to VM, moisture (M), and ash:

$$FC = 1 - M - VM - ASH$$

Moisture content will have a significant impact on the biomass conversion process. Biochemical conversion processes can use biomass with high moisture content, while thermochemical conversion processes generally require biomass with low moisture content. However, gasification processes require some moisture to produce hydrogen, and the amount of hydrogen produced will increase with moisture content. The moisture content used in evaporation is typically not recovered.

The biomass to energy conversion process depends on a number of factors. Two main factors are the desired form of end products and the available feedstock materials.

Biochemical conversion, thermochemical conversion, and physicochemical conversion are the three basic routes for converting biomass to energy. As indicated in, the most fundamental thermochemical conversion processes include combustion, pyrolysis, gasification, and hydrothermal liquefaction (HTL) (Alafif et al. 2019).

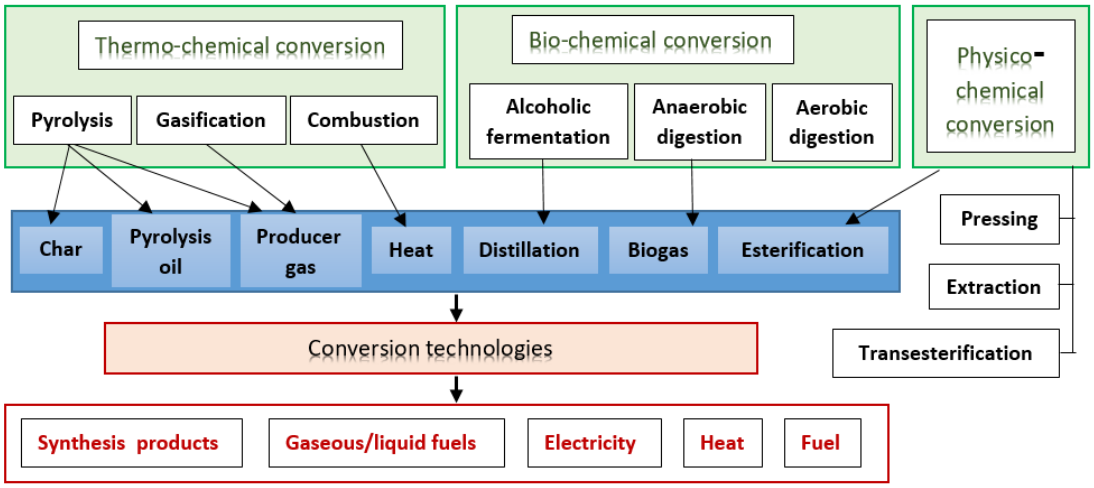

Figure 3.2: Biomass conversion technologies

Two heating values, higher heating value (HHV) and lower heating value (LHV), characterize the energy content of such technology. If water vapor in exhaust gas is excluded, LHV is the energy released from full oxidation. If water vapor in exhaust gas is taken into account, the energy released from full oxidation is (HHV).

3.3.1. Thermochemical conversion

Thermochemical conversion routes can be classified according to the oxygen content used in the process, as seen in

Figure 3.3, including combustion (complete oxidation), gasification (partial oxidation) and pyrolysis (thermal degradation in the absence of oxygen). Hydrothermal processing is an alternative route to processing wet biomass using heat and pressure in the presence of water, which can also be considered a thermal degradation in the absence of oxygen.

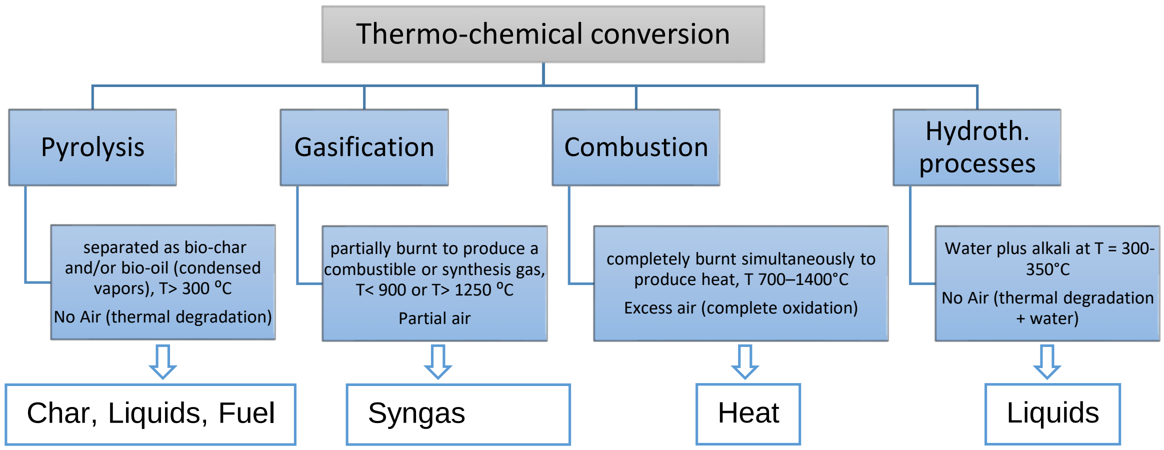

Figure 3.3: Thermochemical conversion

Combustion: thermal conversion of organic matter with an oxidant (normally oxygen) to produce primarily carbon dioxide and water. Depending on the type of biomass, the heat of combustion varies from 17 to 19MJ/kg on an ash-free dry basis. The combustion reaction for the main elements is represented by (Demirbas and science 2004, 2015):

$C_xH_yO_z + nO_2 \rightarrow xCO_2 + (^y/_2)H_2O$, with $\quad n = x + (^y/_4) - (^z/_2)$

Stages of combustion of solids:

Drying → Devolatilization (Pyrolysis, gasification) → Flaming combustion → Residual char combustion

A wide range of biomass sources can be considered for combustion. The best quality fuels contain high amounts of carbon and hydrogen and low amounts of other elements (oxygen, nitrogen, sulfur and trace elements).

Fresh woodchips can contain 50% moisture, and leaves can have over 90% moisture. Most furnaces and boilers are designed for biomass with less than 20% moisture. It is extremely difficult to maintain combustion with a moisture content of more than 55%. Low values of the FC/VM ratio lead to high ignition behavior. Combustion of VM is fast compared to combustion of solid charcoal, and a low ratio of FC/VM decreases the residence time in the boiler/furnace.

Direct combustion is currently the principal method of generating electricity around the world via steam turbines. Many combustor types for this purpose are used, such as stoker grate or moving grate, fluidized bed, circulating fluidized bed, entrained flow.

Gasification is a thermochemical process of converting solid biomass into a gaseous fuel known as synthesis gas, or shortly syngas or producer gas, under a reduced oxygen atmosphere to avoid complete combustion. The overall gasification process is endothermic, and runs at temperatures ranging from 600°C to 1500°C. Biomass is fed into contact with a gasification agent. Reactions between oxygen and carbon take place at gasifier temperature through a direct heating (autothermal) or an indirect heating (allothermal) phase. Produced gas mixtures consist of H_2, CO, CO_2, CH_4 and N_2 are known as synthesis gases. The most common gasification agents are steam, air, oxygen, and carbon dioxide. Gasification offers large feedstock flexibility (e.g. woody biomass, agricultural residues, but also wastes and waste-derived fuel). Characteristics of biomass such as moisture content, ash content, volatile compounds, and particle size have an effect on gasification performance.

A simple way of representing the gasification reaction is shown below.

$$Biomass + O_2(g) \rightarrow CO(g) + H_2(g) + CO_2(g) + CH_4(g) + Tar(l) + H_2O(l) + Char(s) + TraceSpecies$$

Fuel or synthesis gases are the primary products of gasification that can be used in internal and external combustion engines, turbines, and with limitations in fuel cells. Gasification processes depend on many parameters such as gasifier type, which includes small-scale applications (updraft, downdraft), large scale applications (fluidised bed, circulating fluidised bed), and entrained flow. Additionally, temperature, gasification agents, catalysts, moisture, as well as other biomass parameters (e.g., the energy content) influence the product quality as well as the heating value.

Pyrolysis is a thermochemical technology in which organic substances are decomposed at high temperatures under an inert atmosphere. It is the first step after drying in combustion and gasification processes. The pyrolysis mechanism can be divided into three phases: dehydration, fragmentation, and product formation (Chan et al. 2019). Liquid bio-oil (also known as pyrolysis oil, pyrolysis tar, bio-crude, wood liquid, wood oil, or wood distillate), solid bio-char (also known as charcoal), and pyrolytic gas are pyrolysis chemical products.

$$Dry\ Biomass \rightarrow char + (CO, CO_2, H_2, H_2O(g), CH_4) + tars + ash$$

Depending on the operating conditions (heating rate, solid residence time and temperature), pyrolysis processes are classified as torrefaction, slow (conventional) pyrolysis, intermediate pyrolysis, and fast pyrolysis as shown in **Table 3.1**. Each type of pyrolysis produces different proportions of the three types of products (biochar, bio-oil, and gas).

Biomass pyrolysis consists of three main stages: (a) initial evaporation of moisture, (b) primary decomposition, and (c) secondary reactions (oil cracking and repolymerization). At 100°C, the mass of biomass decreases due to the evaporation of free water. Thermal decomposition of biomass begins with extractive devolatilization/decomposition at 220 °C. Hemicellulose is the least stable polymer and breaks down first at temperatures of 220 to 315°C with maximum mass loss at 268°C. The pyrolysis reactions are endothermic between 180 and 270°C. Devolatilization and decomposition in pyrolysis is not a single step reaction and a difference can be made between primary and secondary reactions. The gas and vapor products of primary conversion are unstable under pyrolysis temperatures and, with sufficient residence time, can undergo secondary reactions such as cracking and/or repolymerization of primary volatile compounds. Cellulose has a high degree of polymerization and exhibits higher thermal stability. It decomposes in the temperature range of 315 to 400°C. Lignin is the most difficult component to pyrolyse, which results in a wide temperature range from 160 to 900 °C. The rate of lignin degradation reactions is slower than cellulose and hemicellulose (Nachenius et al. 2013) (Wijekoon et al. 2020) (Kan et al. 2016) (Yang et al. 2007).

Table 3.1: Classification of Pyrolysis methods

Mode	Condition	Liquid	Solid	Gas
Fast	Reactor temperature 500ºC, Very high heating rates >1000ºC/sec, Short hot vapour residence ~1 sec	75%	12% Char	13%
Intermediate	Reactor temperature 400-500ºC, Heating rate range 1-1000ºC/sec,	50%	25% Char	25%

	hot vapour residence time ~ 10-30 sec			
Slow-Carbonization	Reactor temperature 400-500ºC Heating rate up to 1 ºC/sec Long solid residence hrs-days	30%	33% Char	35%
Slow-Torrefaction	Reactor temperature ~ 290ºC, Heating rate up to 1 ºC/sec, Solid residence time ~ 30 min	0-5%	77% Solid	23%

Hydrothermal carbonization is a promising technique to convert wet biomass into carbonaceous solids at relatively high yields by omitting the energy-intensive drying before or during the process. It is an exothermal process, suitable for variety of problematic wastes and contineouty generated biomass streams are used such as, human waste (e.g. excrement's and faecal sludge's), municipal solid wastes as well as agricultural residues and algae, that have high moisture content biomass. Wet biomass, typically with 70 wt% or more water, can be converted using hydrothermal processing, which involves applying heat and pressure to convert biomass in the presence of water into carbonaceous biofuel. Compared to other conversion methods, a low operational temperature is necessary. Water plays an active role as a solvent and reactant. It uses subcritical or supercritical water to convert biomass into end products in the absence of atmospheric oxygen.

Hydrothermal processing can be classified into three processes: hydrothermal carbonization (HTC), hydrothermal liquefaction (HTL) and hydrothermal gasification (HTG) based on reaction parameters such as temperature, pressure, and residence time, as shown in **Table 3.2** (Daful and Chandraratne 2020).

HTC could be used as a fuel, a reducing agent, activated charcoal, or biochar. One of the benefits of this procedure is that the hydrochar can be mechanically drained. It is possible to obtain high conversion efficiency, a low amount of tar, a large amount of H_2, and a low CO content in the product. Until now, the main stumbling block has been scaling up the process to an industrial scale.

Table 3.2: Classification of Hydrothermal processing

	Hydrothermal Carbonization	**Hydrothermal Liquefaction**	**Hydrothermal Gasification**
Reaction medium	Water (liquid)	Water (liquid)	Water (near/above supercritical)
Typical tempreture range	170 – 250 ºC	250 – 350 ºC	350 – 380 ºC / 600 – 700 ºC
Typical presure range	10 – 20 bar(g)	50 – 200 bar(g)	180 – 300 bar(g) / 250 – 300 bar(g)
Typical catalyst	Citric acid or FeSO4	Alkalicarbonates, alkalinehydroxides	Ru, Ni/ none
Typical reaction time	4 – 16 h	10 – 15 min	<1h/1 - 5 min

Main products	Coal-suspension, coal-granulate	Phenol rich, Oily liquid	Hydrogen, carbon dioxide, methane
Product separation	Filtration and drying	Phase separation hydrophobic/hydrophilic	Phase seperation gaseous/liquid

Fuels with 30 % moisture or more reduce the calorific produced gas value. Feedstocks with high moisture content are mostly suitable for bio-thermal conversion technologies such as fermentation, anaerobic digestion, and hydrothermal carbonization (HTC).

Influence of moisture on thermo-chemical conversion. The moisture content of biomass primarily determines the conversion process for the selected biomass. Thermochemical conversions like pyrolysis, gasification, or combustion are ideal for dry biomasses such as wood or straw. Wet conversion processes such as hydrothermal processing and biochemical processing (fermentation and anaerobic digestion) are more suitable to process high moisture content biomass like aquatic biomasses, sewage sludge, food waste, and manures.

Thermochemical conversions generally offer many advantages over biochemical conversions, such as handling a wide variety of feedstocks, better conversion efficiency, high energy efficiency, and shorter reaction times. As a result, in recent years, thermochemical conversions have received greater attention for biofuel production.

3.3.2. Bio-chemical conversion

Bio-chemical conversion can turn biomass into a number of products and intermediates through the selection of different microorganisms or enzymes. The process provides a platform to obtain fuels and chemicals such as biogas, hydrogen, ethanol, butanol, acetone and a wide range of organic acids (Chen and Qiu 2010). **Figure 3.4** depicts these processes.

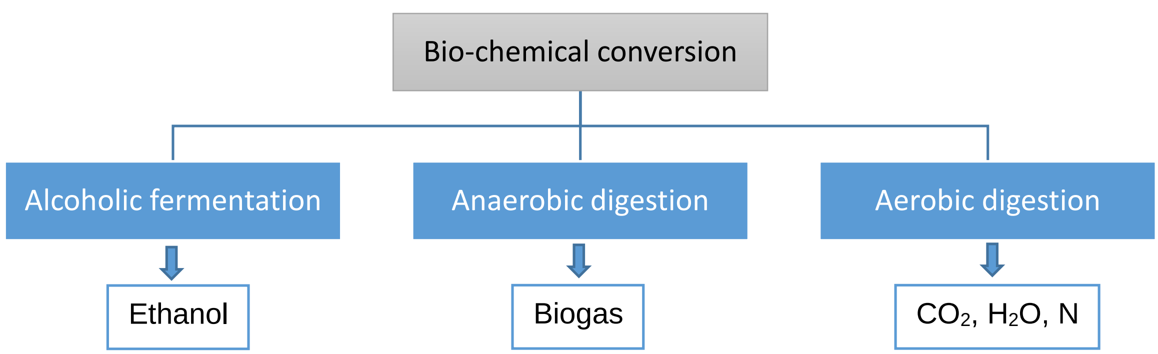

Figure 3.4: Bio-chemical of biomass conversion

Anaerobic digestion is a series of biological processes in which microorganisms break down biodegradable materials in the absence of oxygen. Anaerobic digestion is performed at temperature ranges between 30 and 35°C or 50 and 55°C using two stages. In the first stage, acid-forming bacteria are used to break biomass into simpler compounds such as acetic and propionic acids along with volatiles. The second stage, methane producing bacteria coverts acids into CO_2 and CH_4 that are commonly called biogas.

Carbon dioxide and methane can be collected and used as fuel (biogas). Biogas is most typically made by mixing organic matter with water and stirring and heating it in an airtight container called a digester (Balat 2006). Livestock manure, municipal wastewater solids, food waste, high strength industrial wastewater and residuals, fats, oils, and grease (FOG) could be used as organic waste streams. An anaerobic digestion plant produces two main outputs, biogas and digestate. Both can be further processed or utilized to produce secondary outputs. At the end of its use, the biogas can be used for heating, electricity, transport, or combined heat and power (CHP). The biogas has a heating value of about 22.35 kJ/m^3 for a mixture that contains a ratio (CH_4:CO_2:inerts) of 60:35:5 (Chen and Qiu 2010). There are many factors controlling the conversion of biomass to biogas, such as process temperature, pH values, solid fraction, redox potential, nutrient demand, and trace elements, see **Table 3.3**.

Table 3.3: Factors controlling anaerobic digestion process

Influencing variable	Acidogenesis	Methanogenesis
Temperature	25 …35 °C	Mesophilic 32 …42 °C Thermophilic 50 …58 °C
pH value	5.2 … 6.3	6.7 … 7.5
Solid fraction	< 40 % DM*	< 30 % DM
Redox potential	+400 … -300 mV	< -250 mV
Nutrient demand C,N,P,S	500: 15: 5: 3	600: 15: 5: 3
Trace elements	No special demand	Essential Ni, Co, Mo, Se

*DM: Dry matter

Ethanol Fermentation or bioethanol production process is a biological process which converts biomass residues containing fermentable sugars generated from cellulose and hemicellulose components of biomass in the presence of yeast or bacteria, such as microalgae species, for instance, Chlorella, Chlamydomonas, Scenedesmus, Dunaliella, and Spirulina.

The complex polysaccharides that result are the raw materials needed to make bioethanol. Because the microorganisms have trouble metabolizing the polysaccharides, hydrolysis is used to break them down into simple sugars before feeding them. As shown in **Figure 3.5**, the most frequent hydrolysis procedures use acid/alkali and enzymes. The ethanol is distilled and dehydrated at the end of the conversion process to obtain concentrated alcohol, while the solid leftovers can be utilized as fuel in boilers to produce gas or as livestock feed.

The fermentation of the two most common sugars follows the two reactions below (Tursi 2019):

Sugars → Ethanol + CO_2 + by-products

$C_6H_{12}O_6(\text{Glucose}) \rightarrow 2C_2H_5OH + 2CO_2$

$3C_5H_{10}O_5(\text{Xylose}) \rightarrow 5C_2H_5OH + 5CO_2$

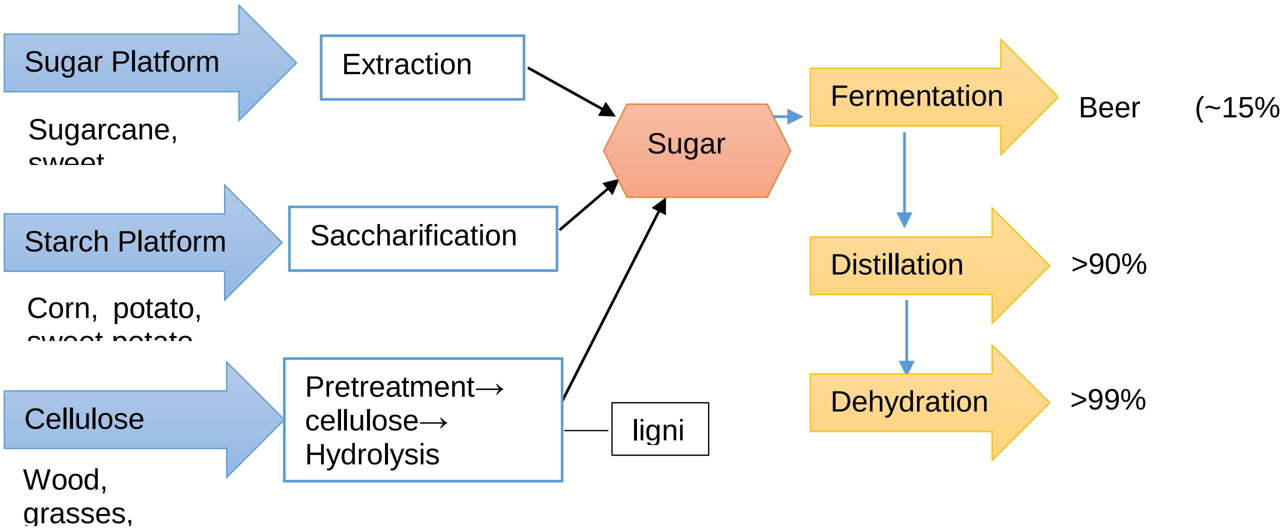

Figure 3.5: Fermentation process

Depending on the starting substrate, multiple metabolic processes could be used to convert carbohydrates to ethanol. Specifically, (a) from hexoses like glucose, via glycolysis or the Embden-Meyerhof pathway (EMP) (Taherzadeh and Karimi, 2008), and (b) from pentoses, via the pentose phosphate pathway (PPP) (Taherzadeh and Karimi, 2008). (PPP). The hexoses' conversion reactions are faster than those of the pentoses.

Aerobic digestion is the degradation of organic sludge solids in the presence of oxygen to reduce the volume of sewage sludge and make it suitable for subsequent use. The micro-organisms in the sludge convert the organic material to carbon dioxide and water, and the ammonia and amino species to nitrate. Aerobic digestion runs at ambient temperature, the process is much less complex and easier to manage. Operating costs are much greater than for anaerobic digestion, but capital costs are generally lower than for anaerobic systems. Aerobic digestion processes have high power costs to supply oxygen, even for very small plants. Shammas and Wang (2007) discovered that it is easier to operate than anaerobic systems and has other advantages (Shammas and Wang 2007).

3.4. Biogas technology

Bioenergy is making its way to energy, environmental, and co-product benefits in the first process of producing biogas from waste, here from municipal waste, agricultural residue, and waste water plant. Biogas is produced after organic materials are broken down by bacteria in an oxygen-free environment in a process called anaerobic digestion. Biogas can be produced through anaerobic digesting biochemical conversion, as shown in **Figure 3.4**. Anaerobic digestion can occur at mesophilic (35-45˚C) or thermophilic (50-60˚C). Both types of digestion typically require supplementary sources of heat to reach their optimal temperature. Biogas creation is also called biomethanation. Biologically derived gases are produced as metabolic products of two groups of microorganisms called bacteria and aArchaea. These microorganisms feed off carbohydrates, fats, and proteins, then, through a complex series of reactions including hydrolysis, acetogenesis, acidogenesis, and methanogenesis produce biogas consisting mainly of carbon dioxide and methane.

Biogas consists of 50-75% methane, 25-45% carbon dioxide, 2-8% water vapor and traces of O_2 N_2, NH_3 H_2 H_2S. The energy content of the gas depends mainly on its methane content. The average calorific value of biogas is about 21-23.5 MJ/m³, so that 1 m³ of biogas corresponds to 0.5-0.6 L of diesel fuel or about 6 kWh (FNR, 2009). The biogas yield of a plant depends not only on the type of feedstock but also on the plant design, fermentation temperature, and retention time. **Table 3.4** shows the gas yield and methane percentage for various substrates.

Table 3.4: Gas yield and methane contents for various substrates at the end of 10-20-day retention time at a process temperature of roughly 30°C

Substrate	Gas yield (L/kg)VS*	Methane content %	Reference
Cow manure	90-310	65	(Kabeyi and Olanrewaju 2021)
Poultry droppings	310-620	60	(Kabeyi and Olanrewaju 2021)
Horse manure	200-300	51	(Wartell et al. 2012) (Mukumba et al. 2017)
Sheep manure	90-310	24-63	(Li et al. 2020) (Nagy et al. 2018)
Barnyard dung	175-280	36-53	(Ashekuzzaman and Poulsen 2010)
Hemp	360	59	(Kabeyi and Olanrewaju 2021)
Grass	280-550	70	(Kabeyi and Olanrewaju 2021)
Vegetable residue	330-360	32.252 ($\pm$12.051%)	(Morales-Polo et al. 2021)
Potato tops/greens	280-490	55–65	(Achinas et al. 2019)
Agriculture waste	310-430	60-70	(Kabeyi and Olanrewaju 2021)
Seeds	620	54.7	(Vijay et al. 2020)
Fallen leaves	210-290	58	(Kabeyi and Olanrewaju 2021)
Sewage sludge	310-740	55-80	(Khairul Anuar et al. 2018)

*VS = Total volatile solids

Biogas can be used in similar ways as natural gas or LPG in gas stoves, lamps, or as fuel for engines. It can be transformed into any kind of thermal, electrical, or mechanical energy as shown in **Figure 3.6**. And can also be compressed, much like natural gas, and used to power motor vehicles (Caposciutti et al. 2020).

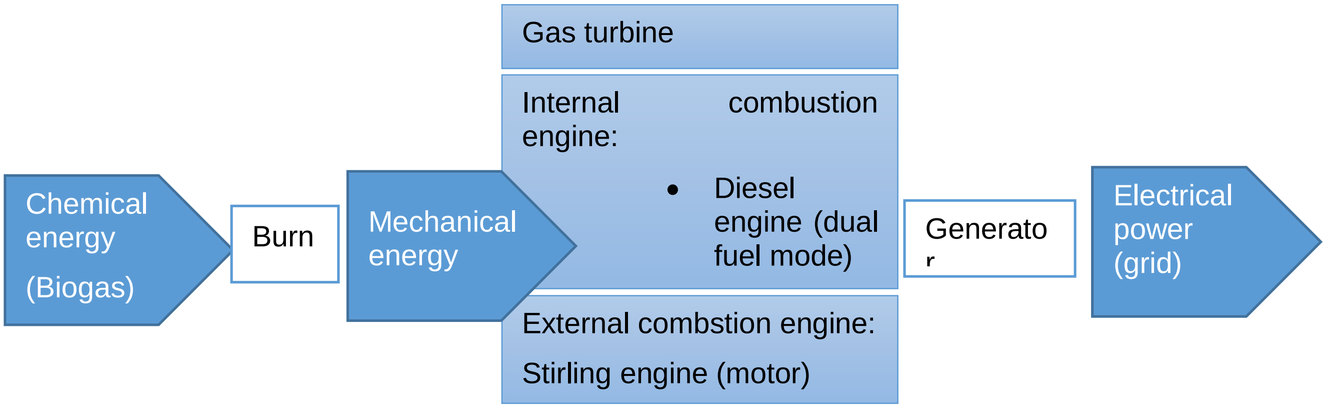

Figure 3.6: Biogas utilization

Sulphur content must be minimized, particularly for use in engines. In fact, the contribution of a methane molecule (CH_4) to the greenhouse effect is 21 times greater than that of a carbon dioxide molecule(SUSANA 2009). Therefore, burning methane, even though it produces CO_2, reduces its impact on the environment. In Germany and other industrialized countries, power generation is the main purpose of biogas plants; the conversion of biogas to electricity has become a standard technology. Producing electricity from biogas is still relatively rare in most developing countries.

There are many factors controlling the conversion of biomass to biogas in addition to process temperature, retention time, and nutrient demand, such as pH-value, toxic substances, organic loading rate (OLR), and alkalinity.

3.5. Photovoltaic solar technology

In Gaza, it is usual to use solar energy in a common way or to use photovoltaic technology to turn it directly into electricity. This has helped to alleviate the electricity shortage situation and is becoming more widely used.

This section describes the basic terminology used in solar photovoltaic energy technology, solar irradiance and solar constant, sun position and sun angles, and photovoltaic solar cell principle of operation and types of cell technology, finally a briefly depict of the solar cell configuration is displayed:

3.5.1. Solar Irradiance and solar constant

Solar radiation is the electromagnetic radiation emitted by the sun. The distribution of solar radiation as a function of wavelength is called the solar spectrum. The sun's total radiation output is approximately equivalent to that of a blackbody at 5776 K. The mean distance between the sun and the earth is (149,597,870 km) is known as the astronomical unit (AU).

The solar constant is the amount of solar radiation received outside the earth's atmosphere on a surface normal to the incident radiation per unit time and per unit area at the earth's mean distance from the sun. It is an important value for the studies of global energy balance and climate. It is the average amount of solar irradiance that arrives above the Earth's atmosphere, which is approximately (1353W/m^2) The analysis of satellite data suggests a solar constant of 1366W/m^{-2} with a measurement uncertainty of 73 W/m^2 of the radiant energy emitted from the Sun, approximately 50% lies in the infrared region (40.7 µm), about 40% in the visible region (0.4–0.7 µm), and about 10% in the UV region (0.4 µm).

When describing the sun's energy, there are four commonly used parameters in the PV community:

Solar irradiance: This is a term that describes the intensity of solar power per unit area. Its units are therefore in W/m^2.

Solar irradiation: This is the total amount of solar energy collected per unit area over time (Wh/m^2).

Insolation: This describes the amount of solar irradiation collected during one day ($kWh/m^2/day$).

Solar constant: This is the average amount of solar irradiance that arrives above the earth's atmosphere, which is approximately ($1353 W/m^2$) (Precup et al. 2018).

Consequently, due to atmospheric effects, there are four main types of solar radiation. Solar radiation at the earth's surface is defined as the amount of radiation reaching the earth that is less than that which enters the top of the atmosphere. It is classified into: direct, diffuse, reflected, and global radiation. **Figure 3.7** illustrates the various types of solar radiation.

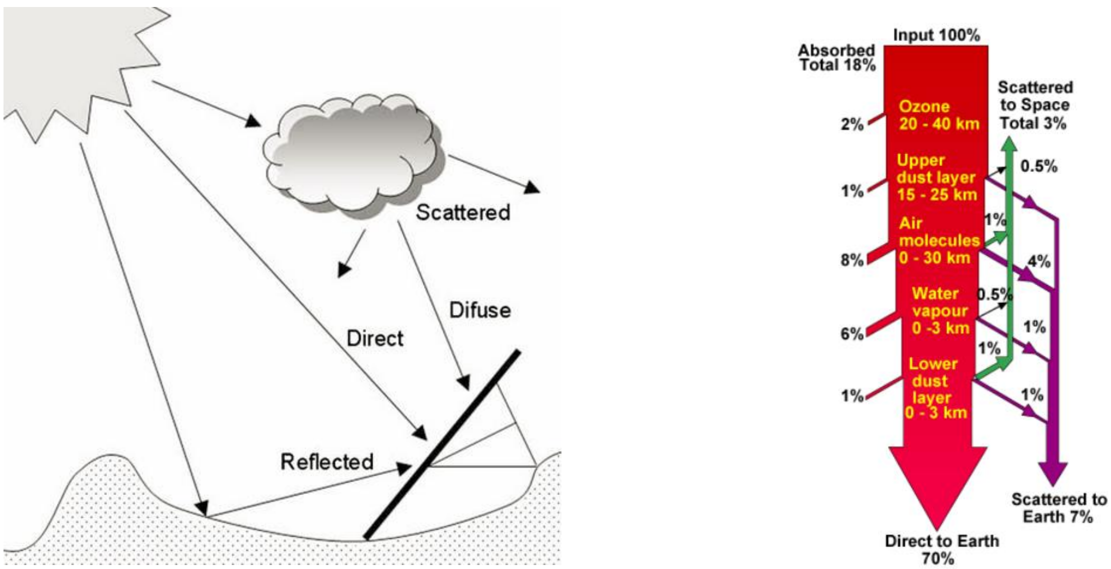

Figure 3.7: (a) various types of solar irradiation (b)the atmospheric effects on the irradiance power density (Keller and Costa 2011)

Direct normal irradiance (DNI): It is the direct beam of light to the solar collector. The radiation coming directly from the sun is received at the earth's surface (without scattering).

Diffuse horizontal irradiance (DHI): It is the light beam that is reflected from clouds and ground albedo and scattered radiation coming from all other directions.

Global horizontal irradiance (GHI): It is the total amount of shortwave radiation received on a surface horizontal to the ground; it is the sum of DNI and DHI.

The amount of solar radiation received at any location on earth depends on the time of day and year, the local latitude, and the orientation of the surface. It is also significantly affected by weather conditions (Günther et al. 2011).

On a clear day when the sun is directly overhead, almost 70% of the incident solar radiation reaches the earth's surface. The magnitude of solar radiation that is scattered or absorbed depends on the amount of atmosphere through which it must travel before reaching the Earth's surface.

Air mass (AM) is the length of the light path through the atmosphere. It represents the amount of atmosphere through which solar radiation must pass before reaching the Earth's surface. The value of AM can be evaluated by using the equation 3.1, by looking at **Figure 3.8** and using the equation AM0 means at the outer surface of the earth, AM1 means the sun is perpendicular to the earth's surface or when the sun is directly overhead at sea level.

$AM = \frac{1}{cos\,\emptyset}$ Eq. (3.1)

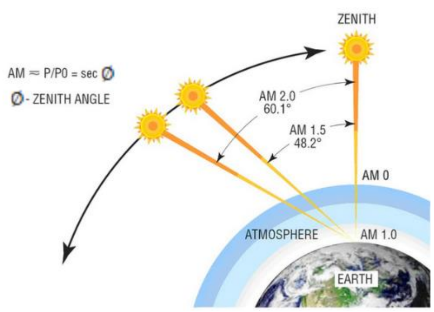

Figure 3.8: Explanation of AM0, AM1 and AM (secØ)

The air mass is a numerical comparison between the bath length which the solar actually traverses and the vertical path through the atmosphere. Thus, at sea level, the air mass AM is unity when the sun is at the zenith, i.e., when Ø=0º (N'tsoukpoe et al. 2009). In general,

$air\ mass = \frac{path\ length\ traversed}{vertical\ depth\ of\ atmosphere}$ Eq. (3.2)

When Ø=48.2º the air mass equals 1.5, which has become the standard for photovoltaic (PV) work (I=1000W/m²). This air mass is mainly valid for countries located within the solar belt. A typical peak value of 1000 W/m^2 is used as the rating condition for PV modules and arrays (Zamft and Conrado 2015). In the far north and the far south, the AM increases and the irradiance decrease. PV utilization is primarily using terrestrial solar radiation, which is sunlight that reaches the earth's surface. Extraterrestrial and terrestrial spectra are depicted in **Figure 3.9** (Dirnberger 2015).

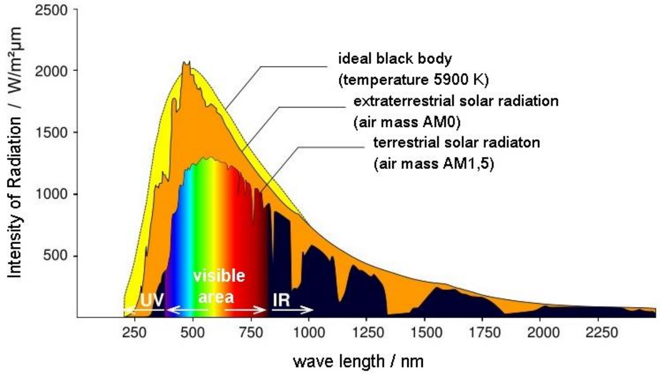

Figure 3.9: Intensity of radiation per Watt/m2µm

Atmospheric Effects

The solar irradiance enters atmosphere at 1367 W/m^2. Solar radiation is absorbed, scattered, and reflected by components of the atmosphere. The irradiance can be calculated by the formula in equation 3.3. In the far north and the far south, the AM increases and, consequently, the irradiance power density decreases. When irradiance enters the atmosphere of 1367W/m^2, then ozone begins to absorb part of it; upper dust layer, air molecules, water vapor, and lower dust layer. Then 3% reflects back to space among clouds, 7% scattered by the clouds and solid molecules in the atmosphere. The direct amount reached on the m^2 is 70% as depicted in the equation.

$I = 1367\ (0.7)^{(AM)^{0.678}}$ Eq.(3.3)

On an average, the irradiance does not exceed 1000 watts per square meter. This gives us an overview of the location effect on the solar irradiance power density.

Irradiation is often expressed as peak sun hours (PSH). It is simply the length of time in hours at the irradiance level of 1kW/m^2 needed to produce the daily irradiation obtained from the integration of irradiance over all daylight hours.

Sun position:

The sun's position and sun angles are considered when the distance between PV strings is calculated. The position of the sun is specified by three angles elevation (altitude) angle α, azimuth angle ψ, and declination angle δ.

Elevation (altitude) angle α:

The solar altitude angle, α, is the angle between the line of collinear with the sun's rays and the horizontal plane.

Azimuth angle ψ:

The solar azimuth angle, ψ, is the angle between a due south line and the projection of the site to the sun line on the horizontal plate. The sign convention used for azimuth angle is positive west of south and negative east of south (Kreith and Kreider 2000). Solar noon happens when the sun is perpendicular to the real south. The azimuth angle starts at the sunrise and ends at the sunset. It is east/west on equinoxes.

Declination angle δ:

Solar declination is the angle between thee equatorial plane and the ecliptic plane. The solar declination angle varies with the season of the year, and ranges between –23.5° and +23.5°. It is defined as the angle of deviation of the sun from directly above the equator, as shown in **Figure 3.10**, and calculated using equation 3.4, where n is the day number in the year that must be considered when calculating the declination angle.

$\delta = 23.45°\ sin\left[\frac{360(n-80)}{365}\right]$ Eq. 3.4)

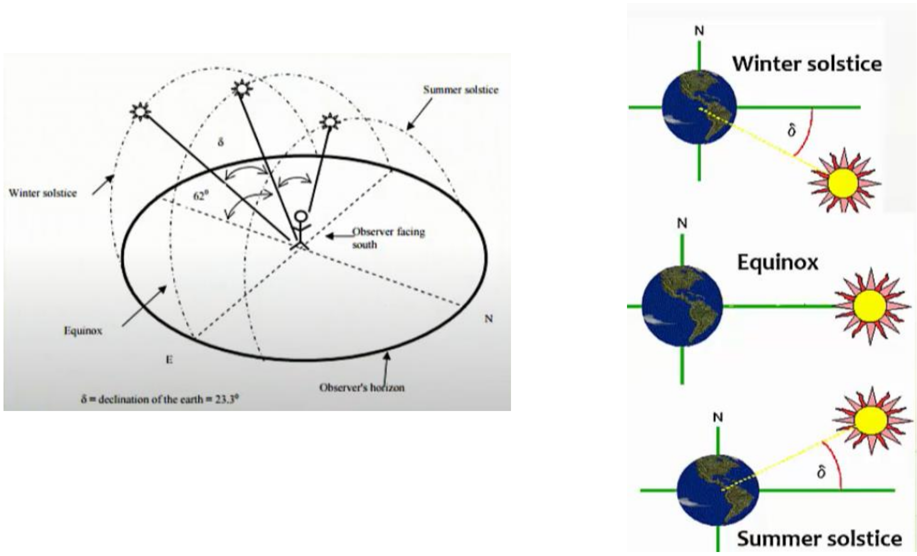

Figure 3.10: Season effects on the declination angle

The solar zenith angle ∅:

The solar zenith angle, ∅, is the angle between the site and the sun line and the vertical at the site.

$\emptyset = 90° - \propto$ Eq. 3.5)

Sun path chart

is used to calculate the shadow of the first string on the next string. **Figure 3.11** displays the sun path diagram of the Gaza city location. The figure shows the solar altitude and azimuth angles for 31.3° latitude. Usually, when two strings of solar arrays have been mounted as shown in **Figure 3.11** , the longest shading and the inter-row spacing between strings of solar arrays are chosen on December 21st, because the sun's elevation is at its lowest possible on the horizon, and hence we will get the longest shadow and calculate the distance between PV strings, where the string of PV is not affected on the next string. The interrow spacing is calculated by ascending h, d, and then X. The lengths substite in the following equations:

$h = L \sin tilt$ Eq. 3.6)

$d = \frac{h}{\tan\alpha}$ Eq. 3.7)

$interrow\ space = d \cos(\alpha)$ Eq. 3.8)

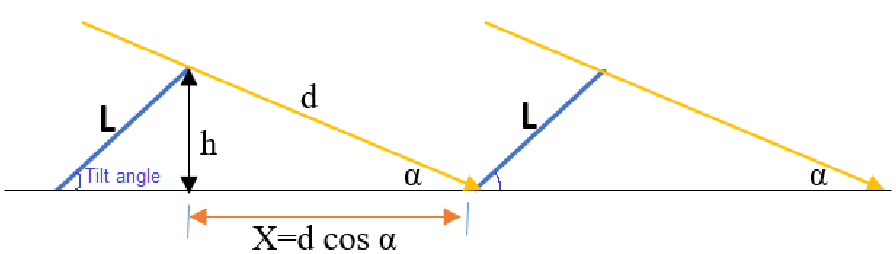

Figure 3.11: Height and distance between two modules

Figure 3.12 displays the sun path chart of Gaza city at a location (Altitude: 49.7 m, Latitude: 31°30´ N, Longitude: 34°27´ E), the x-axis is solar azimuth, y-axis is solar elevation, the solar noon (12 PM) direct south equals zero azimuth angle. For example, to calculate the shading on December 21st at 09:00 AM, for example of the 2 rows of solar array for the previous location, **Figure 3.12** is used to determine azimuth and elevation angles. The solar module dimensions are 1.65 m in length and 1 m in width when mounted portrait. There are two types of solar panels mounted portrait or landscape, it depends upon area, shading, material, and with or without by-pass diode. From the chart 3.9 elevation (altitude) angle α, azimuth angle ψ are 21.5° and 43° (180° minus137°) at the mentioned time.

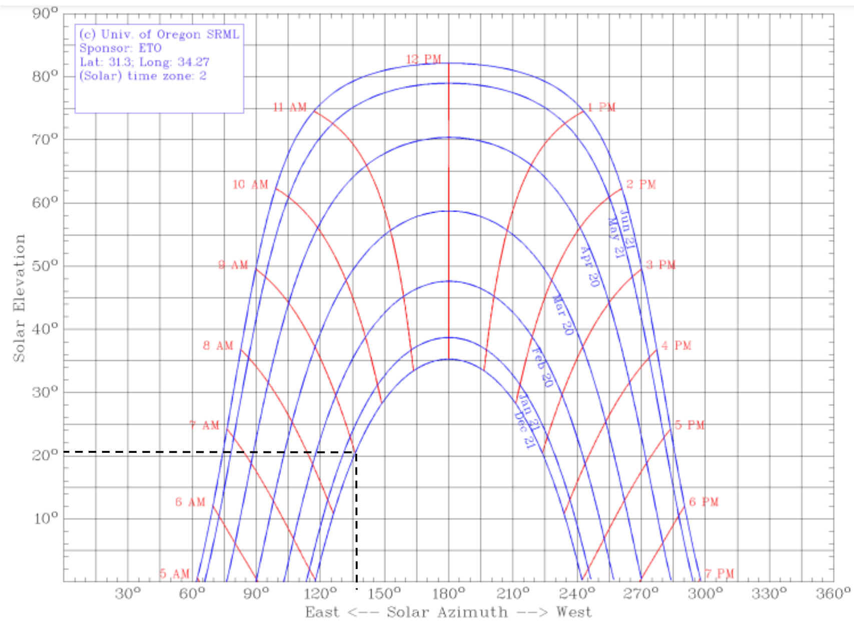

Figure 3.12: Sun path chart of the Gaza city

http://solardat.uoregon.edu/SunChartProgram.html

3.5.2. Photovoltaic solar cell

Photovoltaic (PV) is one of the main types of solar energy technology. Photovoltaic (PV) devices generate electricity directly from sunlight via an electronic process using certain types of material called semiconductors. A solar cell (or PV cell) is the basic component of a photovoltaic (PV) system.

A PV cell is comprised of many layers of materials, each with its own function. The specially treated semiconductor layer is the most important layer in a photovoltaic cell. It is made up of two layers (p-type and n-type), see **Figure 3.13**. Photons ionize the semiconductor material on the solar panel, causing outer electrons to break their atomic bonds. The electrons are forced in one direction by the semiconductor structure, resulting in an electrical current flow.

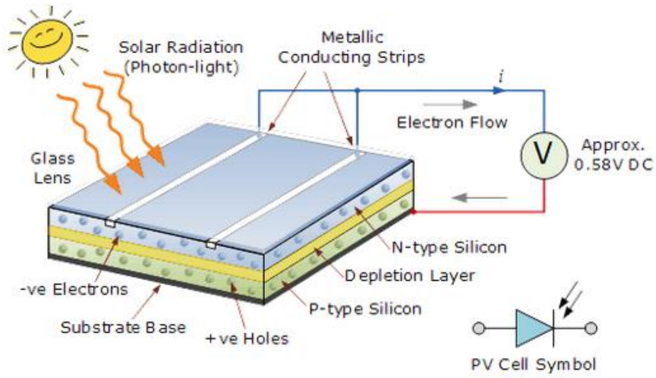

Figure 3.13: Photovoltaics solar cell

Photons strike and ionize semiconductor material on the solar panel, causing outer electrons to break free of their atomic bonds. Due to the semiconductor structure, the electrons are forced in one direction, creating a flow of electrical current. Solar cells made of crystalline silicon are not 100 percent effective, in part because only certain wavelengths of light can be absorbed. Some of the light spectrum is reflected, while others (infrared) are too weak to generate electricity, and still others (ultraviolet) generate heat energy rather than electricity.

According to the photovoltaic report (2020), the percentage of global annual production of mono-Si modules (GW_p) in 2019 records 89.7. See **Figure 3.14**. The highest value due to its high efficiency and more sensitivity to light. The multi-Si production is 39.6. It is preferred in high degradation and less sensitive to shading. The thin film production is 7.5, which is around the percentage of this decade.

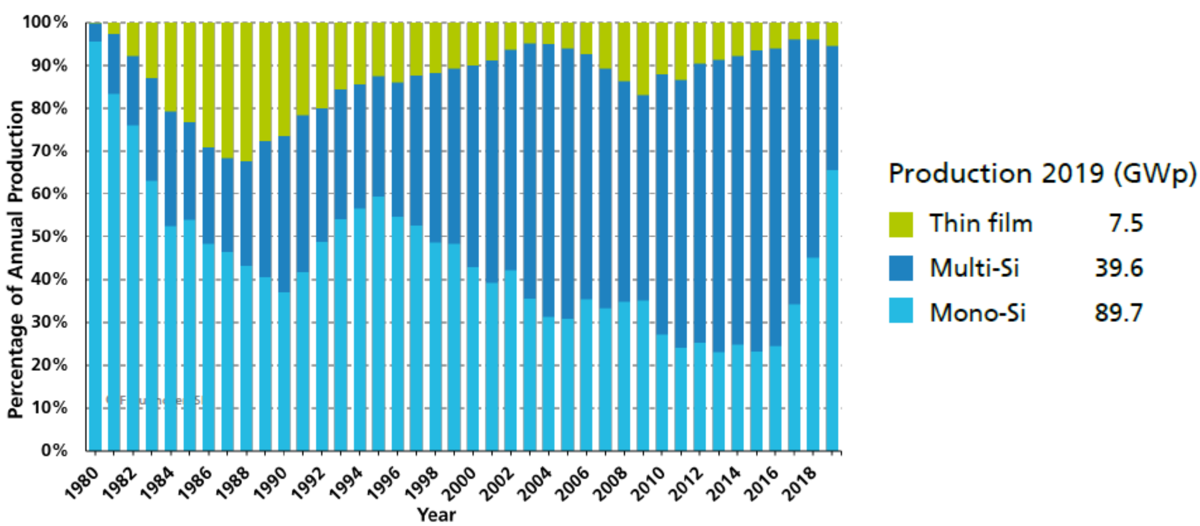

Figure 3.14: Percentage of the PV annual production

Solar cell material

Silicon

The vast majority of solar cells on the market today are made of silicon and offer both low prices and high efficiency. Two cell types are monocrystalline (Mono-c-Si) with a ~20% efficiency rate and polycrystalline (Multi-c-Si) with about 15% efficiency. Mono-Si is highly efficient, durable, and more expensive compared with p-Si, but the latter has a higher degradation value. The different types of PV cells based on cell material are shown in **Figure 3.15**.

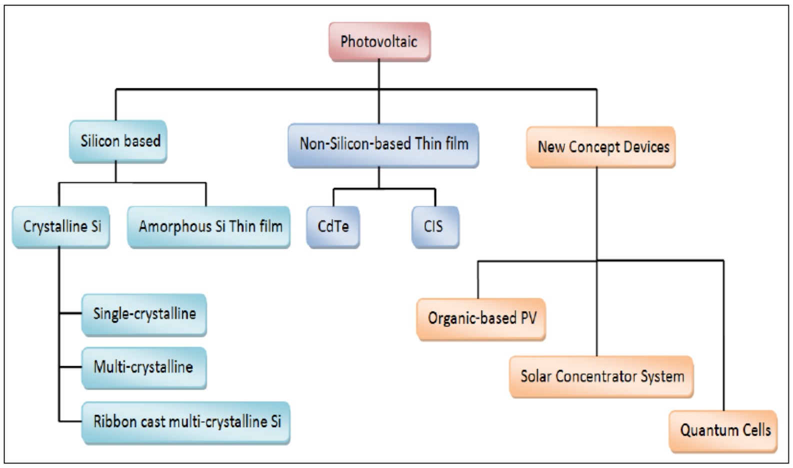

Figure 3.15: Different types of photovoltaic cells based on cell material (Halasah 2009, 2018).

Thin-Film Photovoltaics

Thin film PV modules are another commonly used photovoltaic technology. They are made from very thin layers of semiconductor material on a supporting material such as glass, plastic, or metal. There are two main types of thin-film PV semiconductors on the market today: cadmium telluride (CdTe) and copper indium gallium diselenide (CIGS). Both materials can be deposited directly onto either the front or back of the module surface. The thickness of these cell layers is only a few micrometers and can be deposited directly onto either the front or back of the module surface. Thin-film PV efficiency is about 7-10%. They are generally less efficient, low-cost, flexible, and lightweight than c-Si modules.

Organic Photovoltaics

Organic PV, or OPV, cells are composed of carbon-rich (organic) compounds and can be tailored to enhance a specific function of the PV cell, such as bandgap, transparency, or color. OPV cells are currently only about half as efficient as crystalline silicon cells and have shorter operating lifetimes, but could be less expensive to manufacture in high volumes. They can also be applied to a variety of supporting materials, such as flexible plastic, making OPV able to serve a wide variety of uses.

Perovskite Photovoltaics

Perovskite solar cells are a type of thin-film cell and are named after their characteristic crystal structure. Perovskite cells are built with layers of materials that are printed, coated, or vacuum-deposited onto an underlying support layer, known as the substrate. They are typically easy to assemble and can reach efficiencies similar to crystalline silicon. They are based on hybrid materials with an organic and an inorganic part. Their laboratory yields are already reaching those of other technologies (the record is 23.7%).

Quantum Dots

Quantum dot solar cells conduct electricity through tiny particles of different semiconductor materials just a few nanometers wide, called quantum dots. Quantum dots provide a new way to process semiconductor materials, but it is difficult to create an electrical connection between them, so they're currently not very efficient.

Multijunction Photovoltaics

Another strategy to improve PV cell efficiency is layering multiple semiconductors to make multijunction solar cells. These cells are essentially stacks of different semiconductor materials, as opposed to single-junction cells, which have only one semiconductor. Each layer has a different bandgap, so they each absorb a different part of the solar spectrum, making greater use of sunlight than single-junction cells. Multijunction solar cells can reach record efficiency levels because the light that doesn't get absorbed by the first semiconductor layer is captured by a layer beneath it.

Concentration Photovoltaics

Concentration PV, also known as CPV, focuses sunlight onto a solar cell by using a mirror or lens. By focusing sunlight onto a small area, less PV material is required. PV materials become more efficient as the light becomes more concentrated, so the highest overall efficiencies are obtained with CPV cells and modules. However, more expensive materials, manufacturing techniques, and the ability to track the movement of the sun are required, so demonstrating the necessary cost advantage over today's high-volume silicon modules has become challenging. The CVP cell has a high performance and efficiency rate of about 41%, but it needs a solar tracker and a cooling system.

3.5.3. Solar cell types and technology:

PV cell technologies are classified into two types, **Figure 3.16**: crystaline silicon or first generation cells, which consist of poly/multi-crystaline and mono-crystaline, and the second generation, thin-film cells.

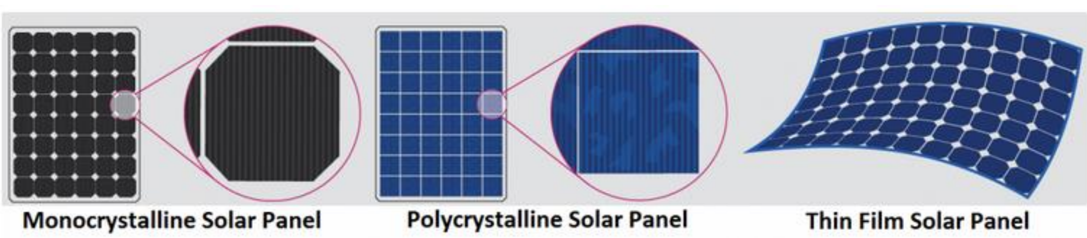

Figure 3.16: PV cell technologies types

PV cell has a voltage which named V_{cell} or $V_{open\ circuit}$, if the PV cells connected in series then the voltage will be doubled while the output current is the same in case both cells receive the same amount of light **Figure 3.17**. When the cells are connected in parallel, the voltage is the same and the current will be summed from each cell. Often the voltage of one cell is near 0.5-0.6-volt open circuit voltage.

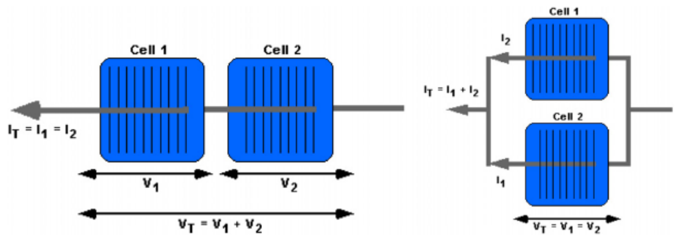

Figure 3.17: Schematic diagram of the series and parallel connected mono-Si solar cells.

PV cells are connected in series or in parallel to build a module. Standard cell numbers per module are 36, 60, and 72 cells. One cell could generate 5 watts as a maximum. The module contains 36 cells most of which provide a 22-volt open circuit, for instance.

Solar cell and module effieciency:

The National Renewable Energy Laboratory, Golden, CO. (NREL) maintains a chart of the highest confirmed conversion efficiencies plotted from 1976 for cells (NREL 2020). The cell efficiency results are provided for 28 different subcategories and indicated by distinctive colored symbols as shown in **Figure 3.18** within families of semiconductors:

- Multijunction cells
- Single-junction gallium arsenide cells
- Crystalline silicon cells
- Thin-film technologies
- Emerging photovoltaics.

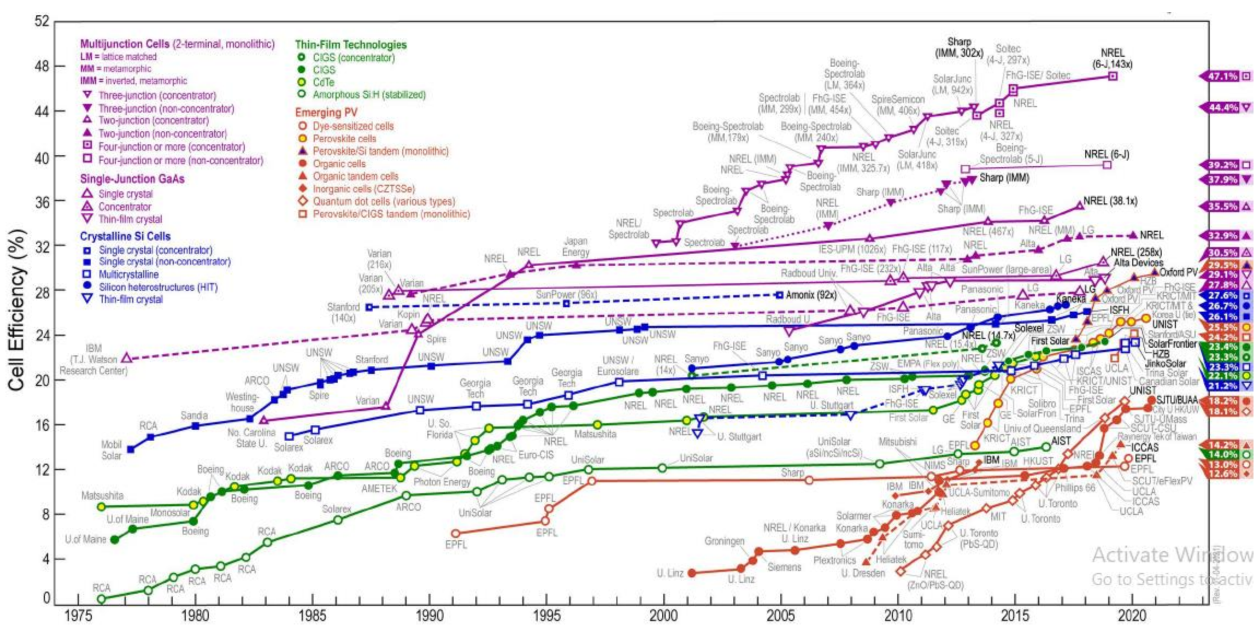

Figure 3.18: Best research-cell efficiencies NREL

A solar cell could be considered as a simple energy converter able to produce an electrical work after the absorption of heat from the sun. In this fundamental vision, the solar cell is represented by an ideally reversible Carnot heat engine. As an ideally reversible is assumed, the sun is a high temperature reservoir, and the ambient atmosphere is a low temperature reservoir. If the sun is at a temperature of *6000K* and the ambient temperature is *300K*, the maximum Carnot efficiency is about *95%* as an upper limit for all kinds of solar converters. The solid angle under which the cell sees the sun is minimizing efficiency. The energy band-gap of a semiconductor *pn* junction solar cell is the most important and critical factor controlling efficiency, where if incident photons with energy higher than the energy gap can be absorbed, creating electron-hole pairs, while those with lower energy are not absorbed, either reflected or transmitted. Other fundamental factors, such as the view factor of the sun seen from the solar cell position, the background radiation, and losses due to recombination. Other fundamental factors should be taken into account, namely; the view factor of the sun seen from the solar cell position; the background radiation, which could be represented as a blackbody at ambient temperature, and losses due to recombination, radiative and non-radiative, which give a more realistic picture of the solar cell efficiency.

The Shockley-Queisser limit or detailed balance limit refers to the calculation of the maximum thoeoretical effeciency of a soler cell made fron a single *pn* junction. It was first calculated by William Shockley and Hans Queisser (Shockley and Queisser 1961). From **Figure 3.18** it can be seen that the most sillicon solar panels are between 26.1 and 27.6 efficient. The minimum module efficiency can be obtained from the equation:

$$Minimum\ module\ effeciency\ \cong \frac{Specified\ rated\ power\ of\ the\ array\ (W)}{Available\ installation\ area\ (m^2)\times 1000\ W/m^2} \qquad \text{Eq. 3.9)}$$

3.5.4. IV-characteristiv of solar module

One of the most commonly used models for photovoltaic modules is the single diode model. In this model, the equivalent circuit of a solar cell consists of a current source, a diode, and two resistors, as shown in **Figure 3.19**-a. I_L represents the current source of the charge carrier generation in the semiconductor layer of the PV cell caused by incident radiation. The shunt diode represents the recombination of these charge carriers at a forward-bias voltage ($V+I.R_s$). High-current paths through the semiconductor along mechanical defects and material dislocations are denoted by the shunt resistor R_{sh} (Boyd et al. 2011). The equivalent circuit of the pv cell contains five independent parameters; thoes are current at maximum power I_{mp}, voltage at maximum power V_{mp}, short-circuit current I_{sc}, open circuit voltage V_{oc}, and temperature coefficients of short-circuit current α_{Isc} and open-circuit voltage β_{Voc}. Even just the measurements at STC that are available on manufacturer datasheets can be used to calculate these five-parameter models analytically.

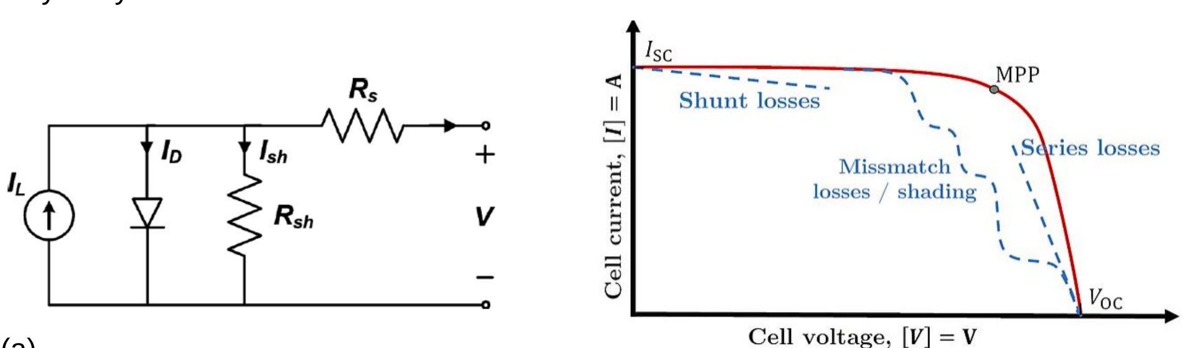

(a)

(b)

Figure 3.19: Equivalent circuit of a photovoltaic solar cell used in the five-parameter model

Solar module performance is tested by STC (Standard Test Condition) at 25° C temperature, and the solar irradiance is 1000W/m^2 at 1.5 AM. **Figure 3.19**-b shows the relation between current and voltage, which is called the iv-charactristic of the PV module. If we test the solar module at different voltages in the same irradiance of 1000W/m^2 , where the positive and negative ends of the module are connected, a short circuit current will pass. This current is the maximum current flow in the module. Open circuit voltage occurs when the circuit is open. When variant resistance is connected at the two ends of the module, the voltage and current will differ in the circuit according to the value of the resistance. The PV module is considered a current source. The maximum power obtained from the solar module is recorded at the maximum power point (MPP). This point depends on the resistance value (load) connected to the solar panel.

The values of short circuit current, current at maximum power point, open circuit voltage, voltage at maximum power point, and maximum power point I_{sc}, I_{mp}, V_{oc}, V_{mp}, and P_{mp} are given in the data sheet of the solar panel. The maximum power is equal to $Vmp \times Imp$. The fill factor is a quality indicator of a solar module that is calculated using the formula.

$$Fill\ factor = \frac{V_{mp} \times I_{mp}}{V_{oc} \times I_{sc}} \quad \text{Eq. 3.10)}$$

The fill factor is the ratio between maximum power divided by the power generated from open voltage multiplied by short current. Any fill factor greater than 0.75 is excellent value. The FF<0.7 refers to bad quality value. This occurs when the panel installation, use of welding, and connection are not perfect.

Effect of temperature and irradiance on the solar module

Solar module IV characteristics are affected under different weather conditions such as temperature and irradiance. Usually, the solar panel specifications such as V_{oc}, I_{sc}, I_{mp}, and V_{mp} are always reported at STC (at cell temperature of 25° C, AM1.5, and 1 kW/m^2 solar irradiance) by the manufacturer. Therefore, the influence of solar irradiance on the temperature coefficient of V_{oc} and V_{mp} is assumed to be insignificant, whereas the temperature coefficient of short-circuit and maximum power point current are scaled by the ratio of the actual irradiance level to the irradiance level at STC. When the solar irradiance decreases to 200 W/m^2 the inverter and the solar module will not work. The data sheets of PV modules specify the temperature coefficients of maximum power point, short-circuit current, and open-circuit voltage. Hence the temperature of the cell can be calculated using equation 3.11, where NOCT is the Normal operating cell tempreture.

$$\boldsymbol{T_{cell}}(°\boldsymbol{C}) = \boldsymbol{T_{air}} + \frac{\boldsymbol{NOCT-20}}{\boldsymbol{800}} * \boldsymbol{G} \quad \text{Eq. 3.11)}$$

PV module open circuit voltage changes with cell temperature. It decreases as the temperature rises due to ambient changes or heat generated by internal power dissipation. As a result, the power output is reduced. Irradiance has an impact on module performance, with a decrease in sunlight resulting in a decrease in current and, as a result, a decrease in power output (Mandadapu et al. 2017).

3.5.5. Solar system configuration

Five solar system configurations that adhere to the IEC standard are illustrated in this section. It is important to note that the grid-connected hybrid system will use the third configuration. As shown in **Figure 3.22**, It consists of solar panels, a grid-tie inverter, a DC disconnect, and an optimizer (*optional*) to improve the performance of the panel.

PV DIRECT SYSTEM

A very simple system which has no batteries to store excess energy and no inverter to convert the direct current DC to an alternative current AC, **Figure 3.20**. It is not connected to the main power grid. It consists of a solar panel that converts light directly to electricity. The solar module consists of cells connected in series or parallel. Then it connects to the array DC disconnect to the controller to the DC load. It is an example of a DC pump. The pump controller monitors the speed and torque of the pump depending on solar irradiance.

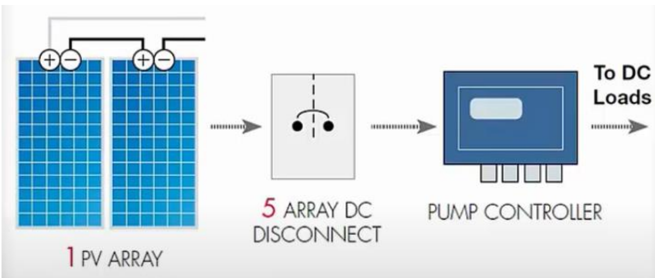

Figure 3.20: PV direct system configuration

OFF-Grid SYSTEMS

The solar panel is connected to a to combiner box (optional) that depends on the number of PV strings. When PV modules are connected in series, they make a PV string or PV panel. Two or more strings make a PV array. As seen in **Figure 3.21**, PV is applied to the charge controller by solar. DC disconnect between the charge controller and the battery bank. The output battery bank can be applied to the system meter to measure voltage, current, power, and energy. A disconnect is required between the battery bank and the inverter. The DC charge controller is a DC/DC converter and monitors the battery charge from the PV panel. The inverter converts the DC supplied from the charger to AC.

AC disconnect between the inverter service panel (circuit breaker panel) that supplies the load. This configuration is known as off-grid connection; if the generator is not used, the configuration is known as off-grid system solar PV system with battery energy storage. If another source of energy, like a wind turbine, is connected to the system by inverter or by service panel, then the system is called a hybrid system. The hybrid system is used to decrease the number of batteries for cost effectiveness and to serve the life span of the battery bank.

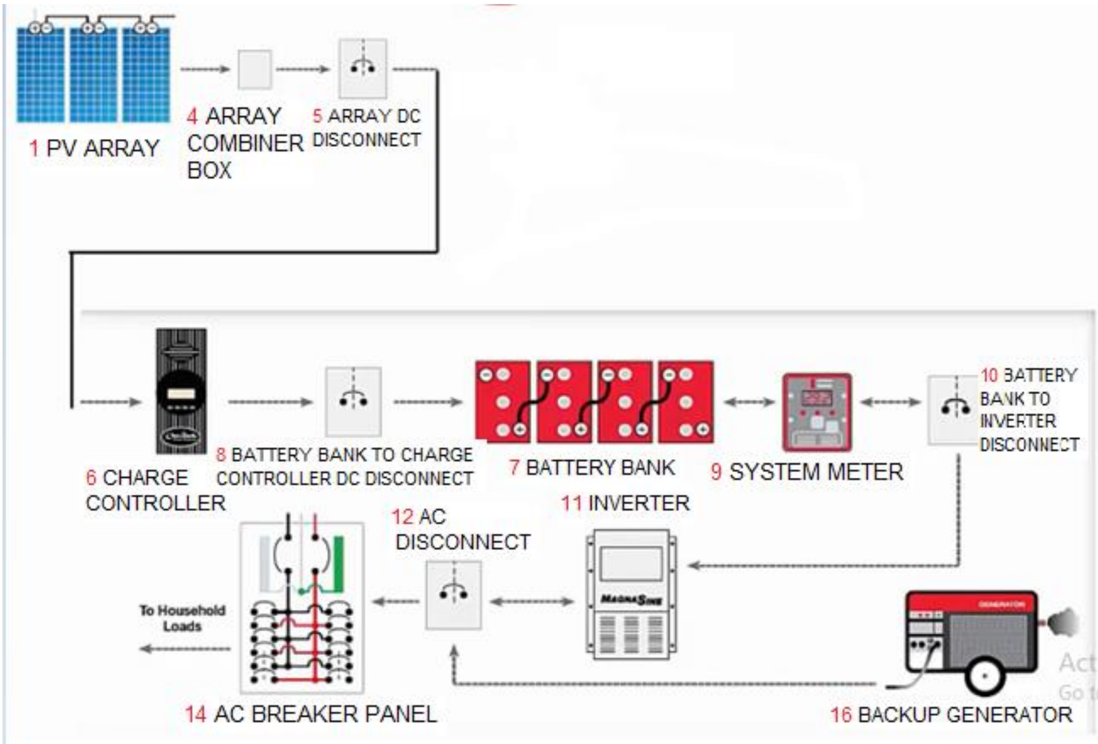

Figure 3.21: PV off grid system

Grid-Tie PV SYSTEMS

This system type is more efficient, indepedenty and cost-effective than an off grid system. A grid-connected system consists of solar panels with an optimizer (optional) to enhance the performance of the panel. In **Figure 3.22**, a PV output panel is connected to the DC disconnect, then to the grid-tie inverter. The output of the inverter connects to AC the disconnect. In the case of 100 kW PV production, PV production monitoring should be used, otherwise the inverter is connected to the service panel at the load side with a double line or three-line circuit breaker. Finally, inverter output goes to the bidirectional kWh meter to the grid as depicted in **Figure 3.22**.

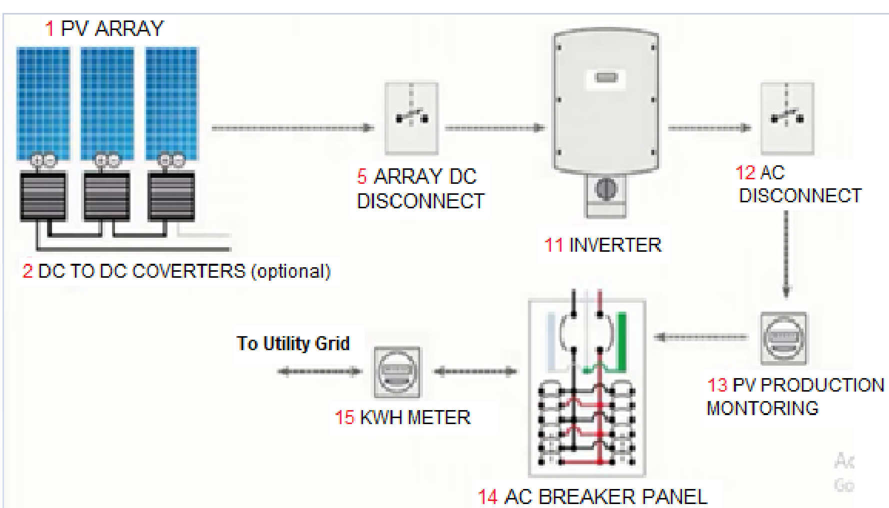

Figure 3.22: PV grid tie system

Grid-Tie PV SYSTEM with battery storage (DC-Coupled)

The first type of grid connected with battery storage is a DC coupling **Figure 3.23**. Firstly, it combines PV panels, combiner box, and DC disconnect. Then the power from the PV system goes to the charge controller. In the case of the battery, a usage charge controller is needed. A DC disconnect is applied between the charge controller and battery bank. An off-grid multimode inverter is installed and connected with service and backup panels during AC disconnect. This multimode inverter can send to and receive from the utility grid at the same time and to subpanel backup load. If the batteries are full, the solar panels will feed the load. If the load is less than solar production, the excess energy goes to the grid or not. The multimode inverter can charge the batteries from the grid; it acts as an inverter charger. When there is a power outage on the grid, the AC disconnect only feeds the backup load.

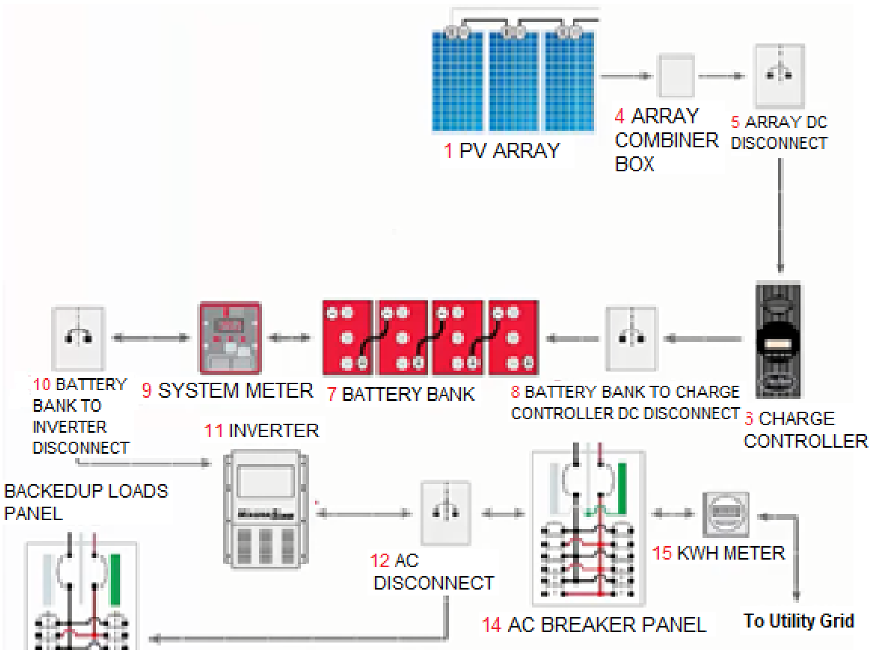

Figure 3.23: PV grid tie system with battry storage (DC-Coupled)

Grid-Tie PV SYSTEMS with battery storage (AC Coupled)

In this configuration, there are two inverters: grid-tied and multimode inverters. In a grid-tied inverter, the connection is the same as configuration three above, but here we add batteries, a multimode inverter, and a backup subpanel for the important loads such as lighting, some sockets, and a refrigerator in residential load **Figure 3.24**.

The PV panel will feed the main service panel. If the load is less than the consumption, then the excess energy is sent to the utility. In the event we need to charge batteries, the PV panels and utility are two sources: the main service panel and a multimode inverter (utility source) that depends on the load and the source. When the PV generation is more than the load and batteries need to charge, then it will be charged from PV, not from the grid.

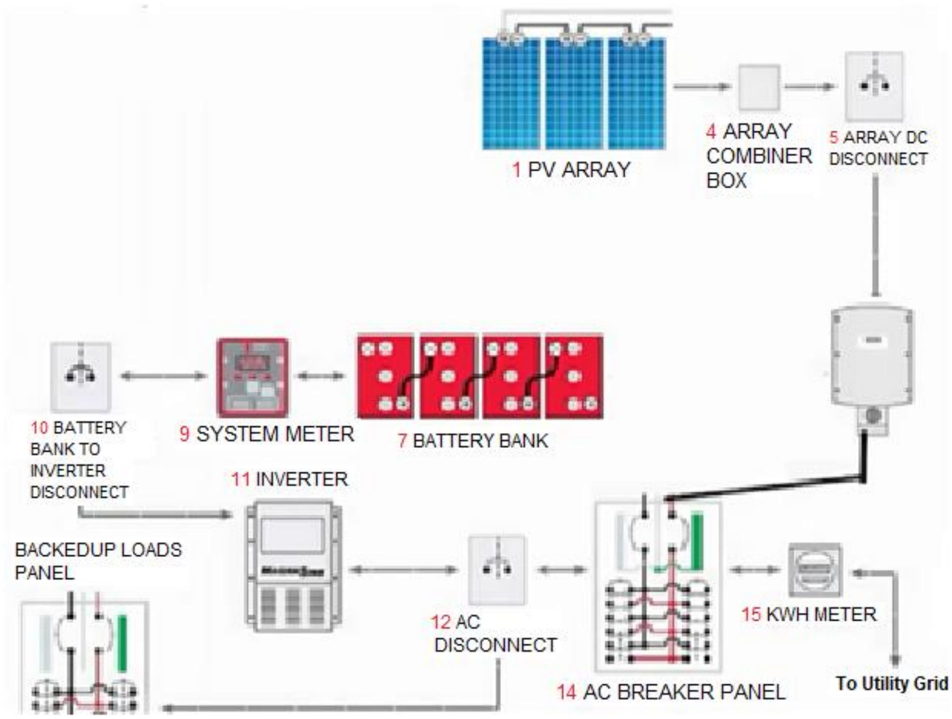

Figure 3.24: PV grid tie system with battry storage (DC-Coupled)

Factors influencing the annual performance of PV modules.

The power produced by a PV system depends on many factors influencing the annual performance of PV modules. The factors and their percentages are as follows:

Cumulative solar irradiance Surface orientation and tracking affect long-term irradiance profiles. In comparison to a latitude-tilt fixed system, this factor ranges from roughly a 25% reduction for a vertical surface to over a 30% increase for two-axis tracking. The impact of module orientation is taken into account.

Module power rating at standard test conditions A comparison of multiple PV technologies revealed that, given the same power rating, all technologies were similar in terms of annual energy generation within a 5% calculation error.

Maximum power point voltage dependence on irradiance level at low irradiance levels, a-Si and CdTe modules have a large value of the maximum power point voltage. This statistic alone might result in a 10% improvement in annual energy production.

Soiling Soiling may account for up to a 10% reduction in the annual energy production.

Variation in the solar spectrum On an annual scale, the impacts of the hourly change of the sun's spectrum essentially cancel out. The most sensitive technology to this impact is amorphous silicon, but the observed changes are usually less than 3%.

Optical losses when the sun is at a high angle of incidence (AOI) The optical losses are due to the increased reflectance of the cover glass of the PV modules for AOI greater than approximately 60%.

4. Methodology

The goal of this research is to design an optimal grid-connected hybrid renewable energy system, including biomass energy as a particular renewable energy source.

The microgrid was developed to provide electricity to a high-density residential district. For this, I used the following methodological procedures:

1. A survey study involves an investigation of the research area and geographic location based on the study area. Identifying renewable and nonrenewable energy resources in terms of energy balance and energy mix. Energy costs and load profiles are determined.
2. Developing mathematical formulas and using RE simulation software tools to assess energy outputs from a variety of renewable resources in the study area. The electrical yield is obtained as a result. Individual and integration maps depict each energy's potential.
3. Developing a mathematical model for calculating hybrid renewable bio-shared grid-connected system component capacities.
4. Use HOMER Pro (Multiple Energy Resources Hybrid Optimization) software to simulate microgrid experiments and generate an optimal solution.
5. Drawing a single line diagram of the network and the necessary connections.

4.1. Materials and data collection

An estimated evaluation is applied to determine the potential of available renewable resources in the GS, and then an integrated assessment is given. Recent meteorological observations and statistical data have been used for this purpose. The most recent available data of biomass resources in this study could be utilized to extrapolate the current situation, according to experts in this field. These data could be compensated by biomass amount variables to evaluate the energy yield and then compare the assessment results with the electrical energy demand at the corresponding time. The input biomass data consists of many arguments that vary due to population inhabitants and their activities. The second challenge encountered in data collection is the absence of a meteorological station in the study area. This problem is overcome by depending on neighboring area data, which is close in meteorological conditions to the interested study area.

Biomass data comprises statistical data pertaining to municipal solid waste (MSW), sewage sludge, and agricultural waste. Municipal waste, being the main dry biomass source (kg/person/year), was supplied by the Municipal Development and Lending Fund (MDLF). MDLF is a semi-governmental funding channel involved in the GS and is one of the 19 different waste recovery stockholders in 2017. Sewage sludge data, the sewage treatment station number, and treated water volume (m^3/day), were provided by the Palestinian Water Authority (PWA) in 2018, and by the Coastal Municipalities Water Utility (CMWU) in 2017. Data on agricultural waste was derived from the MoA in 2017. Agriculture data comprises annual yields of waste (kg/ha) of plants for 2013–2014 and animal dung production.

Solar energy harvested from the sun mainly depends on the irradiance reading (W/m^2), which is obtained using the solar energy tool in the ArcGIS 10.1 software maintained by the Environmental Systems Research Institute (ESRI). Furthermore, the diffuse solar radiation was obtained from the Photovoltaic Geographical Information Systems (PVGIS) dataset (Choi et al. 2019, PVGIS 2021).

Because Ashdod has a similar climate to Gaza, the meteorological input data used for wind energy potential are taken from Ashdod data for the years (1991 to 2010). Ashdod is located in the Mediterranean coastal area, 30 km away from Gaza at the same elevation. The wind speed data at 10 m height can reach over 13 m/s for a few hours on certain days. Most of the time, the wind comes from the sea; this means from between south–southwest and north–northwest. Based on wind speed meteorological input data, most readings lie between 2 and 6 m/s; the average speed reading mostly exceeds 4 m/s, while the highest recorded readings are in February and September (Juaidi et al. 2016, PENRA 2020).

The calculation of wave potential relies on the value readings recorded by the Centre for Meteorology of the Ministry of Transport and Communications in Gaza. Values are presented for the period 2001–2006 taken at the "Gaza Station". The minimum and maximum values of the average wave period (3.2–3.6 s) were recorded in 2006 and 2001, respectively; the minimum and maximum values of the average wave height (56.1–67.0 cm) were recorded in 2005 and 2001, respectively (MTC 2021).

GEDCo provides residential demand energy costs (US$/kWh) as well as electric data for the district, such as the annual electrical consumption load profile for 2020 and utility grid details. institute provides an overview of the energy sector and the legal and institutional framework of duties. additional to a national strategy objective of the energy sector in Palestine (2017-2022), including diversification of resources, energy exchange with neighboring countries, energy mix, and energy balance. The cost and manufacture of the selected system components were inserted depending on the local market price and the private companies' working in solar system installation and distributed diesel generator operators.

4.2. Renewable resources assessment

Estimation procedures involve four sources of renewable energy: biomass, solar, wind, and wave.

4.2.1. Biomass assessment

Proposed equations formulas are developed to assess potential biomass-based energy production in the GS. The energy production was derived from the equations calculating the annual energy (MJ/year) of the biomass resources over a given year(s).

Municipal Solid Waste

The GS currently operates three main landfills, located in Gaza, Deir Elalah, and Rafah. MSW material can be generally categorized as compostable, recyclable, or inert. The compostable category (organic fraction) includes food waste, residues from the vegetable market, and garden waste. Recyclables are comprised of paper, plastic, metal, and glass. Inert is the fraction of MSW which can neither be composted nor recycled.

A high organic content of around 65% for the solid waste is depicted in equation 4.1. This percentage is an indication to calculate the density of the waste and the amount of gas that would be obtained from an anaerobic bio-thermal conversion (MDLF 2017). The biogas production has been selected since most of the organic waste in Gaza is quite wet and the technology is relatively simple to apply (in comparison to a combustion process with a steam cycle). The methane (CH_4) yield from MSW was measured and converted to energy using Equation (4.1):

$$SY_i = \sum SW * \frac{SP}{ST} * 0.65 * G_P \qquad \text{Eq. 4.1)}$$

SY_i (MJ/year) represents the local energy output from municipal organic solid waste, SW (ton/year) represents the total MSW in the study area, i represents the time period, which is one year in our case (2015), SP (ton/year) represents the local quantity of one landfill, and ST (ton/year) represents the total quantity of MSW across all landfills in the study area. G_P is the methane production (Nm^3/ton vs.) (Sumit Sharma et al. 2014), where 1 m^3 CH_4 = 36 MJ (Thomas Amon et al. 2007).

On the other hand, the considered energy from the remaining inorganic amount of MSW, some of the fractions of MSW that are not compostable, not recyclable, and reusable but could be combusted, was determined based on (Kitani and Hal 1989), using Equation (4.2):

$$GY_i = P * (0.23) * Y_a * AVH \qquad \text{Eq. (4.2)}$$

GY_i (MJ/year) is the lower heating value of waste burning, i is the time period (2015), P is the population, taking into account that only 23% of total waste will be burned, Y_a is the average waste production per capita (kg/year), and AVH (MJ/kg) is the average calorific value of the MSW.

Sewage in Wastewater

Sewage sludge originates from three primary wastewater treatment plants located in the areas of Beit Lahia, Gaza, and Rafah, as well as two intermediate treatment plants in Khan Younis (Mawasi) and the Wadi Gaza wastewater treatment plant (WWTP). According to a study on anaerobic digestion of sewage sludge (Al-Najjar et al. 2020), the long-term potential for methane production and its energy output from local sewage sludge (ton/year) was calculated using Equation (4.3):

$$WY_i = (0.69) * P * \frac{S}{W} * Y_a * G_p \qquad \text{Eq. (4.3)}$$

where WY_i (MJ/year) is the annual energy output that could be generated from waste water treatment plants, *i* is the time period (2015), *P* is the number of inhabitants connected to the waste water network, which is equal to 69% of local people, and the wastewater network covers an area equivalent to 69% distributed among the GS Governorates (PWA 2016). Cesspits will dispose of water from areas that are not connected to wastewater networks. Y_a(kg/year) is the average per capita wastewater generation, S/W is the sludge wastewater (SS) ratio, and G_p is methane (Nm^3/ton vs.) production, where 1 m^3 CH_4 = 36 MJ.

Residues in Agriculture

Agricultural land is about 16,400 ha, according to the MoA annual report 2013–2014, classified into 5600 ha of vegetables, 8000 ha of garden trees, 2800 ha of field crops, and 20.8 ha of herbs (MOA 2018). On the other hand, the production of agricultural waste amounts to around 1197 tons of organic waste per day. Research in (Babaee and Shayegan 2011) obtained the amount of methane released by anaerobic digestion of vegetable and fruit waste. The total amount of methane produced from garden trees was calculated according to (Murphy et al. 2011) method. The biogas can be produced from crops and herbalists was obtained from Letomaki (Lehtomäki 2006). Using Equation (4.4), the methane generated from anaerobic digestion can be detected for agricultural land and its energy production.

$$PY_i = \sum(\int * Y)_i * G_p \qquad \text{Eq.(4.4)}$$

where PY_i (MJ/year) is the energy output of the plant area, $\int$ (ha) is the area, Y_i (kg/ha) is the average plant waste yield, *i* is the time period (2017), and G_p is the methane production from vegetable waste (Nm^3/kg vs.), where 1 m^3 CH_4 = 36 MJ

Production of animal waste in Gaza comes from sheep, goats, camels, cattle, calves, rabbits, and poultry. Poultry types in the study area are broilers, layers, broiler mothers, and turkeys. Broilers refer to the chicks that can be kept to produce white meat, with 50 days as a maximum period. Layers refer to the chicks kept to produce table eggs, typically not longer than 30 months in life span. Based on methane yields obtained, the amount of methane from livestock units was evaluated and implies anaerobic digestion (Díaz-Vázquez et al. 2020). The density of veal, ovine, and poultry manure is 103, 103, and 970 kg/m^3, respectively (Thomas Amon et al. 2007). The total volume of methane in the animal waste and the energy yield were determined using Equation (4.5).

$$AY_i = \sum L_f * Y_f * G_p \qquad \text{Eq. (4.5)}$$

where AY_i (MJ/year) is the potential energy output of a livestock farm, i is the time period (2013–2014), L_f represents the farm's livestock unit, Y_f (m^3) is the daily waste yield from the livestock, and G_p is the average methane production from animal waste (Nm^3/kg vs.), where 1 m^3 CH_4 = 36 MJ.

The potential energy$B_{int}(\mathrm{MJ/year})$ derived from biomass was assessed using Equation (4.6). The method suggests anaerobic digestion, but combustion will be carried out on non-organic MSW. **Figure 4.1** shows the incorporated energy (MJ/year) from the different biomass sources in the work area. It is worth noting that digested animal organic waste after biochemical treatment can be used as compost.

$$B_{int} = \sum(SY_i + GY_i + WY_i + PY_i + AY_i) \qquad \text{Eq. (4.6)}$$

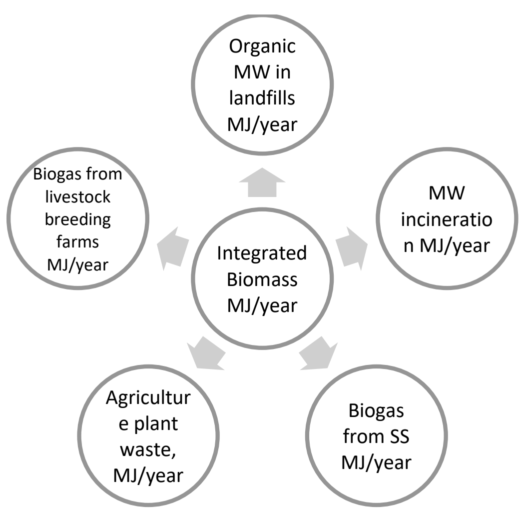

Figure 4.1: Integrated energy (MJ/year) from available sources of biomass in GS.

4.2.2. Solar Energy Assessment

GIS methods are used for solar radiation modelling. ArcGIS 10.1 (ESRI) has a module for calculating solar radiation in a given area. The characteristics of the analyzed area are derived from a Digital Elevation Model (DEM) (Tar et al. 2015). The DEM is obtained from the Shuttle Radar Topography Mission (SRTM). The solar radiation module uses a predicted coordinate scheme, which can then calculate the inclination angle of the sun's radiation. The diffuse radiation values were obtained from the PVGIS dataset and from the Tar and co-workers' method (Tar et al. 2015), respectively. A PVGIS is an open-source online tool to assess the solar electrical energy production from a PV system; consequently, a solar radiation map of the GS was created.

A generalized procedure was defined to convert the solar energy potential into energy output using Equation (4.7).

$$PV_r = \eta_{pv} * A_{pv} * GR_i \qquad \text{Eq. (4.7)}$$

where PV_r (kWh/year) is the solar energy potential in the study area, η_{pv} is the efficiency of the PV array, A_{pv} is the area of a PV module (in m^2), GR_i (kWh/m^2/year) is the amount of global radiation in a given governorate, and *i* is the modelled period for one year (2016). The output of a PV system needed for an average household in the GS is 2.86 kW. In this study, crystalline silicon technology PV system were modelled with a 1 kW capacity and a 7.0 m^2 roof area for each. Total solar energy potential is estimated based on the number of study area households, and one PV system was assumed for each dwelling.

4.2.3. Wind Energy Assessment

WindSim 9.0.0 software (https://windsim.com/) was used to estimate the wind energy. The software has been developed by the Norwegian company Vector AS. The software is based on computational fluid dynamics (CFD) simulations of wind flows and requires a high-resolution DEM of the region. The input wind parameters for the simulations included the eight-wind direction speed based on the wind measurements at Ashdod Station (1991 to 2010), refer to Section 4.1. The wind turbine installation depends on authorities' permits and environmental regulations. In addition to territorial environmental consideration restrictions (Benedek et al. 2018). Turbine locations were then entered into ArcGIS.

The areas suitable for wind farm installation were determined based on the methods of Staffell and Pfenninger (Staffell and Pfenninger 2016), while the total wind energy production was estimated (Benedek et al. 2018) using Equation (4.8):

$$W_{pot} = \int_i * T_p * T_m \qquad \text{Eq. (4.8)}$$

where W_{pot} (MWh/year) is the wind power produced locally, $\int$ (km^2) is the area available for wind turbine installation, and T_p is the turbine performance (MW/km^2). The utilized fraction of the wind potential depends on many ecological factors and was estimated at 5 MW/km^2, while it decreases in the mountains (2009, Benedek et al. 2018). T_m is the turbine performance of a given area in the WindSim 9.0.0 simulation. The T_m values reflect the average output of the 400 kW (low capacity) turbines from Vestas WD34, expressing a mean potential value not limited by the investment scale.

4.2.4. Wave Energy Assessment

The west coast of the GS, 31.192°–31.354° N, 34.138°–34.293° E, has a coastline which is roughly 41 km long. The GS overlooks the Mediterranean the West and extends from the South to the North, making Gaza an exploitable area for renewable wave energy (El-Zaza 2009). The GS coast is located in the eastern Mediterranean region. A very high-resolution integrated atmospheric/wave modelling system was developed for simulating the atmospheric circulation and sea wave evolution in the area over a period of 10 years in the Levantine Basin, Eastern Mediterranean and is presented in Zodiatis et al. (Zodiatis et al. 2014a). The most energetic offshore areas of the Levantine Basin are characterized by a relatively low 10-year mean wave energy potential of about 2.5 kW/m and show a generally stable yearly behavior of wave power values. The wave model WAM, ECMWF (European Centre for Medium-Range Weather Forecasts) (https://www.ecmwf.int/), version CY33R1 has been used (Janssen 2000, 2004). The wave energy potential is affected directly according to the control and simulation of two main parameters, which are the considerable wave height and wave energy period.

The state of the sea/ocean, the installation and maintenance of mechanical and electrical equipment, as well as its efficiency, type of bed sea, and other factors are all important considerations when deciding on a wave energy conversion (WEC) system and the power produced (Alamian et al. 2014). WEC systems have been developed to extract energy from the shoreline out to the deeper waters offshore. These devices are generally categorized by the installation location, such as shoreline, near-shore, and offshore, and the Power Take-Off (PTO) system (Rodrigues 2008).

The annual available energy (AAE) density, in MWh/m, is used as a site's resource parameter (Neary et al. 2018). The wave energy period (T_e) and considerable wave height (H_s) are ultimately determine the wave power density (J) of the specific site. The factor for random waves is 1/16, as opposed to 1/8 for periodic waves:

$$J = \frac{\rho g}{16} * H_s^2 * C_g(T_e, h) \qquad \text{Eq. (4.9)}$$

where C_g is the wave group velocity, which is a function of distance (the depth (*h*)) and wave energy time T_e. The AAE density is calculated as a function of peak cycle (period) time (T_p):

$$AAE(T_p) = T_{year} \sum J(T_p) f(J, Tp) \qquad \text{Eq. (4.10)}$$

where T_{year} is the number of hours in a year (8766h), and $f(J, Tp)$ is the combined probability of the partitioned wave power density J and peak cycle time T_p. The total AAE density is gathering over all peak time:

$$AAE = \sum AAE(T_p) \qquad \text{Eq. (4.11)}$$

The average annual power density of shoreline waves is determined by dividing the total AAE density in MWh/m by the number of hours in a year, assuming no energy conversion losses. The annual means for a typical period (2001–2006) of J, H_s, and T_e are 1.29 kW/m, 61.6 cm, and 3.4 s. The equivalent absorbed power (kW) produced from the simulation of point absorber simulation in OpenWEC is evaluated by the force of 8 × 10^3 N and 5 m depth.

4.3. Proposed system and mathematical model

Research proceeds on to the third stage in this section after evaluating the potential of energy resources, especially renewable resources. This step is contingent on the results of the second step, which demonstrated that solar and biomass are the most abundant resources that can be integrated into a grid-connected system. As a consequence, a mathematical model is used to estimate the capacity of the hybrid system components, and a hybrid biomass-solar grid-tied system is exhibited.

The Hybrid Renewable Energy System (HRES) is configured to provide maximum residential AC loads. Depending on the outcomes of the step before, solar and biomass are candidates to share in the desired system. A grid-tied system of solar and biomass renewable sources involves a diesel generator and lead-acid chemical battery storage as back up, as maintained in **Figure 4.2**. Biomass is incorporated as a renewable resource into a hybrid renewable system by using a biogas engine generator. The study assumes anaerobic digestion technology to produce biogas from biomass.

For the electrification of the load demand, the hybrid system utilizes existing public grid infrastructure. The grid provides the microgrid at night. While sunrise and sunset, battery storage and two generator types are used as backups, the system contains several options to satisfy stability and minimize battery dependence.

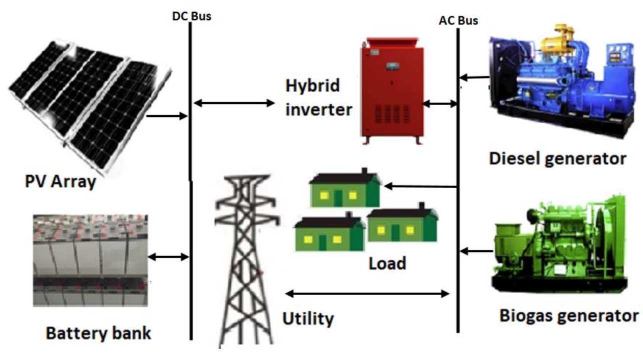

Figure 4.2: Architecture of the desired HRES

The solar system installation assumes a centralized photovoltaic plant because our study involves microgrid implementation to use renewable resources and support the grid while using its infrastructure. Land scarcity, management and control issues are concerned. Many advantages of a centralized method are discussed in the distribution of similar PV capacity (Kasaeian et al. 2019).

4.3.1. Mathematical model and sizing system

Grid-Connected Hybrid System

The structure of the grid-connected HRES is shown in **Figure 4.2**. It is composed of a PV array of a three-phase DC-AC converter, a biogas engine, a diesel generator, and battery storage. In general, the most common methods for sizing a hybrid system are empirical, analytical, and numerical. Most significantly, weather data for the specific location and end user requirements where the system will be mounted are essential to ensure that the sizing method is correct as explained in the next chapter. Generally, system design entails optimising the size of the system components, the size of the PV system, the size of diesel and biogas generators, and the grid ability. It is important to determine the size of a hybrid system for a specific application in order to achieve the best return on investment (ROI). The determination of the designed system of residential load for the expected lifetime would help to reduce economic waste (V K Sharma et al. 1995).

In this section, sizing the hybrid renewable systems that are connected to the utility grid is focused on. This can be achieved depending on the most commonly used techniques intuitive method in the literature. For HRES sizing, the intuitive relies on the hybrid designer's experience in sizing and will be involved with analytical and mathematical equations. In brief, the intuitive method involves estimating the daily load demand, optimizing the tilt angle, calculating the size of the PV system, and determining the size of the battery bank using simple mathematical equations. Similarly, the size of system components can be determined by considering their efficiency and the maximum AC power that can be delivered.

Figure 4.3 provides a summary of the main steps involved in sizing a grid tied HRES system. Sizing the system is done assuming all modules are identical. N is the number of modules, if the located area to install the system is available, then the $P_{\mathrm{PV,array}}$ can be determine using the daily load energy required $E_{req,day}$ and has to be devided by the PSH. Otherwise, the equation of the area under consideration as a variable is required. Module efficiency has to be used. PSH can be determined by dividing global incident irradiation (G_t) over square meters by irradiance at the STC for the worst calendar month of the year, section 3.5.1. The rated power harvest of the PV array takes into account the system efficiency. The system efficiency involves the efficiency of the cables, inverters, and batteries.

Moreover, the battery capacity (Ah) considers the number of days of autonomy $N_{aut}$and DOD_{max} the maximum depth-of-discharge of the batteries, Or can be obtained by dividing total energy of the battery $\mathrm{E_{Tbatt}}$ by the DC system voltage $\mathrm{V_{DC,sys}}$. The total number of batteries is determined by the total energy required from the batteries divided by the individual energy of each battery. The number of batteries connected in parallel $N_{p,batt}$and in series $N_{s,batt}$can be calculated depending on the $V_{DC,sys}$.

The bio-engine generator values totally depend on the biogas locally generated in the plant and collected in the store. The biogas is assumed to be anaerobic digestion of the municipal waste or biomass in the desired hybrid system. The diesel generator is more reliable in spite of its high operating cost. The diesel generator (s) operates in the morning and evening, and the minimum load required has to be met at the third capacity of the generated power from the generator.

Start

Daily energy required ($E_{req,day}$)

Determine location, meteorological data, PSH

$$P_{PV,array} = {}^{E_{req,day}}\!/_{PSH} \times \eta_{system} \qquad \text{Eq. (4.12)}$$

$$\eta_{system} = \eta_{cable} \times \eta_{invs} \times \eta_{batt} \qquad \text{Eq. (4.13)}$$

Determine $V_{DC,sys}$, P_{invs}

$$N = \frac{P_{PV,array}}{Panel_{pk}} \qquad Eq.\ (4.14)$$

$$Batt(Ah) = \frac{\frac{E_{req,day}}{V_{DC,sys}} \times N_{aut}}{DOD} = \frac{E_{Tbatt}}{V_{DC,sys}} \qquad \text{Eq. (4.15)}$$

$$N_{T,batt} = \frac{E_{Tbatt}}{E_{batt}},\ N_{s,batt} = \frac{V_{DC,sys}}{V_{batt}},\ N_{p,batt} = \frac{N_{T,batt}}{N_{s,batt}} \qquad \text{Eq. (4.16)}$$

$$G_{Bio}, G_{Dsl}$$

Figure 4.3: Mathematical model steps of components sizing

4.3.2. Major components of a hybrid system

PV system:

A photovoltaic system mainly consists of an array of photovoltaic modules or panels, inverters, batteries (for off grid) and interconnection wires. However, the balance of system (BOS) components in a PV system include mounting materials for the modules, wires, distribution panel, junction box, lighting protectors, grounding connections, battery fuses, battery cables, and battery containers. In general, PV systems can be grouped into grid-connected or autonomous (or stand-alone) systems. The national electricity grid is not linked to a standalone or autonomous PV system. The key components of this system are depicted in **Figure 4.4**:

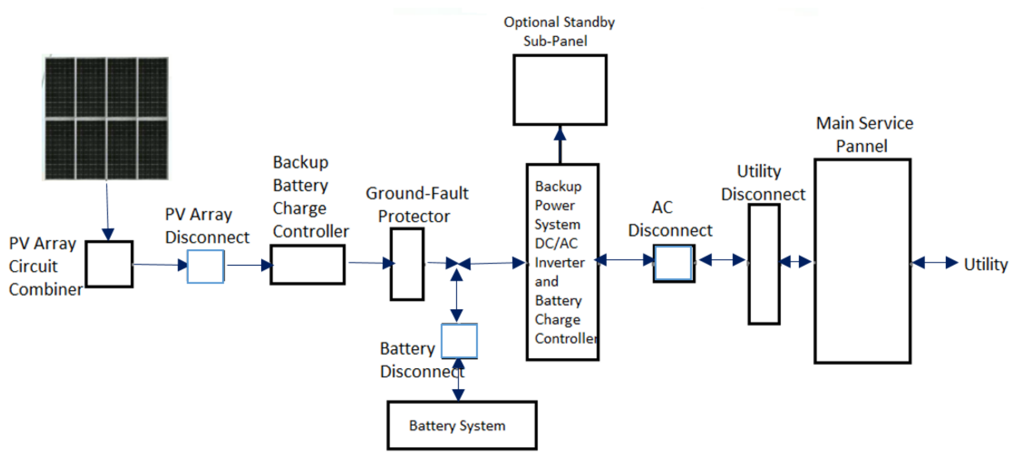

Figure 4.4: Block diagram of PV system with battery backup

A PV system has a DC circuit that requires a special design and equipment. It can have multiple strings, and special disconnects are required to isolate components. Energy flows in such systems could be bi-directional as depicted in **Figure 4.4**. Utility-Interactive PV systems require an interface with the AC utility grid and special consideration must be adopted. Thus, in the following description, the main parts of the PV system and the required calculations employed to determine its component capacity are displayed.

PV module:

Solar power is an abundant, sustainable, and clean source of energy. PV modules harvest the solar energy and convert it into electricity. Manufactures and ambient factors affect the energy collected. Temperature, solar radiation, and the module efficiency arise in HOMER equations to calculate the power output of a PV array (Kasaeian et al. 2019) (Mandal et al. 2018). The average temperature effect in the specified study area would not have considered the output solar energy, since its average is around 20.99 °C, while the temperature coefficient of power is −0.25%/°C at the standard test conditions (STC) (25 °C), hence the PV output energy is

$$E_{pv} = Y_{pv} f_{pv} \times PSH \qquad \text{Eq.(4.17)}$$

And,

$$\text{PSH} = \left(\frac{G_T}{G_T.STC}\right) \qquad \text{Eq. (4.18)}$$

Where

Y_{pv} (W): Rated capacity of the PV panel,

f_{pv} (%): De-rating factor of the panel due to ambient factors such as dust, shadow, wiring energy losses and others, it is taken as 0.85

G_T (Wh/m^2): Solar radiation incident on the PV array,

$G_T.STC$ (W/m^2): Irradiation at STC (25 °C).

The hybrid system design uses a Canadian Solar 400 Watt, 37.2V Mono-crystalline Solar Panel with 132 [2 X (11 X 6)] (SOLAR 2020), Appendix A. The fixed-mounted installation of the modules is assumed at the optimal tilt angle above the ground equivalent to 29° of the site latitude, 31°30' in Palestine, and south-facing in the north earth part with an azimuth angle of zero according to the (Abdallah et al. 2020) study.

The cost of a solar PV module is determined based on the local market price. It depends on the brand, manufacturer, technology (e.g., mono-crystalline), and the size of the panel. The lifetime of the PV array is set to 25 years. The cost of the module in the local market at this time is 75US$. Considering that the wattage tariff for solar panels is the same as the IEC slandered, which is US$0.25/W. The total module cost includes installation and accessories, maintenance, and replacement costs. Table 5.7, section 5.5 displays in detail these values. The replacement cost is taken as zero as the project life equals the module lifespan. The electrical data sheet of the module can be found in Appendix A.

Inverter

This device is responsible for converting the PV panel's direct current (DC) into an alternating current (AC) that can be fed to the residential load or the utility grid. A-three phase inverter is applied. The function of a three-phase inverter is to manipulate the input DC voltage and current with switching signals to change it into the desired three-phase AC current.

The inverter system can be successfully connected to the grid if two steps are accomplished. First, the inverter system should start to generate three-phase voltage that has the same magnitude as the grid side voltage in isolation from the grid using a transformer. Second, the inverter system output has the same frequency and same phase as the grid. to connect the inverter to the grid at the moment.

A hybrid inverter, or a hybrid grid-tied inverter, is an electrical converter that converts the direct current (DC) generated by solar panels into alternating current (AC) and vice versa in a so-called battery-based inverter. Residential loads operate with AC current, which is fed by the utility grid. Each household electricity subscription is supplied with 32 A of electric current as a fixed capacity measure for each power meter. Hybrid inverters therefore operate multiple modes and dual functionality such as on grid, off grid, as well as hybrid (with or without grid), and backup that enable energy management. In a hybrid system, different types of energy generators could be supplied to the inverter but a single current supply to the load as the output of the inverter (Muh and Tabet 2019). Inverter capacity was preemptively determined to be higher than the peak nominal AC load requirement. The inverter capacity can be obtained by using equation 4.21 (Hossain et al. 2020).

$$C_{inv} = \left(\frac{L_{max}}{\eta_{inv}}\right) \times \sigma_{sf} \qquad \text{Eq.(4.19)}$$

Therefore, 10% compensation for inverter efficiency and safety factor σ_{sf}. Where L_{max} is the AC_{max} load (kW), η_{inv} is the inverter efficiency, and σ_{sf} is the safety factor. For hybrid system design, a 30 kW BLUESUN solar power hybrid inverter on-off grid is considered. Technical specifications for the instance of utility-interactive mode in **Table 4.1** are retained (BLUESUN 2016). Based on website data, the purchase price of the hybrid inverter depends on capacity (kW), number of units, application (on/off grid), and manufacturer specification. The capital is the same as the replacement cost of the inverter is US$5000 per unit in the local market as shown in **Table 5.7** section 5.5. The lifetime is assumed to be 15 years, the line efficiency is 95%, and there is zero maintenance cost per inverter.

Table 4.1: Technical specifications for instant of utility-interactive mode

Parameter	Specification
Model	BSMG2-30K-EX
DC Input	
Battery voltage range	400V(250~520V)
Batter DC Max Current	90A
PV Voltage Range	520~900V (MPPT 520V~800V)
PV DC. Max Current (in case of completely consumption)	116A
AC Output	
AC voltage	400V(340V~460V)
AC current	44A
Nominal power	30kW
AC frequency	50/60Hz(±2.5Hz)
Output THDI	≤3%
AC PF	Listed: 0.8~1 leading or lagging (Controllable) Actual: 0.1~1 leading or lagging (Controllable)

Charge Controller:

A charge controller or a charger regulator aims to control the rate of current flow into and out of storage batteries. This is done to prevent overcharging and deep discharging of the battery, which can severely reduce battery performance and lifetime.

Battery Bank:

Batteries are the heart of an autonomous solar electric system. They are the reservoirs for storing electrical energy. The size of a battery is measured in terms of its storage capacity in amperehours (Ah). There are different types of battery technologies, including lithium ion, lead acid, nickel cadmium, and many others. The depth of discharge (DOD) is the amount a solar battery is discharged. Lead-acid batteries are the most convenient choice based on cost. It is widely utilized in solar systems, while Li-ion batteries are suitable for electronic appliances. **Table 4.2** displays the main characteristics of these batteries (Lasseter 2007).

Li-ion batteries, as shown in **Table 4.2**, are less sensitive to high temperatures and require fewer cells in series to achieve a given voltage compared to lead acid, Also, it has a high efficiency because they do not have deposits every charge/discharge cycle. The only disadvantage is the high cost.

Table 4.2: Comparison between three different types of battery technologies

	Lead-Acid	**Ni-Ca**	**Li-ion**
Cell voltage	2	1.2	3.6
Specific energy (Wh/kg)	1-60	20 - 55	3 - 100
Specific power (W/kg)	< 300	150 - 300	100 - 1000
Energy density (kWh/m3)	25-60	25	80 - 200
Power density (Wh/m3)	< 0.6	0.125	0.4 - 2
Maximum cycles	200 - 700	500 - 1000	3000
Discharge time range	>1 min	1 min – 8 hr	10 sec – 1 hr
Cost (US$/kWh)	125	600	600
Cost (US$/kW)	200	600	1100
Effeciency (%)	75-90	75	99

Chemical storage BAE SECURA PVS solar Vented lead-acid battery (VLA) battery model is a candidate from the HOMER catalog depending on nominal voltage (V) and maximum capacity (Ah) (SOLAR 2020). A Lead–acid battery consists of lead dioxide as the positive electrode and a negative electrode with a separator to isolate both electrodes. BAE solar batteries are used in renewable energy applications such as photovoltaic power generation, hybrid applications, as well as stand-alone photovoltaic systems. A battery bank is important for backup hybrid electric systems (HES) in parallel with electric generators. In this work, a kinetic model, battery storage system is sized to meet the load demand of one night, thereby one day of autonomy. Battery sizing depends on many factors, such as depth of discharge, battery capacity and efficiency, and battery system voltage. The battery system energy P_{Batt} can be calculated based on equation 4.22 (Hossain et al. 2020).

$$P_{Batt} = \frac{P_{load} \times T}{DOD \times \eta_{Batt} \times \eta_{DC-AC}} \qquad \text{Eq. 4.20)}$$

Where P_{load} is the daily demand electrical AC load, T the backup time as days of autonomy, DOD the depth of discharge, $\eta_{Batt}, \eta_{DC-AC}$ the efficiencies of the battery and the AC load conversion respectively. DOD is an important capacity of battery bank selection that tells how deeply the battery is discharged along with the battery state of charge (SOC), where $\mathrm{DOD} = 1 - \mathrm{SOC}$ (Ahmad and Alam 2018), and it is set to 50%, as depict in **Figure 4.5** which mean 3000 life cycles of the battery during its life time. Less DOD leads to higher battery lifetimes. The number of batteries in series and parallel depends on the DC system bus voltage that is equal to 48V in the system designed (Hossain et al. 2020). **Table 4.3** and **Table 5.7** (section 5.5) summarize the technical and costs specifications details of BAE solar battery.

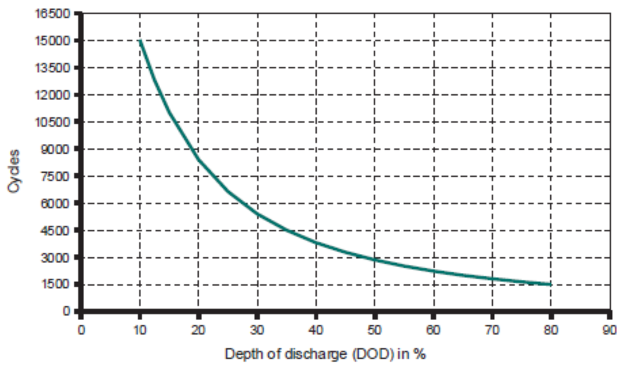

Figure 4.5: Number of cycles as function of depth of discharge

Table 4.3: Technical parameters of the battery

Parameter	Unit	Value
Maximum Capacity	Ah	$2.46 * 10^3$
Nominal Voltage	V	2
Max. Charge Current	A	376
Max. Discharge Current	A	$2.56 * 10^3$
Roundtrip efficiency	%	85
Min. storage lifetime	yrs	5

Diesel generator

Diesel generators also act as a backup in this work to increase the reliability and effectiveness in meeting peak load demand. Engine generators in HRES which are grid-tied could reduce dependence on the storage system, specifically at times when renewable sources are unavailable or frequent grid outages occur (Kasaeian et al. 2019). In addition, the reduced burdens of battery disposal and short lifetime have to be mentioned. Diesel price is about 1.3US$/L in Gaza. A Caterpillar 25 kW diesel generator will be used for the simulation (Caterpillar 2020). The capital cost of each generator is evaluated using information from the manufacturer’s website, while operations and maintenance costs are 4.0 US$/op.hour, which was estimated from common market prices in the country.

Biogas generator

Energy could be extracted from biomass by using a variety of conversion technologies such as boilers with a steam-cycle or a gasifier coupled with an engine. In a boiler, direct combustion of the biomass is performed to generate steam and superheated steam to operate a turbine in a CHP station (Nunes et al. 2017) (Jahangiri et al. 2018). A gasifier converts the biomass into purified producer gas through a combination of a gasifier followed by a purifier (Jie et al. 2019), while the digester in biogas technology produces biogas through an anaerobic digestion process. The use of gasifier or digester to produce biofuel depends on the volume of biogas required to the application, type and scale of the project, converting process time, biomass type, and cost (Kasaeian et al. 2019).

In a small scale project and relatively high organic continent as well as moisture of the biomass, digestion is favorable to gasification to produce biogas in a biological process namely anaerobic digestion. The biogas can be used in combustion engine that is coupled with a generator and a controller to generate electricity.

In HOMER, the term "biogas" refers to gasified biomass. Biomass gasified via thermo-chemical gasification or biological processes such as digestion. The product can be called one of several different names, including synthesis gas, syngas, producer gas, or wood gas (HOMER 2019). This is in contradiction to scientific literature (biogas for anaerobic digestion, product/producer/syn-gas for gasification). Biomass feedstock in the study area combined of municipal waste, agricultural residue, and animals' dung.

The hourly output energy produced from the biogas digester system is evaluated by the equation 4.23 according to the reference (Chauhan and Saini 2017).

$$E_{BGG}(t) = \frac{Biogas\ availability(m^3/day)\times CV_{BGG}\times \eta_{BGG}\times \Delta t}{860\times h_{BGG}} \qquad \text{Eq. (4.21)}$$

Where, E_{BGG} is the energy output of the biogas digester; η_{BGG} is the system conversion efficiency. CV_{BGG} is the biogas digester calorific value (4700 kcal/kg) and it is divided by 860 to convert kcal to kWh (1 kWh = 860 kcal), $h_{BGG}$is the operating hour of the biogas generator (alternator) in a day (Anand et al. 2019).

The capital, replacement, and maintenance costs of a 10 kW and 25 kW biogas generator were set at US$2800 and US$5000 (ONEW 2020) as shown in **Table 5.7** section 5.5. The generator's lifetime hours have been set at 9125hr of operation. And the minimum load ratio was assumed to be around 20% of the capacity.

4.4. HOMER Pro

The HOMER tool software is the global standard and has been employed for developing and analyzing microgrids from an early stage. initially in the national renewable energy Laboratory of the US Department of Energy (NREL, USA). HOMER focuses on both off-grid and grid-connected hybrid renewable microgrids (Duman and Güler 2018) (Sawle et al. 2016), incorporating various sources of energy and storage, such as biomass with photovoltaic and batteries. Chronologically conducted, three main tasks are simulation, optimization, and sensitivity analysis to derive techno-economic decision analysis (Sinha and Chandel 2014). Throughout the year, the HOMER configured the system in terms of component prices, percentage of renewable energy use, carbon emissions, and electrical loading specifications. Considering the on-grid hybrid system, excess electricity generated can be sold back to the grid. This in turn increases reliability, affordability, and quality of electrification for HRES design and planning and the cost-effectiveness of the contribution of biomass in such a hybrid system. HOMER lists the optimal system configuration, defined as the one with the least Net Present Cost (NPC) and Cost of Electricity (COE), and then results in this work were refined further by performing sensitivity analysis on parameters such as fuel price, load size, reliability requirement, biomass potential, solar irradiance, and variations to optimize the system under different conditions. Renewable solar and biomass resources are considered for this purpose, while battery storage and generators (diesel and gas) are used as device backups. Simulations are carried out at the lowest cost to meet the load requirement and provide a general structure to be applied to other clusters in the same area.

Many studies of renewable hybrid energy generation have used similar methodology, according to a review of the literature (Sawle et al. 2018) (Ayodele et al. 2019) (Rad et al. 2020). The selected and applied methodology involves important and necessary criteria so that the evaluation of the optimum system design can be analyzed correctly. The input data involves determination of the intended location as well as conventional and renewable resources of energy as the first step of the techno-economic feasibility analysis of the hybrid system for electrification. **Figure 4.6** shows the optimum analysis process of HRES in HOMER. The required input data, such as an electric load profile, geographic location, and resources available in a specific area, are defined here. After identifying the hybrid system components and gathering the technical, size, and economic information about these hybrid system components, the simulation process is started (Azerefegn et al. 2020). Based on the results, it can be decided whether or not the previous inputs meet the load requirement. If the component size is not adjusted, the optimization is achieved by simulation to obtain the techno-economically optimum system sizing. The sensitivity analysis evaluates the effects of system parameters on the whole process, such as fuel price and irradiation values. The output of the economic results, such as COE, total cash flow, and NPC, was then presented in ascending order. Excess energy fraction, fuel consumption, and renewable source contribution are calculated.

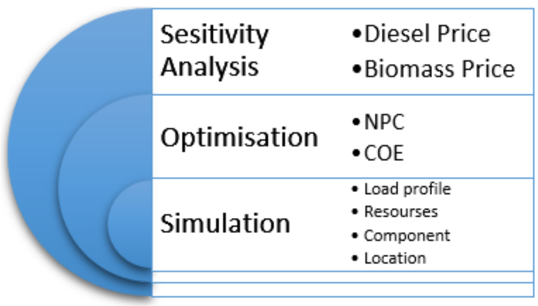

Figure 4.6: Simulation, Optimization, and Sensitivity Analysis in HOMER

4.4.1. Simulation, optimization, and sensitivity analysis:

Firstly, using the HOMER Pro simulation stage over time steps of the year, in each interval balance calculations are performed by comparing demand to the energy produced by the system and calculating the flow of energy to and from each component of the system. The component controller specifies the HOMER system operation during the simulation in what is called a dispatch strategy or control algorithm. In the case of multiple controllers added to the model, the results are optimized and comparable performances are presented. For example, HOMER determines how to run the generators and whether to charge or discharge the batteries at any given interval in systems including storage and fuel generators. Also, the life-cycle cost of the system is determined at this stage (Lambert et al. 2006). At the optimization process, two optimization algorithms of HOMER Pro simulate the system configurations in the search space and rank the feasible ones via Total Net Present Cost (TNPC), sometimes called life-cycle cost, that can be used to compare system design options, since single optimization includes multiple simulations. **Table 5.6** in section 5.4 displays both the search space and the HOMER optimizer parameters used in the design of the proposed optimal hybrid system for different components considered. In the proposed system as a backup, a biogas generator is comprised (Lilienthal 2005). The last stage, sensitivity analysis **Figure 4.6**, HOMER repeats the optimization phase for a range of sensitivity input variables that are specified, which means one sensitivity analysis is composed of different optimizations. In our model; we define many sensitive variables as described in subsection 6.3. These variables (**Table 6.2**) help us to quantify the effects of uncertainty and systemic changes (Lambert et al. 2006).

4.4.2. Economic parameters

This work aims at optimizing the design of a hybrid grid system that uses solar as well as biomass in all scenarios to electrify a residential area. Economic assumption is an essential part of sustainability since a better economy automatically achieves more sustainability. HOMER uses basic principal economic cost parameters to assess which system is optimal. Those include the effects of total net present cost (TNPC), levelised cost of energy (LCOE), and salvage cost (HOMER 2019). The cost summary of the system components is shown in **Table 5.7** Section 5.5.

Total net present cost (TNPC)

HOMER software defines the total net present cost (TNPC) of a system as the present value of all the costs the system incurs over its lifetime, except the present value of all the revenue that is earned over the same duration. The costs of the system include capital costs, replacement costs, operating and maintenance (O&M) costs, fuel costs, emissions penalties, and the cost of buying power from the grid. While the revenues include salvage value and grid sales revenue. The TNPC is the fundamental economic value of HOMER, the value by which all system configurations are ranked in the optimisation results. Mathematically. TNPC is calculated by dividing the total annualized cost, which is the annualized value of the total net present cost, by the capital recovery factor ratio. The capital recovery ratio is a function of the real discount rate (%) and the number of years (N) of the project lifetime. It is a ratio used to calculate the present value of a series of equal annual cash flows as depicted in equation 4.25. The mathematical formula of the TNPC is as follows

$$C_{TNPC} = \frac{C_{ann,tot}}{CRF(i, R_{proj})} \qquad \text{Eq. 4.22)}$$

$$CRF_{(i,N)} = \frac{i(1+i)^N}{(1+i)^N - 1} \qquad \text{Eq. 4.23)}$$

Where

$C_{ann,tot}$ = total annual cost of the system (US$/yr)

$CRF_{(i,N)}$ = recovery ratio depends on the interest rate (%) and project lifespan R_{proj}, i is real discount rate, N: the number of years.

https://www.homerenergy.com/products/pro/docs/latest/capital_recovery_factor.html

Net present cost (NPC)

The present value of all costs of installing and operating the component over the project's lifetime, minus the present value of all revenues produced during that time. It is the component's net present cost (life-cycle cost).

Levelized cost of energy (LCOE)

The average cost per kWh of useful electrical energy provided by the HOMER simulated system is defined as the levelized cost of energy (LCOE), and the cost of energy will equal the total annual cost of the system divided by the total electrical load served.

The total annual cost is the sum of the annualized costs of each system component plus the other annualized costs. HOMER used its value to evaluate both LCOE and TNPC. To calculate the LCOE the following formula is used

$$COE = \frac{C_{ann,tot} - C_{th}}{E_{served}} \qquad \text{Eq.(4.24)}$$

Where:

$C_{ann,tot}$ = total annual cost of the system (US$/yr)

C_{th} = total cost of thermal load served cost (US$/yr)

E_{served} = total electrical load served (kWh/yr)

Salvage cost

Salvage value is the value remaining in a component of the power system at the end of the project's useful time. Accordingly, it depends on the replacement cost rather than the initial capital cost. HOMER assumes linear component depreciation, implying that a component's salvage value is directly proportional to its remaining life. The salvage value S is determined by the multiplication of the costs of replacement of the component by the ratio of total life to product life. The remaining life R_{rem} is the remaining life of the component at the end of the project lifetime, which is equal the lifetime of the component plus the replacement cost duration, minus the lifespan of the project excluding project lifetime (yr). Using the following equation:

$$S = C_{rep} \frac{R_{rem}}{R_{comp}} \qquad \text{Eq. (4.25)}$$

Where S = Salvage cost.

C_{rep} = replacement cost of the component (US$)

R_{rem} = the remaining life of the component at the end of the project lifetime (yr)

R_{comp} = lifetime of the component (yr)

5. Implementation

As demonstrated in the previous chapter, methodology, modeling, and analytical procedures were developed to construct a microgrid with the optimum hybrid renewable energy system. The hybrid system serves a residential district area and can be finally used for general development of hybrid energy systems for decentralized applications. The procedures began with a surveying study and the collection of geographic, statistical, and meteorological data, after which the energy yield was estimated using software tools and mathematical formulas. The dominant resources in previous steps were candidates in the proposed hybrid system. The main aim was to construct a mathematical model for calculating the capacities of system components in order to come up with an optimal solution.

HOMER Pro software is used to run the simulation experiments for the techno-economic solution. The optimized system is developed with the framework conditions that the defined technical considerations are implemented. This chapter focuses on how each procedure is implemented, as well as the software and tools that accompany it.

5.1. Location area

The hybrid system has been designed and optimized to electrify a residential district located at Gaza city, Gaza Strip (GS). Gaza is one of the most densely populated cities in the world, where 629,723 people live on an area of 45 km^2. The city is located on the Mediterranean coastal route in the north of GS. Statistical results showed that 99.9% of city households are connected to the electrical grid through 750 electrical transformers distributed over the city, and the monthly average household electric energy consumption is 265 kWh. The average monthly household expenditure (US$) in the Strip is 785 at 2017, of 5 years' periodicity, the fraction of energy on these expenses is 3.7%. The average household size is 6.1 people. The average electricity price (US$) in the Strip Governorates is 0.14 per kilowatt hour, with a fixed fee of US$ 2.9. People depend on other traditional energy sources such as liquefied petroleum gas (LPG), firewood, kerosene, and solar power besides electricity. The next source of energy in Gaza is LPG, as it is used in various vital activities and matters of life. It is used in cooking, heating water, food factories, gas for refrigerators, and fuel for vehicles. LPG is less expensive than other available (non-renewable) alternatives. In comparison to other fossil fuels, it is relatively environmentally friendly.

The study area concerns a residential district fed by a 400 kVA transformer capacity for 94 electric meters (subscriptions), which is applied to domestic load. The location as indicated by ArcGIS (10.6.1) maps in **Figure 5.1** is (Altitude: 49.7 m, Latitude: 31°30´ N, Longitude: 34°27´ E)

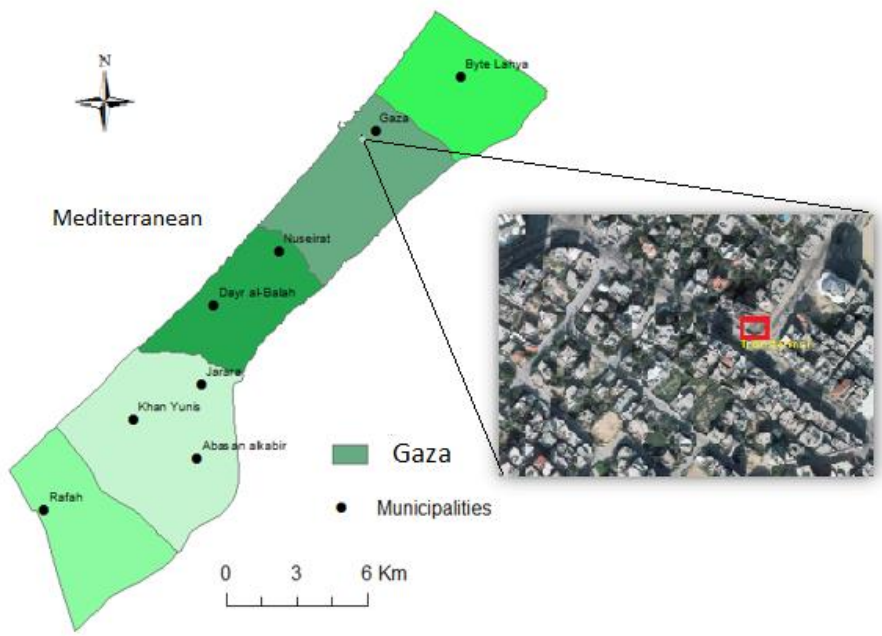

Figure 5.1: Transformer location and served study area, ArcGIS

5.2. Load estimation

These can be a combination of either DC or AC appliances that are connected to the system. The vast majority of present-day appliances require AC power. DC-coupled systems do not require AC converters, which reduces overall system cost and increases system efficiency.

Determine the daily load

Monthly energy consumption rates tend to converge throughout the year, but this is particularly noticeable in the winter due to the demand for heating, as shown in the seasonal profile of **Figure 5.2**. September, as an example, is the peak month of maximum day average of 83.55 (kW). The upper, middle, and lower lines of **Figure 5.2** represent the maximum, medium, and minimum average power consumed in each month, while the upper and lower box borders represent the first and third quartiles of the value of power consumed. **Figure 5.2** displays the seasonal load profile as box plots for twelve months. It is clear that the amount of power used is comparable, and the mean power value is close to one another throughout the year, with the exception of the last five months. September and November had the greatest and lowest mean values, respectively. The longest whisker, in October, indicates greater variability or dispersion between the least and greatest amount of electricity used in that month. November's short box indicates that power consumption has been consistently around the median.

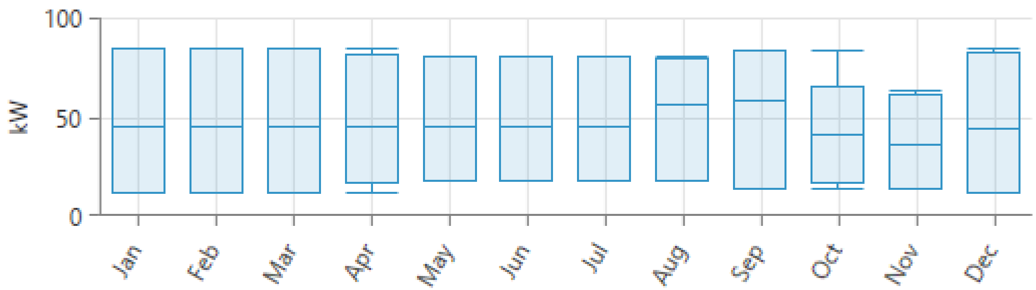

Figure 5.2: Seasonal profile of the desired residential district.

The seasonal trend of consumption in summer is different than in winter. The curves appear to be reflexed as seen in **Figure. 5.3**, but both have nearly the same daily consumption. The annual load profile shows that average daily energy consumption (kWh/day) is 1,098 and peak power (kW_p) of 84.46 for a 45.76 average power (kW) AC load type.

Calculate daily requirment

The domestic load includes lighting, fans, mobile charging points, computers, water pumps, televisions, refrigerators, and laundry machines as essential loads, and other loads such as irons, microwaves, and air conditioning as extended loads. **Table 5.1** presents the typical domestic load analysis based on the survey data, GEDCo. Water pumps (motors), water heating, outdoor lighting, elevators, chillers, and irons could be considered as deferrable loads. The table presents the most widely used appliances in normal seasonal daily life. For example, if we suppose that 10% of the homes in our sample use air conditioning for 3 hours per day and just throughout the months of July and August, the average daily energy consumption that can be concerned is 75 (Wh/day) of one house for this sample of 94 houses.

Table 5.1: Electrical domestic load estimation (Wh/day).

Sr. No	Household load	Quantity	Avg. power (W)	Operating time (h)	Energy demand/day (Wh)
1	Compact fluorescent lamps (CFLs)	4	20	2.5	200
2	Pedestal fan	2	150	1	300
3	Electronic appliance	3	20	2.5	150
4	Water pump	1	1000	0.05	50
5	Laundry machine	1	350	0.5	175
6	Electric iron	1	800	0.25	200
7	Kitchen appliance	4	150	4	2400
8	Air conditioner	1	1500	0.05	75
	Total load for 1 household	3,550			
	Total load for 94 households			754,350	

The load profiles used in this work were obtained from GEDCo. In the 2020 winter and summer seasons, both the January and July load curves briefly show load variance throughout the 24-hour period. Both **Figure. 5.3**-a and **Figure. 5.3**-b are prepared by the HOMER software based on the input data of the daily load profile. The load peak values in January and July occur around 17:00 p.m. and 12:00 a.m., respectively. Evidently, both load curves are distinct in the distribution of energy consumption; the maximum load requirements depend on three main reasons: the weather; existence of family members at homes; and working days. The overall daily demand is shown to be similar during the most demanding months in summer and winter of about 1,098 (kWh/day).

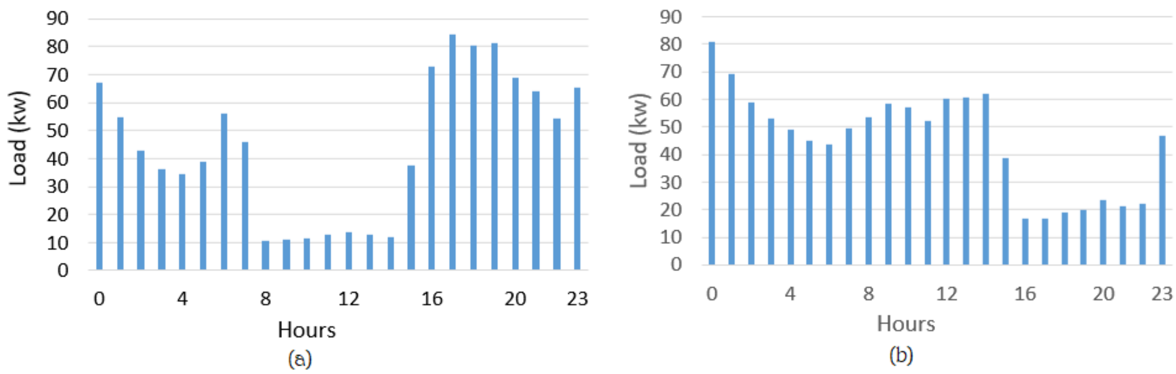

Figure. 5.3: Residential load profile for 24 h: (a) January, (b) July.

5.3. Renewable resources computation and allocation

In this section, we will present the renewable energy potential calculations in GS generally and in particular in Gaza city. The study area was chosen for the residential neighborhood that includes 94 housing units. In conclusion, we also intend to support the electric grid with renewable energy resources. In the case that it is difficult to establish a power plant that relies on renewable resources for the same region.

The current study assumes an anaerobic digestion technique, where methane is estimated from the biomass (MSW, SS, and agriculture waste). Then extract the energy from the inorganic combustible, which is essentially MSW. The capacity to supply methane and electricity from biomass resources in the GS was estimated based on the methodology outlined in Section 4.2.1. The waste from animal manure is considered the largest RE biomass (kton/year), Contributing to overall biomass supplies for thermal energy generation at 71.34% (1368.7 GWh/year), followed by agricultural waste energy at 14.4% (277.2 GWh/year), household solid waste at 13.8% (264.8 GWh/year), and sewage sludge energy at 0.45% (8.8 GWh/year), respectively. **Table 5.2** lists the annual quantity (kton) of biomass for each type; the output of (10^6) methane (Mm^3); the annual thermal energy yield of MWh; and the percentage shar of each biomass source in anaerobic digestion and the mathematical method assumed (Kim et al. 2006). In the same context, it was found that the annual methane production in Gaza from MSW, SS, plants, and animals was 11.01, 0.46, 4.35, and 24.46, respectively, for a sum of 40.28 CH_4 Mm^3/year, equivalent to 1450 TJ or 140.98 GWh_e.

Table 5.2: Biomass resource amounts, potential, and energy yield sharing from anaerobic digestion.

Biomass	Unit	MSW	Sewage Sludge	Plants	Animals
Amount	kton/year	676.71	49.5	132.17	464.49
Methane	MCH_4/year	26.48	0.88	27.724	136.87
Energy yield	MWh/year	264,796	8,801	277,243	1,368,700
	TJ/year	953	31	998	4927
Factor	%	13.8	0.45	14.4	71.3

5.3.1. Distribution of the potential for biomass, solar, wind, and wave energy

This section presents the potential of various kinds of energy in GS, particularly in Gaza city. With the purpose of showing a comparison with neighboring governorates and the profit potential. The biomass potential of the GS and Gaza city are 1450 and 8916.4 TJ/year, depending on the calculations executed over GS in this study, 6910.45 TJ/year comes from anaerobic digestion (refer to **Table 5.2**). Considering the capacity and the efficiency of the equipment used to produce heat and electricity, the electrical energy used is 2377.7 TJ/year, which is equivalent to 671.83 GWh/year, and thus the instantaneous electrical power is 65.15 MW_e from biomass resources.

The prediction of solar energy production in all governorates is 1.195 Twh/year and the average annual global surface irradiation is 2100 kWh/m^2, as seen in **Table 5.3**; the average production of solar energy is around 50% of the total production of RE. Clearly, in the GS governorates, suggesting that appropriate solar energy sites would take into account the increasing population and electricity demand for the installation of the PV systems in the presence of the limited area, all governorates have approximately equal irradiance, hence the study presumes distributed PV installation systems when calculating the solar energy harvested by the PV modules (Sampaio and González 2017) (Toledo et al. 2020).

Table 5.3: Global insolation and solar energy potential in GSs' municipalities.

Municipality	Global Irradiation (kWh/m²/year)	Potential Power of Municipalities (GWh/year)
Northern Gaza	2108.4	218.2
Gaza	2109.4	407.9
Deir al-Balah	2127.7	175.3
Khan Younis	2123.8	244.2
Rafah	2125.5	149.5
Total	Avg.: 2100	1195.1

The potential for wind energy depends much on the topography of a region. As a result, considerable potential exists in the flat region. These areas are located mainly in the north-western part of the GS, overlooking the Mediterranean coastal area of the GS. In total, 10% (3600 ha) of the GS's area is available for wind farm installations, with the most significant potential areas being in the municipalities of North Gaza (1300 ha), Gaza (750 ha), and the southern area (1450 ha), while the other governorates are in highly populated areas. The western coast of the GS is considered to be an area that can be exploited to set up wind farms, where the highest wind speeds have been reported in the northern areas of the coast. The average wind speed in the GS ranges from 2 to 6 m/s (Ouda 2001).

The average annual wave power density is determined by dividing the total annual available energy (AAE) density by the number of hours in a year. The largest values of AAE exceed 17.52 MWh/m along the coast. AAE densities are generally between 11.3 and 17.52 MWh/m along the coast. Two wave parameters, including wave height and wave cycle time, are very important for the estimation of wave energy in the sea. The wave period varies between 3.2 sec and 3.6 sec in the northern Mediterranean coastal area of the GS. In addition, the wave height varies between 0.561 m and 0.67 m in different seasons. Given the considerable wave height and the wave period, the average wave power extractable from the Mediterranean shoreline is between 1.2 kW/m and 2 kW/m. Many considerations are taken into account in the choice of a suitable location to install a conversion shoreline device at less than 10 m depth, such as the existence of breaking waves at the site, which would create very strong waves.

Based on the methods outlined in Section 4.2, the probability of producing electricity from biomass, solar, wind, and wave energy sources in the GS was estimated. Biomass is considered the main RES, adding 59.2% (1919.5 GWh/year) to overall RES energy generation, followed by solar energy at 35.8% (1195 GWh/year) and wind and wave at 3.8% (125 GWh/year).

The potential and spatial distribution of various RESs is an important aspect of RES-based country development strategies. **Figure 5.4** shows the distribution of total RESs at the local level. The figure shows biomass, solar, wind, and wave contributions to energy output, and it is also seen that the energy yield in the Gaza Governorate is more than others, in a dark green color, and biomass and solar are the most significant contributors, when biomass exhibits a dominant renewable resource that represents aspects of society such as farming and high population. In all cases, biomass and solar represent the main energy sources, in some cases accounting for 90% of the RESs. The GS has five governorates with roughly the same RES. The reason for this homogeneous distribution is the small overall area and what follows in the similarity of the coastal climate. Additionally, the similar activities and daily life of the population have been practiced, including social habits and thus biomass production.

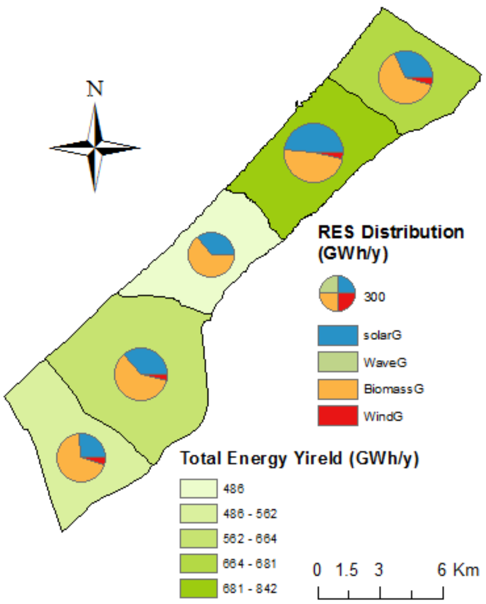

Figure 5.4: Spatial distribution of the total energy yield (GWh/year) from RESs in the GS and the proportion of biomass, solar, wave, and wind energy.

5.2.1. Ratio between Energy Demand and Renewable Energy Production

Average electricity and LPG consumption of household electricity in January 2015 was 306 kWh and 22 kg, respectively, versus 275 kWh and 14 kg in January 2009. The aggregate number of households in the GS was 334,710, meaning GS householders' energy consumption was 1,064,378 MWh/year, while the estimated yield from biomass digestion was 1,919,555 MWh/year. Given the efficiency of the conversion processes, the production of electricity could be 640 GWhe/year. The available electrical energy from biomass is equivalent to 60% of household electrical energy consumption. Solar energy production by considering a hybrid system, covers the total average household demand with biomass. As a result, HRES solutions should be involved in the energy strategy plans of households' electrifications to alleviate the suffering of people due to the permanent long-time interruption of electricity. As a result, biomass and solar are viewed as the main RES in the HRES design of the interest area to electrify households, as demonstrated in the next section.

5.3. Sizing of the hybrid system model components

A summary of the main steps involved in sizing a grid-tied HRES system is depicted in **Figure 5.5** (sizing the system). Assuming all the PV modules are identical, the same manufacture and capacity (kW). As long as the location to install the PV system is available, then the PV system capacity can be determined using a formula independent of the area to be calculated. which is the daily load of energy required during daylight hours $E_{req,day}$ and must be divided by the PSH. Otherwise, the equations of the area as a variable and the module efficiency have to be used.

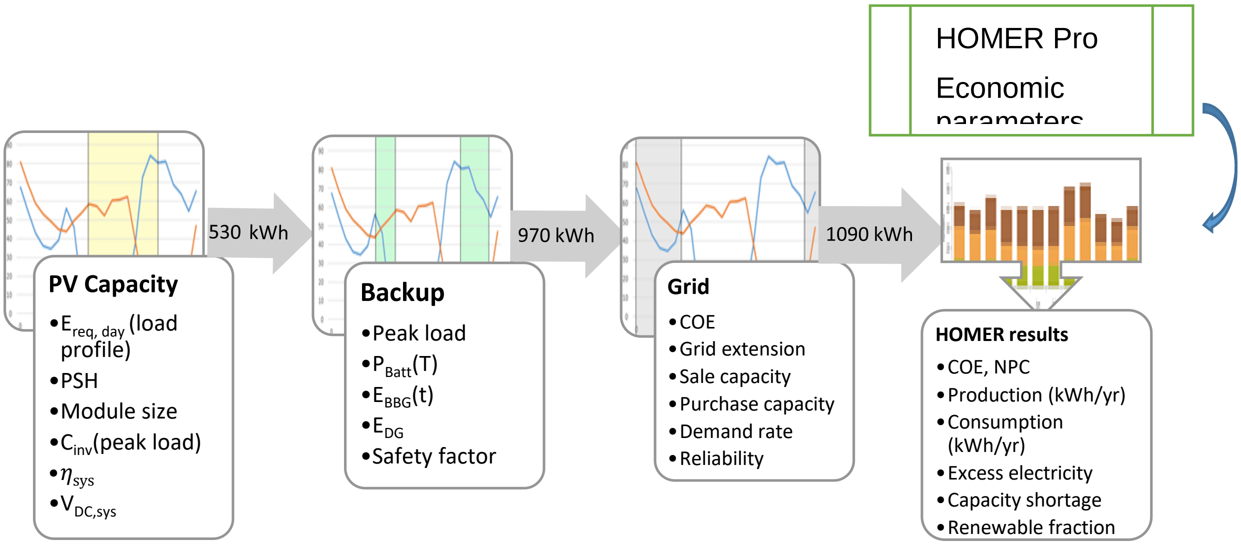

Figure 5.5: Sizing model of the hybrid renewable energy system components.

The inverter capacity is set to meet the peak value of the load. The system efficiency and the safety factor are involved throughout the calculations. The system efficiency comprises the efficiency of the cables, inverters, and batteries. The total energy consumption for the chosen district is 571.592 kWh at (16-23 pm) as shown in **Figure. 5.3**. Then the PV size and energy harvest are calculated based on the rated power of the module, peak demand load value, and considering 0.72 battery and DC-AC converter efficiency.

The load profile is divided into three zones and covered by two types of energy sources: traditional (diesel generator and grid) and renewable resources (solar and biogas). The first zone (yellow) will be covered by solar energy during the day, so the required input values such as PSH and efficiency, as well as the system's DC voltage, will be delivered, as indicated in **Figure 5.5**. At both ends of the day, backup components and biogas engines will be deployed (green). At night, the load will be determined by the utility grid (gray). The calculated components' capacities values are provided to HOMER in the range named the search space, and the economic and technical constraints called the sensitive parameters. The electrical simulation results are therefore displayed and discussed in the next chapter.

5.4. System parameters and constrains

The hybrid renewable system is optimally configured to provide a maximum load of 84.46 kW for residential AC loads. A grid-tied system of solar and biomass renewable sources involving a diesel generator and lead-acid chemical battery storage as a backup is maintained in **Figure 5.5**. By using a biogas engine generator, biomass is incorporated as a renewable resource into a hybrid renewable system. The study assumes anaerobic digestion technology to produce biogas from biomass.

Figure 5.6 depicts the schematic grid-connected configuration design of the HRES model for 45.76 kW average load, which consists of (PV-BIO-DG-BS) components: photovoltaic, three biogas generators (BioGen25 of 25 kW, BioGen50 of 50 kW, BioGen100 of 100 kW), diesel generator (DGen50 of 50 kW), and battery storage (BAE PVS2660) respectively.

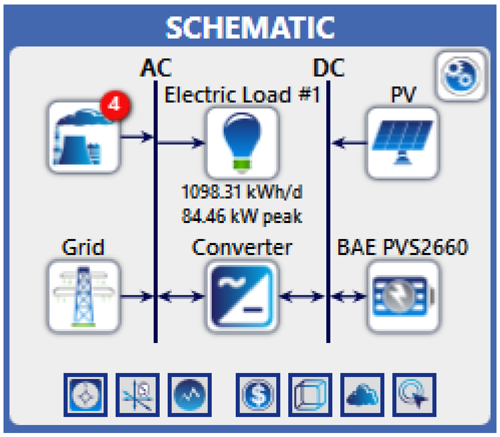

Figure 5.6: Schematic graph of optimum configuration

The designed system consists of a PV system with battery storage. The backup sources are four generator sets; three work with biogas and the fourth generates electricity using diesel. The simulation started at the maximum annual capacity shortage (%) and minimum renewable fraction (%) constraints set to 10% and 60% respectively.

For the electrification of the load demand, the hybrid system utilizes existing public grid infrastructure, whereas the grid provides the microgrid at night. At sunrise and sunset, storage and two generator types are used as backups of the system. Several options are considered to satisfy stability and minimize battery dependence. Depending on the available biomass and the biogas yield from the digestion process, assumptions are presented in **table 5.4**. The average cost of required biomass is at least 45 US$/ton, which includes sorting, transportation, and labor. The annual average available biomass is 719.25 tons/day of the generator's useful life, contains 50% carbon, and has a conversion ratio, which is biogas generated to biomass feedstock consumed (kg/kg) of 0.9 (Teferra and Wubu 2018). The LHV of biogas (MJ/kg) is 20. The fuel consumption (kg/hr) is 1.25 per kW, and the hourly operating costs (US$) are 3, 7, and 10 of the generators' output power (kW) 25, 50, and 100 respectively (Nguyen et al. 2019). The generator schedule option is modified to force on 7 hours all week, where the photovoltaic panels do not work at their full energy. The **Figure 5.7** displays the fuel consumption flow (**Figure 5.7**-a) and efficiency (5.7-b) of the Caterpillar 25 kW diesel generator.

Table 5.4: Biogas yield from different biomass resources

Bio resources	**Availability (kton.yr^{-1})**	**Total (kg*10^3.d^{-1})**	**Recovery factor**	**Biogas yield (m^3/kg)**	**Total Biogas (m^{3}d^{-1})**	**Energy yield (kWh$_e$.d^{-1})**	**Ref.**
MSW	281	771	0.8	0.465	286812	438,822	(Zhang et al. 2007)

Sewage sludge	26	71	0.7	0.244	12166	21,899	(Dubrovskis et al. 2010)
Plant waste	24	67	0.8	0.39	21039	37,871	(Barz et al. 2018)
Animal dung	83	227	0.7	0.036	5734	10,321	(Yimen et al. 2018)

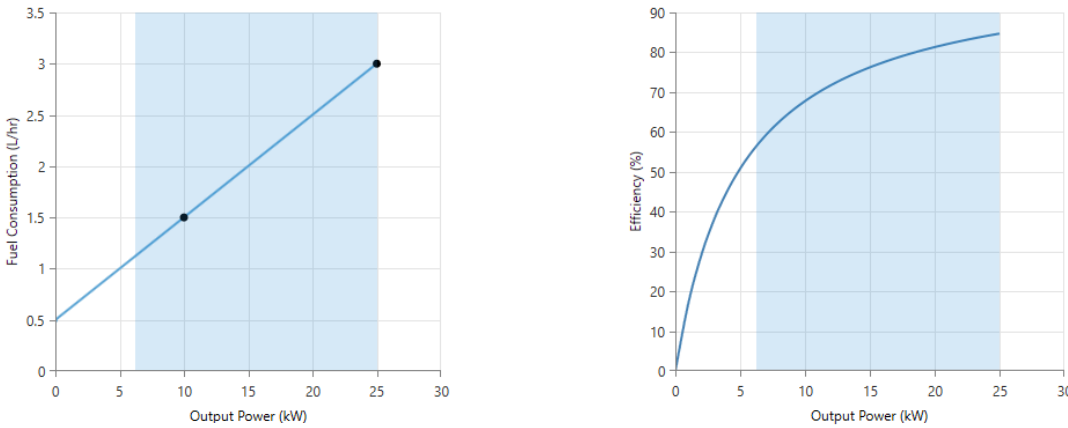

Figure 5.7: Fuel consumption flow (a) and efficiency (b) of Caterpillar 25 kW diesel generator

HOMER uses dispatch strategy, search space values, and sensitivity range variables in optimal solutions such that the load profile meets the maximum utilization of renewable resources, at a minimum renewable fraction (%) constraint of 60% and a miniature system cost (US$/kWh) with less cost of energy (COE). With this assumption, the nominal discount rate is 4%,10%, and expected inflation rate are considered 4%,8 %, and the project lifetime is taken as 25 years. The capacity shortage penalty (US$/kWh) is considered zero. There is no cost penalty that HOMER applies to the system for any capacity shortage that occurs during the year. The electricity scenario is different in the study area because it has 8 on and 8 off utility grid capacity. The system control parameters used in the simulation run constraints are furnished in **Table 5.5**. The set point state of charge is applied and it will not stop until the battery bank reaches 50 percent of its capacity, at which point the system will stop charging the battery.

Table 5.5: System control parameters and input constrains are used in the software.

Parameters	Value used
Project lifetime (year)	25
Load following	Yes
Cycle charging	Yes
Apply set point	Yes
Set point state of charge	50%
Allowing multiple generator	Yes
Multiple generators can operate parallel	Yes
Constrains	
Minimum renewable fraction (%)	0%,60%
Maximum annual capacity shortage (%)	5%, 10%

HOMER simulates 1,490,120 solutions for each of seven different sensitivity cases to perform feasibility and economic analysis of HRES, discarding infeasible configurations. On a 2.3 GHz Intel personal computer, the total simulation time was 22:58:00 hours. and puts all feasible systems in order based on techno-economic assumptions. The feasible results of a grid-tied hybrid electric system are configured to fulfill the needs of a residential electrical load of 94 households per electric power meter.

Table 5.6 lists the parameters of the implemented components and their optimal capacities chosen within the search space. The optimal solution has a 150 kW capacity of the photovoltaic array, a bio generator of 25kW and 50 kW, while the diesel generator and batteries are not chosen. A system converter of 50kW power is used with the cycle charging (CC) dispatch strategy. In CC whenever a generator is required, it operates at full capacity, and surplus power charges the battery bank. Under the Load Following (LF) strategy, when a generator is needed, it produces only enough power to meet the demand. Load following tends to be optimal in systems with a lot of renewable power that sometimes exceeds the load.

Table 5.6: Capacity and search space for optimal hybrid system components.

Parameter	Characteristic	Overall Winner (kW)	Search Space
PV Panel Capacity	Capacity (kW)	150	100, 110, 120, 130, 140, 150
Biogas generators power	Capacity (kW)	0, 25, 50, 100	0, 25, 50, 100.
Diesel generators power	Capacity (kW)	0	0, 50.
Converter	Capacity (kW)	50, 75, 90	50,75, 90, 100, 120.
Battery storage.	#	0, 100	0, 100, 200, 300
Grid annual purchase power	Capacity (kW/yr)	400	400
Dispatch Strategy (DS)	CC	Cycle Charging	CC, LF

According to the results obtained, depending on sensitivity cases, the COE of the on-grid system ranges between 0.341 US$/kWh and 0.438 US$/kWh, and the NPC varied between US$2.30M to US$7.32M. The best solution had a COE of 0.438 US$/kWh and a TNPC of US$2.30M. The ranges of COEs obtained in this study are expected and within reasonable boundaries if compared to other options such as continuous grid power shortages, and high electricity prices from intensive use of the traditional fossil fuel distributed generators, which cost US$0.92/kWh. But the optimum result is still around three times compared to grid power price (US$0.143/kWh). If we take into account the electricity prices of generators, power outages, two-thirds of the day, income level, recommendations of electricity distributors' companies, and 0.5US$/kWh price as a threshold assumption at most for the time being. Higher values than these will certainly be more burdensome.

5.5. Economic parameters

Table 5.7 summarizes the costs of the optimal system, including all necessary components. No system fixed costs are fed to the HOMER, these costs include PV system, inverter, generators, chemical storage costs, and required costs of the grid provided to HOMER, the grid power price is equal to US$0.143 per kWh, which means optimal results should be competitive with this value.

Table 5.7: Economic specification of the Hybrid mini-grid system's main components.

Component	Capital cost	Replacement cost	O&M cost	Life time	Source
PV array	$ 250 kW^{-1}	$ 0 kW^{-1}	$ 2.5 kW^{-1} yr^{-1}	25 yr	(SOLAR 2020)
Inverter	$ 200 kW^{-1}	$ 200 kW^{-1}	–	15 yr	(BLUESUN 2016)
Diesel generator	$ 280 kW^{-1}	$ 280 kW^{-1}	$ 0.16 kW^{-1}	25000 hr	(Caterpillar 2020)
Bio generator	$ 112 kW^{-1}	$ 112 kW^{-1}	$ 0.12 kWh^{-1}	9,125 hr	(ONEW 2020)

Battery	$163 kWh^{-1}	$ 163 kWh^{-1}	$1.6 kWh^{-1}yr^{-1}	15	(SOLAR 2020)
Distribution grid	$0.143 kWh^{-1}	–	–	–	(GEDCo 2020)

5.6. Emission issue

GEDCo receives electricity from outside and from one internal local power generation station, which is unreliable because it relies on imported fuel. A power station, in its best case, covers one third of the demand. The turbines at the station rely on diesel to generate electricity, The emission factor for producing electricity is more than 0.81 kg CO_2/kWh due to the old technologies and equipment used at the station (EPA 2020). The other GHG pollutant generation is from bio resources. The carbon content of biomass is set to 50wt%. In order to calculate the annual emission of pollutants, the characteristics and emission factors of the (g/l) diesel and (g/kg) biogas fuels should be applied. The emission factor includes carbon monoxide, unburned hydrocarbons, particulate matter, the proportion of fuel sulfur converted to PM (%), and nitrogen oxide for both fuels.

6. Results and discussions

The optimization results of the candidate winner system, which is the first solution of the output HOMER calculations, as depicted in **Table 6.1**, meet the following sensitivity analysis parameters: The solar scaled annual average irradiation is 2.50 kWh/m^2/day, the biomass price is 100 (US $/tons), the maximum capacity shortage is 10%, the minimum renewable fraction is 60%, the grid extension distance is 10 km, and the nominal discount and expected inflation rates (%) are 10% and 4%, respectively.

Table 6.1: Optimization results for grid tied HRES (PV-BIO-DG-BS) system for a solar scaled annual average irradiation of 2.50 kWh/m2/day and, biomass price 100 (US$/tons), maximum capacity shortage of 10%, 60% minimum renewable fraction, grid extension distance of 10 km, and Nominal discount and expected inflation rates (%) are 10 and 4 % sensitivity parameters.

			Architecture						Cost				System	
PV (kW)	Bio_Gen (25kW)	Disl_Gen (50kW)	Bio_Gen (50kW)	Bio_Gen (100kW)	BAE PVS2660	Conv.	DS	Initial Capital (US$)	Operating Cost (US$/yr)	NPC (M$)	COE (US$)	Ren Frac (%)	Bios (ton)	Biog (hrs)
150	25		50			50	CC	59,108	171,606	2.30	0.438	64.3	261.3	9,304
150	25			100		50	CC	64,108	183,250	2.45	0.465	63.3	276.3	8,062
150				100		50	CC	61,309	185,180	2.48	0.470	63.2	290.3	5,473
120			50	100		50	CC	58,,059	200,555	2.67	0.506	64.7	304.6	8,235
150	25		50	100		50	CC	69,108	202,034	2.70	0.509	65.3	301.9	11,260
150			50		2400	90	LF	1.98M	211,388	4.74	0.913	64.4	202.4	4,531
150	25		50		2400	90	LF	1.98M	218,292	4.83	0.923	70.2	238.4	7,745
150				100	2400	90	LF	1.98M	222,045	4.89	0.933	72.3	247.6	4,199
150	25			100	2400	75	LF	1.98M	225,489	4.93	0.942	73.1	253.9	7,008
150			50	100	2400	90	LF	1.99M	237,028	5.09	0.971	73.0	258.8	6,606
150		50	50	100	2400	90	LF	2.01M	239,858	5.14	0.982	62.3	205.9	5,664
150	25		50	100	2400	75	LF	1.99M	242,447	5.16	0.985	74.6	271.2	9,232

The first columns show the architecture of the system with the associated dispatch strategy; all solutions involve public grid annual purchase capacity (kW) of 400 capacities. Then cost columns results, including CC, O&M, NPC, and COE costs are displayed. Salvage costs are equal to US$9,593 in nominal cash flow. The battery is included in the results when the dispatch strategy of HOMER is (LF) Load Following.

Generally, optimization results reveal several solutions, including photovoltaic and bio-generators. For the case solution involving battery storage, the system's COE decreases by around 0,097, but NPC will increase to US$3.82M as a maximum difference. Diesel generator is still not recommended, see **Table 6.1**, where the evaluated optimized design should meet the load demand at a tailor-made cost-minimizing power supply with the system restrictions imposed. The multiple generator option is set to active instead of one generator with all capacities to reduce the amount of excess energy. sale to the grid.

Electrical simulation resulted in about (kWh/yr) 452,151 total electrical production to meet the needed 400,884 kWh annual AC primary load, whereas 42.1% of this energy is generated by the biomass generators, 31.7% is produced by the public grid, and 26.2% by the PV array. Excess electricity amounts to 10.2% of the total electricity produced by the system. It should be mentioned here that this excess energy produced would be used on demand since the annual consumption is exceeding the existing load. Due to customers' growth in this district, it is not intended to use this surplus production as a backup. **Figure 6.1** displays the monthly mean (MWh) electrical production of the optimal solution generated from bio generators, solar panels, and the public grid. It shows a semi-high in August and September, the summer season months.

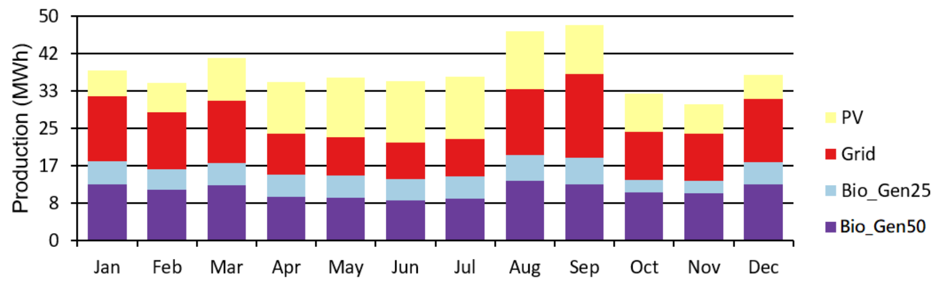

Figure 6.1: Monthly electric production

The cash flow of the hybrid system component during the project life span includes: capital cost, replacement cost, operating and maintenance cost. The resultant cash flow of the optimal results **Figure 6.2** involves 150 (kW) PV panels, 25 and 50 (kW) biogas generators, a 50 kW converter, and the public grid's annual purchase capacity (kW) of 400 capacities. The figure shows clearly the less significant cash flow belongs to the solar component of US$400, followed by the biogas generators of US$44,956. During the project's life, the utility grid has the highest cash flow of US$96,796. The converter cash flow is US$10,000 in the 20th year (capital cost), in case the converter lifetime has been set to 20 years.

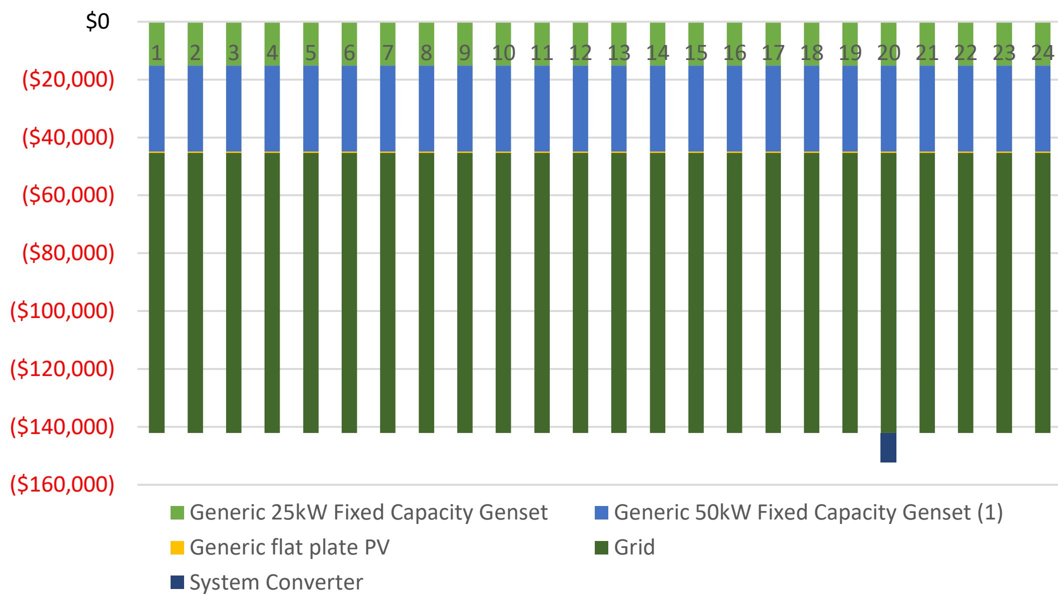

Figure 6.2: Cash flow of the system components

6.1. Grid and breakeven distance

The Gaza Strip (GS) territory is 41 kilometers long and from 6 to 12 kilometers wide, with a total area of 365 km^2. The public electricity grid extension covers most of the territory. The grid-on hybrid designed system uses the entire infrastructure of the grid, and the grid is assumed to provide the load at night. The real time rate of the grid is applied in HOMER of 400 (kW) annual input purchase capacity. The maximum net grid purchase (kWh/yr) of 500,000, the demand rate (US$/kW) or the monthly charge of the electricity bill, is 80 per month, and the grid extension capital cost is 59 US$ per 5 km.

The results show purchase capacity decreases to 143,443 kWh/yr, which contributes to 31.7% of the total electricity proposed. A grid-connected system can sell 1,203 kWh of electricity to the public grid per year. The grid-on or microgrid systems are determined by the distance between the grid and the designed system. The stand-alone system is optimal when the designed system is farther away from the grid, while in the near system, grid extension is optimal. In HOMER, the break-even grid extension distance is defined as “the distance from the grid that makes the net present cost of extending the grid equal to the net present cost of the stand-alone system”, which means determination of this distance is a necessary tradeoff between off-grid and grid extension. Grid purchase production (kW) appears in all solutions with sensitivity parameters combinations and hence the standalone system does not arise as desired solution. In this case, the breakeven distance is not defined, and this is consistent with the current situation, where the grid covers 99.8% of customers. At the breakeven economic distance, the net present cost of the standalone hybrid system and grid-extension is equal (Rajbongshi et al. 2017).

6.2. Renewable fraction

The annual 400,884 kWh AC load is served by the traditional public grid and renewable resources from solar and biomass. Biomass sharing is essential for more sustainability and towards environmental issues that arise in the study area. The renewable fraction is 64.3%. HOMER calculates the renewable penetration by dividing the total electrical load served in a specific time step (kW) by the total renewable electrical power output in this time step (kW). HOMER reports the maximum value of renewable penetration that occurs during the year as 497%. **Figure 6.3** shows a time series plot of renewable penetration (%) during a year related to total electrical load served and total renewable power output. The maximum renewable penetration scored value means that the electric power generated by the renewable resources is about 1/5 compared to the electric load served at this specific time step. Other time intervals between April and August show that the power provided by renewable energy is nearing electric demand.

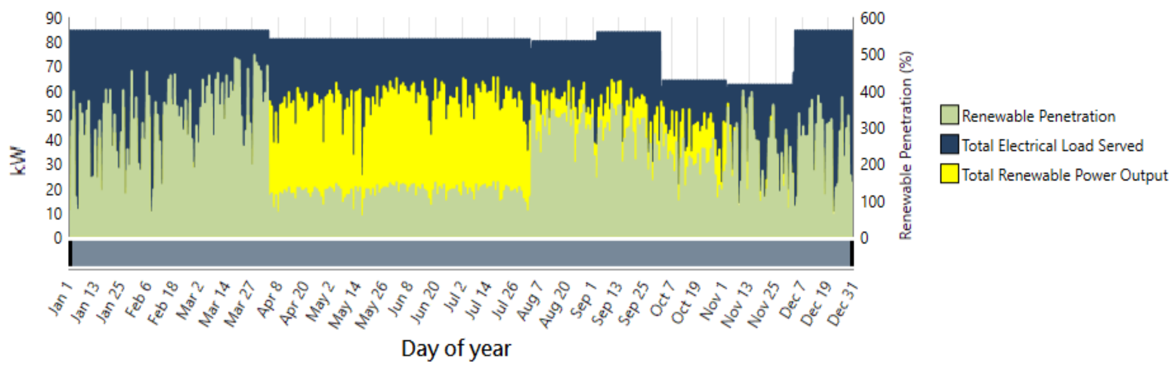

Figure 6.3: Renewable penetration (%) during the year.

6.3. Sensitivity analysis

The sensitivity analysis aims to explore the influence of uncertainty or changes in different input parameters on the behavior of the system. The variant parameters in the designed system are:

biomass price (US$/ton), solar scaled average (kWh/m^2/day), grid extension distance (km), nominal discount rate (%), expected inflation rate (%), the renewable fraction (%) and capacity shortage (%). The variables are set to 60% and 10%. The diesel fuel price (US$) is equal to 1.3 times its normal price. The scaled annual load average parameter is set to 1,098 (kWh/day), which is the default value that equals the baseline annual average. The results show that scaled annual average parameters affects directly on the excess energy. Sensitive input parameters are shown in **Table 6.2**.

Table 6.2: Ranges for the optimal system parameter's sensitivity analysis variables.

Sensitivity variables	Unit	Ranges
Nominal discount rate	%	4, 10
Expected inflation rate	%	4, 8
Minimum renewable fraction (MRF)	%	60
maximum annual capacity shortage (MACS),	%	10
Grid extension distance	km	10, 25
Solar scaled average	kWh/m^2/day	2.5, 5.5
Biomass Price	US$/tones	40,100
PV: De-rating	(%)	90
Diesel price	US$/L	1.3

Sensitivity parameters variant have a clear influence on the simulation results. Figure 6.4 shows the graphical representation of the sensitivity variant on the optimal system results, showing the effect on the economy, technology, and emissions. In figures (**Figure 6.4**-a, b) cost of energy changed according to economic parameters. It is directly proportional to the nominal discount rate and inversely with the expected inflation rate. When the cost of biomass (US$/ton) increases this will reflect on the energy cost directly, as well as the divergence on irradiation, leading to a high energy price in such a hybrid system. (**Figure 6.4**-c) depicts a decrease in the renewable share of electricity production as biomass prices rise and the scaled annual average irradiation kWh/m^2/day rises. Monthly global horizontal irradiation GHI ranges between 2.87 and 8.07 kWh/m^2/day. High scalded (less or more) of this range results in a low renewable fraction. Emissions increase where the renewable fraction decreases or scaled annual average irradiation increases (6.4-d). Low renewable fraction values will force the system to rely on traditional energy sources such as burning fuel, which will increase the amount of greenhouse gases emitted. The excess electricity percent become higher in the case of high sharing of PV (kW) capacity, with remain other capacities, the same occur at increase of scaled solar average as shown in (**Figure 6.4**-e). scaled annual average.

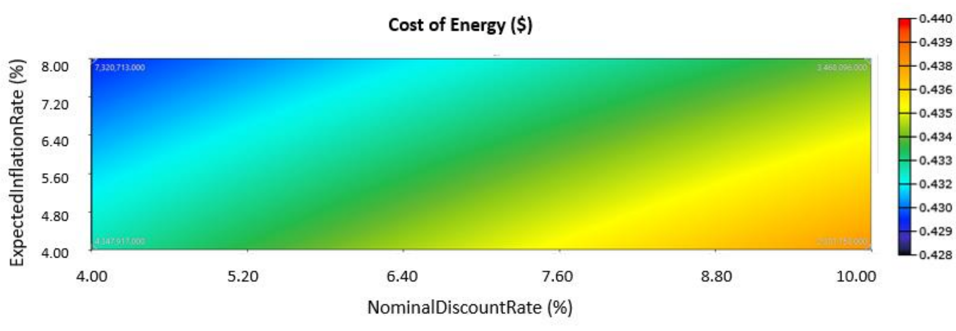

(a)

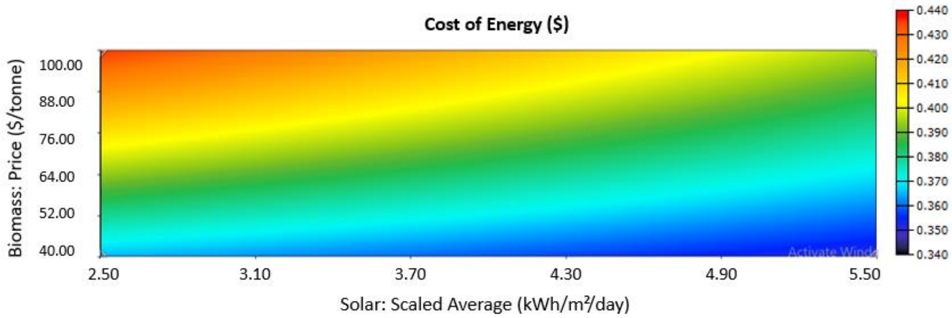

(b)

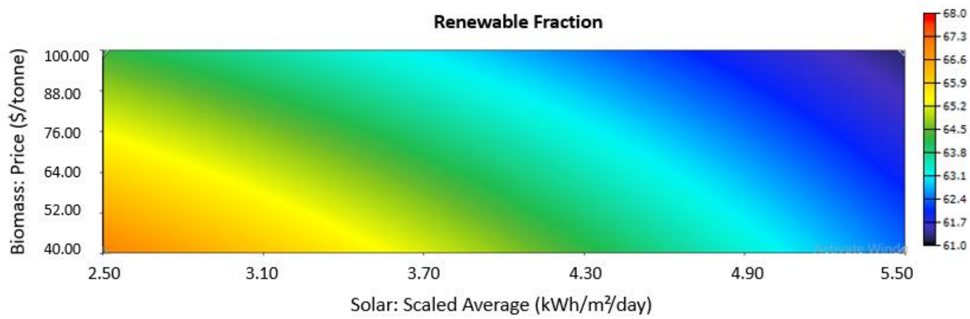

(c)

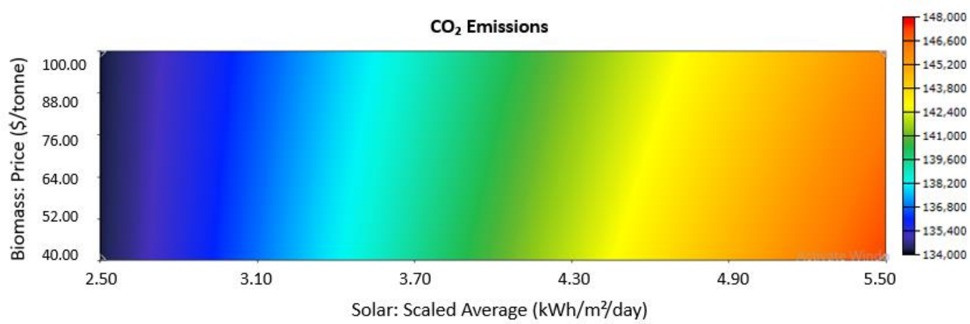

(d)

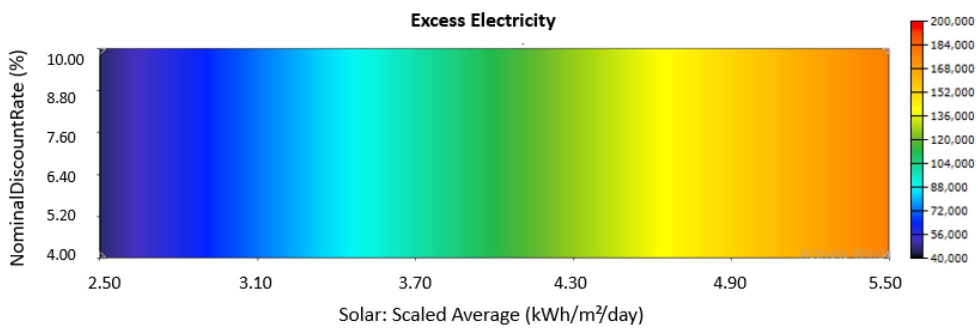

(e)

Figure 6.4: Impact of the sensitivity variables on (a and b) cost of energy (c) renewable fraction (d) CO2 emission (e) Excess electricity

The optimal design was found to be 10% of the maximum annual capacity shortage and 60% of the minimum renewable fraction, with the nominal discount rate and expected inflation rate (%) at

10% and 4%, respectively. The optimal design is at 2.50 (kWh/m^2/day) annual scaled solar radiation with 90% PV de-rating, a biomass price (US$/ton) of 100, and a grid extension distance (km) of 10. The results generally show that variant economic parameters such as NPC, COE, O&M, and CC are directly affected by economic and technical sensitivity variables. COE and O&M costs have opposing effects on economic rates of discount and inflation. The excess electricity will increase when the PV solar capacity increases, but the cost of energy will decrease. The renewable fraction is strongly affected by the biomass price and the de-rating parameter of PV.

6.4. Payback period

Simple payback is the number of years at which the cumulative cash flow of the difference between the current system (winner system) or proposed system and a base case system switches from negative to positive. It is executed by comparison between the winning system/lowest net present cost and the selected base case among optimization results. Payback is an indication of how long it would take to recover the difference in investment costs between the current hybrid system and the base case.

In order to find the payback period of the 84.46 kW$_p$ peak load of the winner grid-tied hybrid (150PV-75BIO) kW system, the base system should be chosen to find the payback period. Any system that appears in the optimization results could be a basic system. Here the system's (120PV-150Bio) kW grid-connected is chosen. For both systems, winner and base, table 6.3 determines the capital, NPC, and O&M for both systems. The LCOE difference between the two systems is US$0.068/kWh. This means increasing solar sharing in hybrid system (winner) leads to more feasible and affordable result. As a compassion between two systems, as shown in **Table 6.3**, the initial and operational costs of the winner system are less than the base system.

Table 6.3: Hybrid and base case system for 84.46 kWp power system

	Public grid (kW)	PV (kW)	Converter (kW)	BG (kW)	Initial capital	Total NPC	O&M $/yr	COE $/kWh
Base case	400	120	50	50, 100	$ 58,059	$ 2.68M	200,555	0.506
Hybrid system	400	150	50	25, 50	$ 59,108	$ 2.30M	171,607	0.438

Figure 6.5 shows the results of graphical representation of both, base system (current system) and hybrid (proposed) systems' cumulative cash flow over project life time. The base system has a higher share of biomass instead of solar energy than the proposed hybrid system. The economic comparison metrics between the winner system and other optimal selection systems (base system) are present worth and annual worth, which are reflected in the cumulative cash flow. Another metric in the payback period is the present worth value (US$) 377,266 is the difference between the NPC of the compared systems. A positive sign indicates that the proposed system saves money over the project lifetime compared to the base case system. The annual worth is (US$/yr) is US$28,868, which is defined as the present worth multiplied by the capital recovery factor as described in section 4.4.2.

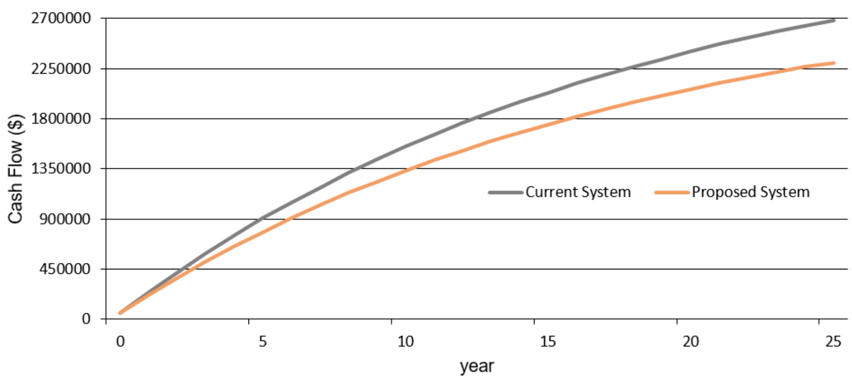

Figure 6.5: Cumulative cash flow over project life time

According to simulation experiments, comparing payback periods between different hybrid systems reveals that the amount and capacity of renewable components have a significant impact on the payback period. This means that at different capacities (kW) of PV arrays included, the resulted payback will be different. In the results obtained in this work, it is obvious that the internal rate of return (IRR) (%) is not applicable, simple payback (yr) and discount payback (yr), are both 0.04.

6.5. Emission

According to HOMER simulation results, the types and values of GHG (kg/yr) are listed in **Table 6.4**.

Table 6.4: Emission quantity generated from hybrid system

Quantity	Value (kg/yr)
Carbon Dioxide,	172,910
Carbon Monoxide	2.99
Unburned Hydrocarbons	0.125
Particular Matter	0.0653
Sulfur Dioxide	535
Nitrogen Oxides	265

We can see that the emissions are reduced significantly compared to about 177,000 tons of CO_2 emissions from the conventional power plant in Gaza for the year 2016 to generate 160 MW (Nassar and Alsadi 2016). In PV and bio generator based systems, there is a reduction in carbon dioxide and sulfur dioxide gases, but there are some other gases present due to diesel fuel used by the public grid in the optimal case (Masters 2013). The percentage of the system's emissions reduction is higher due to the renewable penetration percentage from the solar and biogas.

7. Conclusion

The Gaza Strip's residential sector has a significant and urgent demand for energy, particularly electrical energy, and there aren't many reliable sources available. This prompts the search for alternatives or renewable energy as a solution to this issue. It is expected that the grid-connected hybrid system, which is based on bioenergy and solar energy, can provide an alternative source of electrical energy. The residential area that has power interruptions for more than two-thirds of the day would benefit from the electricity that this hybrid system can assist in providing. We have followed methods to develop an optimal grid-tied hybrid system based on renewable energy, starting with the estimation of the various renewable energies in the relevant geographic area and continuing until the HOMER Pro simulation program achieves optimal results and solutions for the desired hybrid systems.

The key results of the first step consist of evaluating the four most effective renewable energy resources (RESs) that could be implemented in the area of study: solar, wind, wave, and biomass. The energy maps presented show their potential as well. This study has shown that the energy potentials are 1,919.5 GWh/year from biomass, 136.72 GWh/year from wind, and 1,195 GWh/year from solar. Solar and biomass account for over 96% of the overall potential of renewable energy (RE). Furthermore, the ability of productive wind energy is 3.5% of the overall electricity potential. Hence, the construction of wind turbines for this northern coastal region is also recommended, although the potential is relatively low. For these reasons, RESs are recommended for grid injection to electrify households', building projects, as well as remote areas. This work enhances RE market growth in selected target communities by promoting the role of locally generated biomass, wind, wave, and solar energy as the key contributors to a possible future local energy supply. It is worth mentioning that the potential of integrated RESs in the Gaza Strip reaches 3,240.4 GWh/year, which represents more than 95% of the household energy demand in the respective area. To conclude, pursuing renewable resources as a means of energy use is a way of addressing the Gaza energy crisis and offering cultural, social, or environmental benefits. As a conclusion, biomass and solar energy are the most important sources of renewable energy in GS.

The methodology followed in our work and the knowledge gained from the results can be used to replicate electricity production systems and can be transferred to similar societies in other countries with similar geographical and/or political positions. Biomass acts as a renewable resource that has made a significant contribution to the energy yield in the study area, suggesting the significance of future studies in choosing the correct technology between thermos-chemical and biochemical conversion technologies used to generate biomass-based biofuels.

The extremely large amounts of biomass resulting from the population and its activities in the form of MSW demand a serious view of the concept of sustainability. This view is based on environmental, economic, and social considerations of the consequences resulting from the accumulation of these various forms of biomass resources. Our future work will be focused on the development of a hybrid system that incorporates the most contributed renewable resources to meet household demand for electricity and will measure the potential of each resource to achieve a realistic and credible systemic approach.

Analyzing the optimal techno-economic feasibility of a bio-share contribution in a hybrid renewable energy system (HRES) was developed. The HOMER Pro program was utilized to perform this process via a simulation model. As a base case, a specific research area has been selected. The economic and technological input parameters of the components and the project in general are set to meet the 45.76 kW average load of 84.46 kW_p. The biomass introduced in the work assumed anaerobic digestion technology, so the biogas produced was applied to a biogas engine coupled with a generator. In this context, a simulation was carried out over a grid-tied photovoltaic (PV), biogas (BIO), diesel generator (DG), and battery storage (BS) (PV-BIO-DG-BS) HRES configuration, considering a typical summer and winter load profile of 94 households. The optimal solution (PV-BIO) achieved US$0.438/kWh as the lowest energy cost, LCOE, and a US$2.30M net cost NPC.

The optimum choice includes solar and bio-generators (PV-BIO) with the public grid, and excludes the diesel generator and batteries. In the optimal design, a bio-generator is selected in preference to a diesel generator and battery storage because of the high price of diesel, which usually costs about US$1.3/L, and the short lifespan of battery storage.

The most sensitive parameters reflected in the economic, emission, and excess electricity results are the solar scaled average (kWh/m^2/day), economic rates (%), and biomass price (US$/ton). In individual experiments, it was found that the effect of the sensitive parameters could vary the levelised cost of energy and reduce it to less than the grid price. If the PV capital cost multiplier is 0.8 and the expected inflation and nominal discount rates are 8 and 8, for instance, the energy cost will be US$0.119/kWh. The percentage of emissions reduction of the system is higher due to the renewable penetration percentage of around 500% from solar and biogas.

The results demonstrate that PV and biomass generators can produce renewable and sustainable energy and tackle the emission problem; the values of carbon dioxide and sulfur dioxide are substantially reduced. According to the results and calculations, carbon dioxide reduces by 6.4 times the amount produced by a power station for the same amount of generated electricity (Nassar and Alsadi 2016). This means that there is ample room for further benefits from biomass, which can constitute an environmental burden. Bio-share technology also seeks to reduce the system's capital costs, where it clearly affects the cost of energy (US$/kWh) over the project lifespan.

8. Consideration for future research

The study clearly demonstrated how solar energy is the dominating renewable energy in the study area, as well as the case of bioenergy from waste, and in future research, aim will focus more on these two types of renewable sources. In addition to the case study hybrid systems that use alternate energy sources.

References

(2004). The Interaction of Ocean Waves and Wind. Cambridge, University Press; 2004. p. 300 .

(2009). Europe's onshore and offshore wind energy potential, EEA, Copenhagen, 2009.

(2018). Chapter 41 - Engineered Nanomaterials for Energy Applications. Handbook of Nanomaterials for Industrial Applications. C. Mustansar Hussain, Elsevier**:** 751-767.

(2020). ISE. Freiburg,, Fraunhofer Institute for Solar Energy Systems, ISE.

, P., W. and N. Dahmen (2015). Processes for Thermochemical Conversion of Biomass. In Industrial Furnaces and Boilers, 10th European Conference, Papers.

, W. B. (2016). West Bank & Gaza Energy Efficiency Action Plan for 2020-2030 – Final Report, The World Bank, 1818 H Street NW, Washington. DC 20433, USA, fax 202-522-2422, e-mail pubrights@worldbank.org.

, W. B. (2017). Securing Energy for Development in West Bank and Gaza.

Abdallah, R., A. Juaidi, S. Abdel-Fattah and F. Manzano-Agugliaro (2020). "Estimating the Optimum Tilt Angles for South-Facing Surfaces in Palestine." Energies **13**: 623.

Abu-Hafeetha, M. F. (2009). "Planning for Solar Energy as an Energy Option for Palestine." Thesis or Dissertation - Master Degree in Urban and Regional Planning: https://scholar.najah.edu/sites/default/files/all-thesis/planning_for_solar_energy_as_an_energy_option_for_palestine.pdf.

Abu-Zarifa, A. (2014). "Design of a Stand-Alone Power Wind Turbine Optimized for Low Wind Speed in Gaza." International Journal of Energy Engineering: 4(5): 89-93.

Abu Hamed, T., L. Ismail and A. Alshare (2017). "The potential of using olive cake in power generation in the Palestinian territories." International Journal of Sustainable Energy **36**(4): 368-378.

Abusafa, A. and L. Mansour (2019). "Experimental Analysis of Different Solar Water Heating Systems According to Palestinian Environmental Conditions." **12**: 1901-1906.

Achinas, S., Y. Li, V. Achinas and G. J. W. Euverink (2019). "Biogas Potential from the Anaerobic Digestion of Potato Peels: Process Performance and Kinetics Evaluation." **12**(12): 2311.

Ahmad, F. and M. S. Alam (2018). "Economic and ecological aspects for microgrids deployment in India." Sustainable Cities and Society **37**: 407-419.

Al-Najjar, H., C. Pfeifer, R. Al Afif and H. J. El-Khozondar (2020). "Estimated View of Renewable Resources as a Sustainable Electrical Energy Source, Case Study." **4**(3): 32.

Alafif, R., C. Pfeifer and T. Pröll (2019). Bioenergy Recovery from Cotton Stalk. Cotton Research, intechopen.

Alamian, R., R. Shafaghat, S. J. Miri, N. Yazdanshenas and M. Shakeri (2014). "Evaluation of technologies for harvesting wave energy in Caspian Sea." Renewable and Sustainable Energy Reviews **32**: 468-476.

Alsadi, S. and T. Foqha (2021). "Mass flow rate optimization in solar heating systems based on a flat-plate solar collector: A case study." 61-071.

Amon, T., B. Amon, V. Kryvoruchko, A. Machmu ller, K. Hopfner-Sixt, V. Bodiroza, R. Hrbek, J. r. Friedel, E. Po tsch, H. Wagentristl, M. Schreiner and W. Zollitsch (2007). "Methane production through anaerobic digestion of various energy crops grown in sustainable crop rotations." Bioresource Technology **98**(17): 3204-3212.

Amon, T., B. Amon, V. Kryvoruchko, A. Machmüller, K. Hopfner-Sixt, V. Bodiroza, R. Hrbek, J. Friedel, E. Pötsch, H. Wagentristl, M. Schreiner and W. Zollitsch (2007). "Methane production through anaerobic digestion of various energy crops grown in sustainable crop rotations." Bioresource Technology **98**(17): 3204-3212.

Anand, P., S. K. Bath and M. Rizwan (2019). "Renewable energy-based hybrid model for rural electrification." International Journal of Energy Technology and Policy **15**: 86.

Ashekuzzaman, S. M. and T. Poulsen (2010). "Optimizing feed composition for improved methane yield during anaerobic digestion of cow manure based waste mixtures." Bioresource technology **102**: 2213-2218.

Ayodele, E., S. Misra, R. Damasevicius and R. Maskeliunas (2019). "Hybrid microgrid for microfinance institutions in rural areas – A field demonstration in West Africa." Sustainable Energy Technologies and Assessments **35**: 89-97.

Azerefegn, T. M., R. Bhandari and A. V. Ramayya (2020). "Techno-economic analysis of grid-integrated PV/wind systems for electricity reliability enhancement in Ethiopian industrial park." Sustainable Cities and Society **53**: 101915.

Babaee, A. and J. J. C. e. t. Shayegan (2011). "Anaerobic Digestion of Vegetable Waste." **24**: 1291-1296.

Balat, M. (2006). "Biomass Energy and Biochemical Conversion Processing for Fuels and Chemicals." Energy Sources, Part A: Recovery, Utilization, and Environmental Effects **28**(6): 517-525.

Barz, M., M. Delivand and K. Dinkler (2018). "Agricultural Wastes – A Promising Source for Biogas Production in Developing Countries of the Tropical and Subtropical Regions." Revista Forestal Mesoamericana Kurú **16**: 02-12.

Benedek, J., T.-T. Sebestyén and B. Bartók (2018). "Evaluation of renewable energy sources in peripheral areas and renewable energy-based rural development." Renewable and Sustainable Energy Reviews **90**: 516–535.

Besio, G., L. Mentaschi and A. Mazzino (2016). "Wave energy resource assessment in the Mediterranean Sea on the basis of a 35-year hindcast." Energy **94**: 50-63.

BLUESUN (2016). BLUESUN solar power inverter on grid off grid 30kw hybrid on-off grid hybrid inverter.

Boyd, M., S. Klein, D. Reindl and B. Dougherty (2011). "Evaluation and Validation of Equivalent Circuit Photovoltaic Solar Cell Performance Models." Journal of Solar Energy Engineering **133**.

Breeze, P. (2016). Combined Cycle Power Plants**:** 65-75.

Caposciutti, G., A. Baccioli, L. Ferrari and U. Desideri (2020). "Biogas from Anaerobic Digestion: Power Generation or Biomethane Production?" Energies **13**(3).

Caterpillar (2020). AURORA Generators. Commercial & Industrial Diesel Generators.

Chan, Y. H., K. W. Cheah, B. S. How, A. C. M. Loy, M. Shahbaz, H. K. G. Singh, N. a. R. Yusuf, A. F. A. Shuhaili, S. Yusup, W. A. W. A. K. Ghani, J. Rambli, Y. Kansha, H. L. Lam, B. H. Hong and S. L. Ngan (2019). "An overview of biomass thermochemical conversion technologies in Malaysia." Science of The Total Environment **680**: 105-123.

Chauhan, A. and R. P. Saini (2017). "Size optimization and demand response of a stand-alone integrated renewable energy system." Energy **124**: 59-73.

Chen, H. and W. J. B. A. Qiu (2010). "Key technologies for bioethanol production from lignocellulose." **28**(5): 556-562.

Choi, Y., J. Suh and S.-M. Kim (2019). "GIS-Based Solar Radiation Mapping, Site Evaluation, and Potential Assessment: A Review." Applied Sciences **9**(9).

Daful, A. G. and M. R. Chandraratne (2020). "Biochar production from biomass waste-derived material."

Demirbas, A. J. P. i. e. and c. science (2004). "Combustion characteristics of different biomass fuels." **30**(2): 219-230.

Dev, N., Samsher, S. S. Kachhwaha and R. Attri (2012). A REVIEW OF COMBINED CYCLE POWER PLANT THERMODYNAMIC CYCLES.

Dialyna, E. and T. Tsoutsos (2021). "Wave Energy in the Mediterranean Sea: Resource Assessment, Deployed WECs and Prospects." **14**(16): 4764.

Díaz-Vázquez, D., S. C. Alvarado-Cummings, D. Meza-Rodríguez, C. Senés-Guerrero, J. de Anda and M. S. Gradilla-Hernández (2020). "Evaluation of Biogas Potential from Livestock Manures and Multicriteria Site Selection for Centralized Anaerobic Digester Systems: The Case of Jalisco, México." **12**(9): 3527.

Dirnberger, D. (2015). Uncertainties in Energy Rating for Thin-film PV Modules.

Dubrovskis, V., I. Plume, V. Kotelenecs and E. Zabarovskis (2010). "Anaerobic digestion of sewage sludge." **27**.

Duman, A. C. and Ö. Güler (2018). "Techno-economic analysis of off-grid PV/wind/fuel cell hybrid system combinations with a comparison of regularly and seasonally occupied households." Sustainable Cities and Society **42**: 107-126.

EDITION (2020). POLITICS, WORLD,MIDDLE EAST.

El-Zaza, S. Z. (2009). Development of Wave Energy Conversion Device - Gaza Shoreline. Gaza, A thesis of Master of Science in Civil Engineering, IUG.

Elnaggar, M., E. Edwan and M. Ritter (2017). "Wind Energy Potential of Gaza Using Small Wind Turbines: A Feasibility Study." **10**(8): 1229.

EPA (2020). Center for Corporate Climate Leadership GHG Emission Factors Hub. Environmental Protection Agency.

Fathi Nassar, Y. and S. Yassin Alsadi (2019). "Assessment of solar energy potential in Gaza Strip-Palestine." Sustainable Energy Technologies and Assessments **31**: 318-328.

GEDCo (2020). Gaza Electricity Distribution Company.

Günther, M., N. Janotte, A. Mezrhab, K. Hennecke, C. Schillings, S. Wilbert and F. Wolferstätter (2011). Advanced CSP Teaching Materials Chapter 2 Solar Radiation.

Halasah, S. (2009). Life Cycle Energy Analysis of Photovoltaic Systems in the Arava: A Generation Scale Comparison.

HOMER (2019). HOMER Pro 3.13 User Manual, released April 29, 2019. HOMER Energy, HOMER Pro 3.13.

Hossain, M. S., A. Jahid, K. Z. Islam and M. F. Rahman (2020). "Solar PV and Biomass Resources-Based Sustainable Energy Supply for Off-Grid Cellular Base Stations." IEEE Access **8**: 53817-53840.

Hussain, I. (2015). "Effect of Variation in LPG Composition on Heating Value Using Aspen HYSYS." Journal of Petroleum Engineering & Technology **5**: 51-57.

Jahangiri, M., R. A. Rizi and A. A. Shamsabadi (2018). "Feasibility study on simultaneous generation of electricity and heat using renewable energies in Zarrin Shahr, Iran." Sustainable Cities and Society **38**: 647-661.

Janssen, P. (2000). Chapter 3 ECMWF wave modeling and satellite altimeter wave data, Elsevier Oceanography Series

Jie, P., F. Wei, F. Zhang and J. Li (2019). "Evaluating the performance of biomass gasification based combined cooling, heating, and power system operated under different operating strategies." Advances in Mechanical Engineering **11**(2): 1687814019827414.

Juaidi, A., F. Montoya, I. Ibrik and F. Manzano-Agugliaro (2016). "An overview of renewable energy potential in Palestine." Renewable and Sustainable Energy Reviews **65**: 943-960.

Kabeyi, M. and O. Olanrewaju (2021). Development of a Biogas Plant with Electricity Generation, Heating and Fertilizer Recovery Systems.

Kan, T., V. Strezov, T. J. J. R. Evans and s. e. reviews (2016). "Lignocellulosic biomass pyrolysis: A review of product properties and effects of pyrolysis parameters." **57**: 1126-1140.

Kasaeian, A., P. Rahdan, M. A. V. Rad and W.-M. Yan (2019). "Optimal design and technical analysis of a grid-connected hybrid photovoltaic/diesel/biogas under different economic conditions: A case study." Energy Conversion and Management **198**: 111810.

Keller, B. and A. Costa (2011). "A Matlab GUI for Calculating the Solar Radiation and Shading of Surfaces on the Earth." Computer Applications in Engineering Education **19**: 161-170.

Khairul Anuar, N., H. Che Man, S. Idrus and N. N. Nik Daud (2018). "Biochemical methane potential (BMP) from anaerobic co-digestion of sewage sludge and decanter cake." IOP Conference Series: Materials Science and Engineering **368**: 012027.

Kim, J. K., B. R. Oh, Y. N. Chun and S. W. Kim (2006). "Effects of temperature and hydraulic retention time on anaerobic digestion of food waste." Journal of Bioscience and Bioengineering **102**(4): 328-332.

Kitani, O. and C. W. l. Hal (1989). Biomass Handbook, Gordon and Breach science publishers. New York.

Kreith, F. and J. Kreider (2000). Principles of Solar Engineering.

Lambert, T., P. Gilman and P. Lilienthal (2006). Micropower System Modeling with Homer.Integration of alternative sources of energy., John Wiley & Sons.

Langston, L. S. (2020). "Aspects of Gas Turbine Thermal Efficiency." Mechanical Engineering **142**(09): 54-55.

Lasseter, R. (2007). "Microgrids And Distributed Generation." Journal of Energy Engineering-asce - J ENERG ENG-ASCE **133**.

Lehtomäki, A. (2006). "Biogas Production from Energy Crops and Crop Residues." JYVÄSKYLÄ STUDIES IN BIOLOGICAL AND ENVIRONMENTAL SCIENCE 163.

Li, Y., S. Achinas, J. Zhao, B. Geurkink, J. Krooneman and G. J. Willem Euverink (2020). "Co-digestion of cow and sheep manure: Performance evaluation and relative microbial activity." Renewable Energy **153**: 553-563.

Liberti, L., A. Carillo and G. Sannino (2013). "Wave energy resource assessment in the Mediterranean, the Italian perspective." Renewable Energy **50**: 938-949.

Lilienthal, P. (2005). HOMER® micropower optimization model, National Renewable Energy Lab.(NREL), Golden, CO (United States).

Mandadapu, U., V. Vedanayakam and K. Thyagarajan (2017). "EFFECT OF TEMPERATURE AND IRRADIANCE ON THE ELECTRICAL PERFORMANCE OF A PV MODULE." International Journal of Advanced Research **5**: 2018-2027.

Mandal, S., B. K. Das and N. Hoque (2018). "Optimum sizing of a stand-alone hybrid energy system for rural electrification in Bangladesh." Journal of Cleaner Production **200**: 12-27.

Masters, G. M. (2013). Renewable and Efficient Electric Power Systems, 2nd Edition, John Wiley & Sons.

MDLF (2017). Assessment of Existing Waste Recovery Activities in Gaza Strip, Gaza Strip-Palestine: Gaza, Palestine.

meetMED (2020a). Mitigation Enabling Energy Transition in the MEDiterranean region, All rights reserved.All rights reserved. Licensed to the European Union under conditions.

meetMED (2020b). Mitigation Enabling Energy Transition in the MEDiterranean region. Country Report on Energy Efficiency and Renewable Energy Investment Climate, Licensed to the European Union under conditions.

MOA (2018). Ministry of agriculture.

Morales-Polo, C., M. d. M. Cledera-Castro, M. Revuelta-Aramburu and K. Hueso-Kortekaas (2021). "Enhancing Energy Recovery in Form of Biogas, from Vegetable and Fruit Wholesale Markets By-Products and Wastes, with Pretreatments." **10**(7): 1298.

MTC (2021). Ministry of Transport and Communications Palestine, Characteristics of Gaza Sea, 2001–2006.

Muh, E. and F. Tabet (2019). "Comparative analysis of hybrid renewable energy systems for off-grid applications in Southern Cameroons." Renewable Energy **135**: 41-54.

Mukumba, P., G. Makaka and S. Mamphweli (2017). Biogasification of Horse Dung Using a Cylindrical Surface Batch Biodigester. Frontiers in Bioenergy and Biofuels, Eduardo Jacob-Lopes and Leila Queiroz Zepka, IntechOpen,.

MÜLLER-STEINHAGEN, H., F. and F. TRIEB (2004). Concentrating solar power, INSTITUTE OF TECHNICAL THERMODYNAMICS, GERMAN AEROSPACE CENTRE, STUTTGART, GERMANY.

Murphy, J., r. BrAuN, p. WEILAND and A. WELLINGEr (2011). "Biogas from Crop Digestion." IEA Bioenergy.

N'tsoukpoe, K. E., H. Liu, N. Le Pierrès, L. J. R. Luo and S. E. Reviews (2009). "A review on long-term sorption solar energy storage." **13**(9): 2385-2396.

Nachenius, R. W., F. Ronsse, R. Venderbosch and W. Prins (2013). Biomass pyrolysis. Advances in chemical engineering, Elsevier. **42:** 75-139.

Nagy, G., A. Takács, A. Kállay and D. Mentes (2018). "The anaerobic digestion of sheep manure in self-designed low-cost biogas reactor." Analecta Technica Szegedinensia **12**: 13-23.

Nassar, Y. and S. Alsadi (2016). "Economical and Environmental Feasibility of the Renewable Energy as a Sustainable Solution for the Electricity Crisis in the Gaza Strip." International Journal of Engineering Research and Development **12**: PP.35-34.

Nassar, Y., Y. Samer and S. Alsadi (2018). "Wind Energy Potential in Gaza Strip-Palestine state." **7**: 41-57.

Neary, V. S., R. G. Coe, J. Cruz, K. Haas, G. Bacelli, Y. Debruyne, S. Ahn and V. Nevarez (2018). "Classification Systems for Wave Energy Resources and WEC Technologies." International Marine Energy Journal **1**(2).

Nguyen, V., C. Thiep, T. Do and P. Viet (2019). "Research and calculation of the biogas fuel supply system for a small marine diesel engine." Journal of Mechanical Engineering Research and Developments **42**: 64-70.

NREL (2020). Transforming energy. Photovolatic Research.

Nunes, L. J. R., J. C. O. Matias and J. P. S. Catalão (2017). "Biomass in the generation of electricity in Portugal: A review." Renewable and Sustainable Energy Reviews **71**: 373-378.

ONEW (2020). products, natural gas generator. Fuzhou Onew Power Machinery Co., Ltd.

Ouda, M. (2001). Prospects Of Renewable Energy In Gaza Strip.

PCBS (2020). Energy Energy Balance of Palestine 2019. Ramallah - Palestine, Palestinian Central Bureau of Statistics

PENRA (2019). Palestine Energy And Natural Resources Authority.

PENRA (2020). Palestinian Energy and Natural Resources Authority-PENRA.

Precup, R.-E., T. Kamal and S. Hassan (2018). Solar Photovoltaic Power Plants: Advanced Control and Optimization Techniques.

PVGIS (2021). Institute for Energy and Transport: Photovoltaic Geographical Information System.

PWA (2016). Feasibility Study for Wastewater Reuse at Southern Part of Gaza Strip (Kahnyounis and Rafah). Gaza Strip-Palestine, Palestinian Water Authority: Gaza City.

Rad, M. A. V., R. Ghasempour, P. Rahdan, S. Mousavi and M. Arastounia (2020). "Techno-economic analysis of a hybrid power system based on the cost-effective hydrogen production method for rural electrification, a case study in Iran." Energy **190**: 116421.

Rajbongshi, R., D. Borgohain and S. Mahapatra (2017). "Optimization of PV-biomass-diesel and grid base hybrid energy systems for rural electrification by using HOMER." Energy **126**: 461-474.

Razali, M. N. (2016). "Formulation of bitumen from industrial waste." ARPN Journal of Engineering and Applied Sciences **11**: 5244-5250.

Rehman, S. and L. M. Al-Hadhrami (2010). "Study of a solar PV–diesel–battery hybrid power system for a remotely located population near Rafha, Saudi Arabia." Energy **35**(12): 4986-4995.

Rodrigues , L. (2008). "Wave power conversion systems for electrical energy production." **1**(6).

Salameh, T., C. Ghenai, A. Merabet and M. Alkasrawi (2020). "Techno-economical optimization of an integrated stand-alone hybrid solar PV tracking and diesel generator power system in Khorfakkan, United Arab Emirates." Energy **190**: 116475.

Salem, H. S. (2019). "The Potential of Wind Energy in Palestine with Healthcare and Residential Examples in the West Bank and the Gaza Strip." Journal of Nature Science and Sustainable Technology **13**(2): 73-97.

Sampaio, P. G. V. and M. O. A. González (2017). "Photovoltaic solar energy: Conceptual framework." Renewable and Sustainable Energy Reviews **74**: 590-601.

Sawle, Y., S. C. Gupta and A. K. Bohre (2018). "Review of hybrid renewable energy systems with comparative analysis of off-grid hybrid system." Renewable and Sustainable Energy Reviews **81**: 2217-2235.

Sawle, Y., S. C. Gupta and A. Kumar Bohre (2016). "PV-wind hybrid system: A review with case study." Cogent Engineering **3**(1): 1189305.

Schumacher, G. and L. Juniper (2013). 15 - Coal utilisation in the cement and concrete industries. The Coal Handbook: Towards Cleaner Production. D. Osborne, Woodhead Publishing. **2:** 387-426.

Shammas, N. K. and L. K. Wang (2007). Aerobic Digestion. (eds) Biosolids Treatment Processes. Handbook of Environmental Engineering, Humana Press. **6**.

Sharma, S., R. Meena, A. Sharma and P. Goyal (2014). "Biomass Conversion Technologies for Renewable Energy and Fuels: A Review Note." IOSR Journal of Mechanical and Civil Engineering **11**: 28-35.

Sharma, V. K., A. Colangelo and G. Spagna (1995). "Photovoltaic technology: basic concepts, sizing of a stand alone photovoltaic system for domestic applications and preliminary economic analysis." Medium: X; Size: pp. 161-174.

Shockley, W. and H. J. J. J. o. a. p. Queisser (1961). "Detailed balance limit of efficiency of p-n junction solar cells." **32**(3): 510-519.

Sinha, S. and S. S. Chandel (2014). "Review of software tools for hybrid renewable energy systems." Renewable and Sustainable Energy Reviews **32**: 192-205.

SOLAR, F. (2020). Products, Batteries (Lead-Acid), BAE Secura PVS Cell Solar Series.

Staffell, I. and S. Pfenninger (2016). "Using bias-corrected reanalysis to simulate current and future wind power output." Energy **114**: 1224-1239.

SUSANA (2009).

Tar, K., A. Kircsi, B. Bartok, S. Szegedi, L. István, R. Vass, A. Bai and T. Toth (2015). "Estimation of solar and wind energy potential in the Hernad Valley." Quarterly Journa of the Hungarian Meteorological Service **119**(4): 537– 555.

Teferra, D. M. and W. Wubu (2018). Biogas for Clean Energy In (Ed.). Anaerobic Digestion, IntechOpen.

Toledo, C., A. M. Gracia Amillo, G. Bardizza, J. Abad and A. Urbina (2020). "Evaluation of Solar Radiation Transposition Models for Passive Energy Management and Building Integrated Photovoltaics." Energies **13**(3).

Tursi, A. J. B. R. J. (2019). "A review on biomass: importance, chemistry, classification, and conversion."

Vasserman, A. and M. Shutenko (2017). "Methods of increasing thermal efficiency of steam and gas turbine plants." Journal of Physics: Conference Series **891**: 012248.

Vijay, V., P. Subbarao and R. Chandra (2020). "Identification of potential waste seeds of wildly growing tree species for the production of biogas." Environmental Science and Pollution Research **27**: 14515–14528.

Wartell, B. A., V. Krumins, J. Alt, K. Kang, B. J. Schwab and D. E. Fennell (2012). "Methane production from horse manure and stall waste with softwood bedding." Bioresource Technology **112**: 42-50.

Wijekoon, P., C. Wickramasinghe, B. Athapattu, M. Narayana, A. de Alwis, M. J. B. C. Vithanage and Biorefinery (2020). "Biomass valorization and phytoremediation as integrated technology for municipal solid waste management for developing economic context." 1-20.

Yang, H., R. Yan, H. Chen, D. H. Lee and C. J. F. Zheng (2007). "Characteristics of hemicellulose, cellulose and lignin pyrolysis." **86**(12-13): 1781-1788.

Yimen, N., O. Hamandjoda, L. Meva'a, N. Bénoît and J. Nganhou (2018). "Analyzing of a Photovoltaic/Wind/Biogas/Pumped-Hydro Off-Grid Hybrid System for Rural Electrification in Sub-Saharan Africa—Case study of Djoundé in Northern Cameroon." Energies **11**: 2644.

Zamft, B. and R. Conrado (2015). "Engineering plants to reflect light: Strategies for engineering water-efficient plants to adapt to a changing climate." Plant biotechnology journal **13**.

Zhang, R., H. M. El-Mashad, K. Hartman, F. Wang, G. Liu, C. Choate and P. Gamble (2007). "Characterization of food waste as feedstock for anaerobic digestion." Bioresource Technology **98**(4): 929-935.

Zodiatis, G., G. Galanis, A. Nikolaidis, C. Kalogeri, D. Hayes, G. C. Georgiou, P. C. Chu and G. Kallos (2014a). "Wave energy potential in the Eastern Mediterranean Levantine Basin. An integrated 10-year study." Renewable Energy **69**: 311-323.

Zodiatis, G., G. Galanis, A. Nikolaidis, C. Kalogeri, D. Hayes, G. C. Georgiou, P. C. Chu and G. Kallos (2014b). "Wave energy potential in the Eastern Mediterranean Levantine Basin. An integrated 10-year study." Renewable Energy **69**: 311-323.

List of abbreviations

AVH	Average Heating Value
CC	Cycle Charging
CCGT	Combined Cycle Gas Turbine
CCPP	Combined Cycle Power Plant
CMWU	Coastal Municipalities Water Utility
COE	Cost of Electricity
CSP	Concentrated Solar Power
ETC	Evacuated Tube Collectors
FPC	Flat Plate Collectors
GEDCo	Gaza Electricity Distribution Company
GHG	Green House Gasses
GPP	Gaza Power Plant
GS	Gaza Strip
LCB	Lignocellulose Biomass
LCOE	Levelised Cost of Energy or Cost of Energy
LF	Load Following
HES	Hybrid Electric System
HHV	Higher Heating Value
HOMER	Multiple Energy Resources Hybrid Optimization
HRES	Hybrid Renewable Energy System
kW	Kilowatt
MoA	Ministry of Agriculture
MSW	Municipal Solid Waste
NPC	Net Present Cost
O&M	Operating and Maintenance
PC	Palestinian Cabinet
PCBS	Palestinian Central Bureau of Statistics
PENRA	The Palestinian Energy and Natural Resources Authority
PETL	Palestinian Electricity Transmission Line
PLC	Palestinian Legislative Council
PSH	Peak Sun Hours
PT	Palestinian Territories
PV	Photovoltaic
RE	Renewable Energy
SS	Sewage Sludge
SWH	Solar Water Heating
TJ	Tera (1012) Joule
UNOPS	United Nation Office for Project Services
UNDP/DHV	United Nations Development Program
WECs	Wave Energy Converters
WWTP	Waste Water Treatment Plants

List of Tables

List of Figures

Appendix A

ELECTRICAL DATA | STC*

CS3N	400MS	405MS	410MS	415MS	420MS	425MS
Nominal Max. Power (Pmax)	400 W	405 W	410 W	415 W	420 W	425 W
Opt. Operating Voltage (Vmp)	37.2 V	37.4 V	37.6 V	37.8 V	38.0 V	38.2 V
Opt. Operating Current (Imp)	10.76 A	10.83 A	10.92 A	10.98 A	11.06 A	11.13 A
Open Circuit Voltage (Voc)	44.5 V	44.7 V	44.9 V	45.1 V	45.3 V	45.5 V
Short Circuit Current (Isc)	11.50 A	11.56 A	11.62 A	11.68 A	11.74 A	11.80 A
Module Efficiency	19.7%	19.9%	20.2%	20.4%	20.7%	20.9%
Operating Temperature	-40°C ~ +85°C					
Max. System Voltage	1500V (IEC/UL) or 1000V (IEC/UL)					
Module Fire Performance	TYPE 1 (UL 61730 1500V) or TYPE 2 (UL 61730 1000V) or CLASS C (IEC 61730)					
Max. Series Fuse Rating	20 A					
Application Classification	Class A					
Power Tolerance	0 ~ + 10 W					

* Under Standard Test Conditions (STC) of irradiance of 1000 W/m², spectrum AM 1.5 and cell temperature of 25°C.

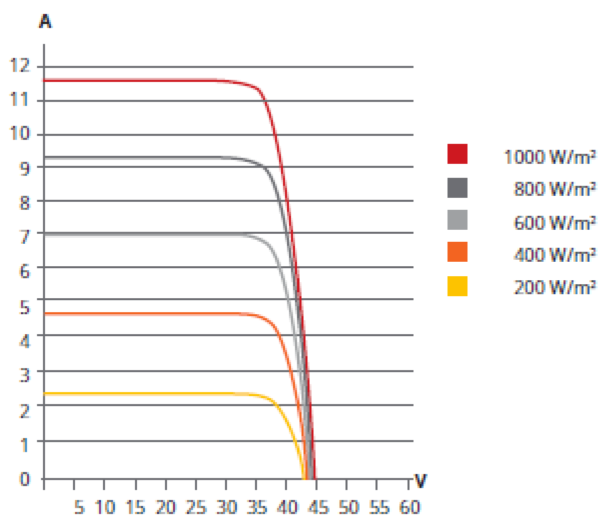

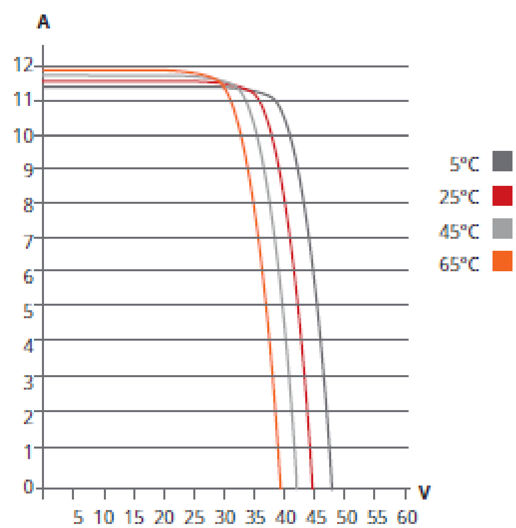

TEMPERATURE CHARACTERISTICS

Specification	Data
Temperature Coefficient (Pmax)	-0.35 % / °C
Temperature Coefficient (Voc)	-0.27 % / °C
Temperature Coefficient (Isc)	0.05 % / °C
Nominal Module Operating Temperature	42 ± 3°C